TECHNICKÁ UNIVERZITA V LIBERCI

Faculty of Mechatronics, Informatics and Interdisciplinary Studies

A chitosan-poly(3-hydroxybutyrate) bioconjugate for greener synthesis of metal nanocatalysts

Ph.D. Thesis

Liberec 2023 **Mgr. Daniele Silvestri**

TECHNICKÁ UNIVERZITA V LIBERCI

Disertační práce

A chitosan-poly(3-hydroxybutyrate) bioconjugate for greener synthesis of metal nanocatalysts

Studijní program: P3942 Nanotechnologie
Studijní obor: Nanotechnologie

Autor práce: **Mgr. Daniele Silvestri**
Školitel práce: doc. Ing. Stanislaw Waclawek, Ph.D.
Ústav nových technologií a aplikované informatiky

Liberec 2023

Prohlášení

Prohlašuji, že svou disertační práci jsem vypracoval samostatně jako původní dílo s použitím uvedené literatury a na základě konzultací s vedoucím mé disertační práce a konzultantem.

Jsem si vědom toho, že na mou disertační práci se plně vztahuje zákon č. 121/2000 Sb., o právu autorském, zejména § 60 – školní dílo.

Beru na vědomí, že Technická univerzita v Liberci nezasahuje do mých autorských práv užitím mé disertační práce pro vnitřní potřebu Technické univerzity v Liberci.

Užiji-li disertační práci nebo poskytnu-li licenci k jejímu využití, jsem si vědom povinnosti informovat o této skutečnosti Technickou univerzitu v Liberci; v tomto případě má Technická univerzita v Liberci právo ode mne požadovat úhradu nákladů, které vynaložila na vytvoření díla, až do jejich skutečné výše.

Současně čestně prohlašuji, že text elektronické podoby práce vložený do IS/STAG se shoduje s textem tištěné podoby práce.

Beru na vědomí, že má disertační práce bude zveřejněna Technickou univerzitou v Liberci v souladu s § 47b zákona č. 111/1998 Sb., o vysokých školách a o změně a doplnění dalších zákonů (zákon o vysokých školách), ve znění pozdějších předpisů.

Jsem si vědom následků, které podle zákona o vysokých školách mohou vyplývat z porušení tohoto prohlášení.

8. února 2023 Mgr. Daniele Silvestri

ACKNOWLEDGEMENTS

First of all, I would like to thank Prof. Petrangeli Papini and Prof. Dr. Ing. Miroslav Černík, CSc, for giving me the opportunity to start traveling through nanomaterials. I will never forget the support and effort I received from my supervisor. doc. Ing. Stanisław Wacławek, Ph.D. Thanks to him it was possible to carry out my PhD. Also, I would like to thank my parents and family who have supported me in many ways. Many thanks to all the CXI people who helped me during my PhD. Furthermore, I would also like to thank the partial financial assistance provided by the NanoEnviCz Research Infrastructure (Project No. LM2015073) supported by the Ministry of Education, Youth and Sports of the Czech Republic. Computational resources were supplied by the project "e-Infrastruktura CZ" (e-INFRA CZ LM2018140) supported by the Ministry of Education, Youth and Sports of the Czech Republic.

Abstract

Biopolymers are inspiring interest due to various characteristics, including biocompatibility, antibacterial properties and the stabilisation of various nanostructures. Furthermore, some can also act as a reducing agent for nanoparticle synthesis. In addition, several biopolymers are biodegradable as well, which is an important point for developing harmless products. Among the biopolymers, chitosan and polyhydroxybutyrate (PHB) have attracted the interest of many researchers around the world. However, given some of their characteristics, the use of these biopolymers is limited in some fields, such as catalysis and the synthesis of nanostructures. One of the main problems is related to the solubility of these two polymers in water at neutral pH. Chitosan is soluble under acidic conditions while PHB needs organic solvents, such as chloroform in order to be solubilised. Therefore, finding an environmentally-friendly way to conjugate chitosan and PHB, and make the polymer conjugate soluble in a wide range of pH in water, could open new perspectives in research. For example, it could be employed for the green synthesis and stabilisation of nanoparticles and to improve their catalytic behaviour. Therefore, the first part of work focused on obtaining the chitosan–polyhydroxybutyrate polymeric conjugate (Cs–PHB). The conjugate was obtained using a procedure for the conjugation of chitosan with folic acid. The goal achieved was to minimise the use of toxic solvents. Indeed, for the synthesis of Cs–PHB only acidified water was used as solvent (nitric acid, 310 µL/100 mL). Therefore, to confirm the successful conjugation, chitosan, PHB and Cs–PHB were characterised by different techniques, such as nuclear magnetic resonance, gel permeation chromatography and Fourier–transform infrared spectroscopy. Furthermore, the favourable outcome of the conjugation procedure was also confirmed by density functional theory.

Another goal achieved was the use of the Cs–PHB conjugate for the synthesis of various metallic and bimetallic nanoparticles. First, the gold nanoparticles were synthesised following the green synthesis approach. The conjugate was employed as a green reducing/capping agent. Cs–PHB–Au showed higher catalytic activity through the hydrogenation of nitroarenes than gold nanoparticles synthesised using only chitosan as reducing/capping agent (about 20% higher). Furthermore, using the Cs–PHB conjugate, it is possible to modulate the shape of the nanoparticles as demonstrated in the synthesis of Pd/Pt bimetallic nanoparticles. By adjusting the synthesis,

nanoparticles with three different shapes were obtained. Furthermore, the different bimetallic nanoparticles obtained show different catalytic activity compared to 4–nitrophenol. Furthermore, it was also possible to synthesise silver nanoparticles following a green approach. The procedure developed with respect to those reported in the literature (synthesis of silver nanoparticles using chitosan) has numerous advantages, such as reduced synthesis times and lower synthesis temperature. Moreover, silver nanoparticles synthesised using Cs–PHB as a reducing/capping agent showed extraordinary results for the hydrogenation of 4–NP (apparent first–order kinetic constant = 0.921 min^{-1}, activity parameter = 151 L g^{-1} s^{-1} and activity parameter/specific surface area = 11.6 L m^{-2} s^{-1}). Finally, Cs–PHB was used as a green capping agent to stabilise zero valent iron nanoparticles and enhance its persulfate activation properties. The results suggest that the remarkable results for the oxidation of the model pollutant could be attributed to the presence of functional groups on the Cs–PHB–nZVI surface.

To summarise, the present work shows the potential applicability of a bioconjugate obtained without the use of toxic solvents as an effective reducing/capping agent of different nanostructures. The synthesised nanoparticles showed increased catalytic activity in both the reduction and oxidation processes.

Keywords: Bio–conjugate, Nanoparticles, Catalysts, Reduction, Oxidation.

Abstract

Biopolymery vzbuzují zájem kvůli různým charakteristikám, včetně biokompatibility, antibakteriálních vlastností a stabilizace různých nanostruktur. Kromě toho, některé mohou také působit jako redukční činidlo pro syntézu nanočástic. Několik biopolymerů je navíc také biologicky odbouratelných, což je důležitý bod pro vývoj nezávadných produktů. Mezi biopolymery přitáhly chitosan a polyhydroxybutyrát (PHB) zájem mnoha výzkumníků po celém světě. Vzhledem k některým jejich vlastnostem je však použití těchto biopolymerů v některých oblastech, jako je katalýza a syntéza nanostruktur, omezené. Jeden z hlavních problémů souvisí s rozpustností těchto dvou polymerů ve vodě při neutrálním pH. Chitosan je rozpustný za kyselých podmínek, zatímco PHB potřebuje organická rozpouštědla, jako je chloroform, aby byl solubilizován. Nalezení šetrného enviromentálního způsobu, jak konjugovat chitosan a PHB a učinit polymerní konjugát rozpustným ve vodě v širokém rozmezí pH, by tak mohlo otevřít nové perspektivy ve výzkumu. Příkladem by mohlo být použití pro zelenou syntézu a stabilizaci nanočástic, a pro zlepšení jejich katalytického chování. První část práce je proto zaměřená na získání polymerního konjugátu chitosan–polyhydroxybutyrátu (Cs–PHB). Konjugát byl získán za použití postupu pro konjugaci chitosanu s kyselinou listovou. Cílem bylo minimalizovat použití toxických rozpouštědel. Pro syntézu Cs–PHB byla totiž jako rozpouštědlo použita pouze okyselená voda (kyselina dusičná, 310 µL/100 mL). Pro potvrzení úspěšné konjugace byly chitosan, PHB a Cs–PHB charakterizovány různými technikami, jako je nukleární magnetická rezonance, gelová permeační chromatografie a infračervená spektroskopie s Fourierovou transformací. Příznivý výsledek konjugačního postupu byl navíc potvrzen také teorií funkce hustoty.

Dalším dosaženým cílem bylo využití konjugátu Cs–PHB pro syntézu různých kovových a bimetalických nanočástic. Nejprve byly syntetizovány zlaté nanočástice podle postupu zelené syntézy. Konjugát byl použit jako zelené redukční/uzavírací činidlo. Cs–PHB–Au vykazovaly vyšší katalytickou aktivitu prostřednictvím hydrogenace nitroarenů než nanočástice zlata syntetizované pouze za použití chitosanu jako redukčního/uzavřeného činidla (asi o 20 % vyšší). Dále je pomocí konjugátu Cs–PHB možné modulovat tvar nanočástic, jak bylo prokázáno při syntéze bimetalických nanočástic Pd/Pt. Úpravou syntézy byly získány nanočástice tří různých tvarů. Kromě toho, různé získané bimetalické nanočástice vykazují odlišnou katalytickou aktivitu ve srovnání s 4–

nitrofenolem. Dále bylo také možné syntetizovat stříbrné nanočástice podle zeleného přístupu. Postup vyvinutý s ohledem na postupy uváděné v literatuře (syntéza nanočástic stříbra pomocí chitosanu) má řadu výhod, jako je zkrácení doby a nižší teplota syntézy. Nanočástice stříbra syntetizované pomocí Cs–PHB jako redukčního/uzavřeného činidla navíc vykazovaly mimořádné výsledky pro hydrogenaci 4–NP (zdánlivá kinetická konstanta prvního řádu = 0,921 min^{-1}, parametr aktivity = 151 L g^{-1} s^{-1} a parametr aktivity / měrný povrch = m^{-2} s^{-1}). Nakonec byl Cs–PHB použit jako zelené krycí činidlo pro stabilizaci nZVI a zvýšení jeho katalytických vlastností. Výsledky naznačují, že výsledky oxidace modelového polutantu (jako oxidant byl použit persíran) lze přičíst přítomnosti funkčních skupin na povrchu Cs–PHB–nZVI.

Tato práce ukazuje potenciální použitelnost biokonjugátu získaného bez použití toxických rozpouštědel jako účinného redukčního/uzavíracího činidla různých nanostruktur. Syntetizované nanočástice vykazovaly zvýšenou katalytickou aktivitu v redukčních i oxidačních procesech.

Klíčová slova: Bio–konjugát, Nanočástice, Katalyzátory, Redukce, Oxidace.

Contents

ABBREVIATIONS 10
INTRODUCTION 11
Chitin 14
Chitosan 15
Chitosan use 20
Use of chitosan in nanomaterial synthesis 20
Chitosan modification 23
Polyhydroxyalkanoates 25
Polyhydroxybutyrate 26
Polyhydroxybutyrate application 26
Use of polyhydroxybutyrate in nanomaterial synthesis 27
Polyhydroxybutyrate modification 29
Catalysis 32
RESULTS AND DISCUSSION 35
A poly(3–hydroxybutyrate)–chitosan polymer conjugate for the synthesis of safer gold nanoparticles and their applications 38
The use of a biopolymer conjugate for an eco-friendly one-pot synthesis of palladium-platinum alloys 47
Synthesis of Ag nanoparticles by a chitosan-poly(3-hydroxybutyrate) polymer conjugate and their superb catalytic activity 62
Modification of nZVI with a bio-conjugate containing amine and carbonyl functional groups for catalytic activation of persulfate 71
CONCLUSIONS 83
Attachments 84

ABBREVIATIONS

PHB – Polyhydroxybutyrate

TMNPs – Transition metal nanoparticles

4–NP – 4–nitrophenol

4–AM – 4–aminophenol

MO – Methyl Orange

NMR – Nuclear magnetic resonance

DA – Acetylation degree

DDA – Degree of deacetylation

FTIR – Fourier transform infrared spectroscopy

MW – Molecular weight

DS – Substitution degree

PHA – Polyhydroxyalkanoates

PLA/PHB–rubber – Poly(lactic acid) and poly(hydroxybutyrate) –rubber copolymer

PHBV – Poly(hydroxybutyrate–valerate)

rGO – reduced graphene oxide

SEM – Scanning Electron Microscopy

PEG – Polyethylene glycol

nZVI – Zero valent iron nanoparticles

PDS – Persulfate

GPC – Gel permeation chromatography

DFT – density functional theory

Cs–PHB – Chitosan–Polyhydroxybutyrate

INTRODUCTION

Nowadays, society is dealing with several challenges related to different fields, such as sustainability and the environment. Therefore, the need to develop new materials is undeniable. These materials could improve the quality of life and help develop advanced technologies. Over the past two decades, polymers have attracted attention in various fields due to their characteristics [1–3]. For instance, in medical applications, polymers have been used for the production of bones and implants [4,5]. Polymers are also used in the food packaging industry to achieve a more sustainable environmental impact of the waste [6]. Furthermore, nanotechnologies often use polymers and bio–polymers for different applications. For example, polymers could be used for drug delivery, to enhance antibacterial properties, as a carbon source in bioremediation, for green synthesis of several nanostructures and for the stabilisation of nanomaterials. Often nanomaterials stabilised, and therefore coated, by polymeric substances show improved properties due to the synergistic effect of such materials.

Jöns Jakob, a Swedish scientist, was the first to coin the name polymer. A polymer could be defined as a large molecule that is composed of repeated chemical units. Overall, polymers can be classified as bio– and synthetic. In turn, biopolymers can be generally divided into two big groups as reported by George et al. [7] namely bio–degradable and non–biodegradable. Most biopolymer research focuses on bio–degradable polymers because it is critical in developing safe products. It should be noted that non–degradable biopolymers make up the majority. Among the bio–degradable polymers, chitosan and polyhydroxybutyrate (PHB) attracted the attention of researchers in several scientific fields due to their unique characteristics [8–11]. As the figure shows, the number of articles concerning chitosan and PHB has been growing over the years (Fig. 1).

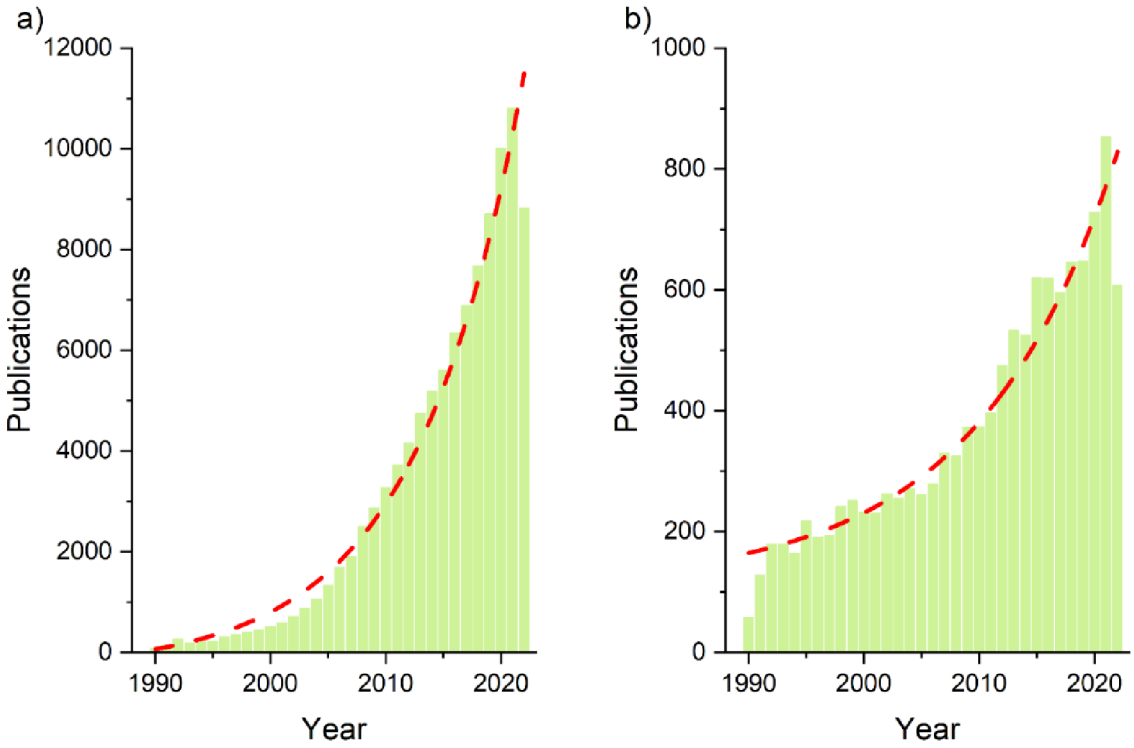

Fig. 1 Number of publications per year of papers containing the keywords a) 'chitosan' and b) a combination of 'polyhydroxybutyrate' and 'PHB' (WOS 20–11–22).

However, the use of these two polymers is strongly limited due to a few factors, such as cost production [12] and the non–solubility of chitosan and PHB in water (chitosan requires acidic conditions, while PHB needs solvents, such as chloroform). Therefore, a modification is needed to obtain a water–soluble polymer to reduce the use of non–environmentally friendly substances.

The synthesis of transition metal nanoparticles (TMNPs) can be achieved in two different ways: bottom–up and top–down. In the bottom–up method, nanoparticles are produced starting from a bulk material (chemical and physical treatments) and thus, this method is based on the dimensional reduction of the starting material. However, this method shows some shortcomings. For example, it is not possible to produce ultra–small nanoparticles and the surface is strongly affected [13] (change in chemistry and physicochemical properties of the surface). On the other hand, the synthesis of TMNPs with the bottom–up method involves the use of smaller molecules or small particles. A typical example of the bottom–up method is the synthesis of nanoparticles from a salt precursor; the salt precursor is reduced by a reducing agent (e.g., sodium borohydride

or green reducing agent), which results in the formation of TMNPs [14]. Over the years, various synthesis methods have been proposed for the formation of TMNPs, the most used are reported in Table 1.

Table 1 Synthesis of transition metal elements

	Nanoparticles	Methods	Procedure	Size (nm)	Reference
Top–down methods	Gold	Ball milling	Gold powder was milled (4, 8, 12, 16, and 20 h) using tungsten carbide (10 mm) and zirconia balls (3 mm).	22	[15]
	Gold	Laser ablation	A gold plate was placed in sodium dodecyl sulfate aqueous solution (10 mL). Then, the gold was irradiated by laser (1064 nm or 532 nm at 10 Hz).	1–5	[16]
	Platinum	Laser ablation	A platinum plate was placed in sodium dodecyl sulfate aqueous solution (10 mL). Then, the gold was irradiated by laser (1064 nm or 532 nm at 10 Hz).	1–7	[17]
Bottom–up methods	Gold	Physical vapor deposition	Deposition was carried out by a custom–built DC magnetron sputterer (2.5 mTorr, Argon).	~1.5	[18]
	TiO_2	Sol gel method	A solution containing 0.3 mL anhydrous ethanol, 0.15 mL distilled water, and 11.1 mL of acetic acid was mixed drop by drop to a solution containing 3 mL titanium tetra–isopropoxide and were mixed with 10.6 mL of anhydrous ethanol. After gel formation it was dried at 110 °C for 24 h. The resulting powder was calcined at 450 °C.	5–10	[19]
	Iron	Chemical reduction	$FeCl_3 \cdot 6H_2O$ (1g) was dissolved in ethanol (50 mL), then, a sodium borohydride solution (1 g, 50 mL D.I.) was added dropwise.	~80	[20]
	Silver	Hydrothermal synthesis	Silver nitrate solution (15 mL 3.40 g) was added to glucose solution (5 mL, 0.12 g). Then, polyvinylpyrrolidone (5 mL, 0.12 g) was added to the solution and finally sodium chloride (15 mL, 0.04 M, 2.33 g). The obtained solution was placed in an autoclave and heated (160 °C for 22 h).	45–65	[21]
	Gold	Solvothermal method	$HAuCl_4$ (50 µL 30 wt %) acidic solution was added to oleylamine solution (1.5 mL, 60 °C), after 15 min temperature was raised at 120 °C and after 30 min temperature was increased at 210 °C and kept for 1 h.	7–9	[22]

However, the synthesis of nanoparticles often involves toxic substances that should be avoided in order to make the process environmentally friendly. In addition, TMNPs frequently need to be stabilised, in order to minimise the aggregation of nanoparticles. The aggregation of nanoparticles is one of the main problems related to nanomaterials [23,24]. This issue is extremely

important especially in environmental applications where the surface area of the nanoparticles plays a key role. Therefore, a homogeneous dispersion leads to a narrow particle size distribution and as the size decreases, the specific surface area of the particles increases. TMNPs are usually stabilised by the formation of a layer around the nanoparticles' surface [25]. The coating process of the nanoparticles can employ natural or synthetic polymers, such as chitosan [26] and polyvinylpyrrolidone [27]; however, in this dissertation, the synthetic polymers will not be discussed. Nanoparticles' coating is important not only to reduce the agglomeration but also to influence the nanoparticles' behaviour. As a matter of fact, an improved catalytic performance due to functional groups shown on the nanoparticles' surface [28–31] and different zeta potential [32] of nanoparticles were reported.

TMNPs are often employed for contaminant removal in water and soil [33,34]. TMNPs can be used in different processes, such as adsorption [35], reduction [36] and additionally in oxidation processes [37]. Several pollutants can be treated using TMNPs, such as heavy metals [38], nitroarenes [39] and dyes [40]. Therefore, for this dissertation, model pollutants were chosen; 4–nitrophenol (4–NP) and Methyl Orange (MO) were considered as benchmarks in environmental applications, similar to other works [41–44].

Chitin

Among the biopolymers, chitin is one of the most abundant polymers present in nature (2nd after cellulose [45]) with a yearly bio–synthesis estimated at 100 billion tons, as reported by Tharanathan and Kittur [46]. Therefore, it is not surprising that chitosan, a derivative of chitin, is one of the most studied and very often used biopolymers for the synthesis of TMNPs.

Chitin [poly (β–(1→4)–N–acetyl–D–glucosamine)] is a natural mucopolysaccharide first isolated in 1811 by a French researcher named Braconnot from the cell walls of champignons [47]. However, it was not until 1823 that Odier renamed this compound from fungine to chitin. Chitin is used as support material in different micro and macro–organisms (e.g., in insects, such as cockroaches, beetles, ants and others and in crustacea, such as prawns, lobsters, krill and others) [48], it is used for exoskeleton, while in fungi (*Ascomycetes*, *Basidiomycetes*, *Phycomycetes* and others), it is present in the cell walls [49].

To date, two source–dependent chitin allomorphs have been identified (based on crystalline structure), known as α– and β–chitin. While, the existence of γ– is matter of debate [50].
It is possible to distinguish these compounds by characterisation techniques [e.g., Nuclear magnetic resonance (NMR) and X–ray diffraction (XRD)] [51].

α–chitin is the most abundant form of chitin found in fungi, insects, crustacea and yeast. While, β–chitin occur in *Siboglinidae*, squid pens and some worms to form microtubules [52]. The crystal structure of α–chitin consists of two antiparallel molecules per unit cell, whereas β–chitin has only one molecule per unit cell, in a parallel arrangement [53]. Both α– and β–chitin exhibit a hydrogen bond in their molecular structure. These hydrogen bonds influence reactivity, solubility as well as the swelling behaviour of chitin chains [51]. Unfortunately, both α– and β–chitin are insoluble in water and most common solvents and therefore, chitin application is strongly limited [54].

The procedure for chitin extraction depends on the starting materials. For example, chitin in crustaceans is complex with proteins and minerals (i.e., calcium carbonate). Hence, the process involves demineralisation and deproteinisation using a chemical or biological approach [52]. The chemical methods use bases, such as NaOH or KOH and acids, such as HCl to dissolve proteins and calcium carbonates [55].
It goes without saying that the chemical method has some disadvantages as it is not ecological, and the solubilised protein and minerals cannot be used for animal or human nutrients [55]. However, the short time required for the extraction make this procedure the most used treatment [55]. Because the use of bases and acids is dangerous for the environment, biological treatment is a valid alternative to the chemical one. In the biological treatment, lactic acid bacteria and proteases are used for demineralisation and deproteinisation respectively [50]. However, this process needs a long time and is limited to the scale of a laboratory.

Chitin has many derivatives which are classified into two groups, anionic and cationic [50]. Of the derivatives, chitosan is considered the most important.

Chitosan

Chitosan is a polymer obtained from the deacetylation of chitin by removing acetyl groups [56]. The acetylation degree (DA) is used to differentiate chitin from chitosan [55]. If the DA (molar

%) is >50 mol%, the product is called chitosan and is soluble in acidic solutions. However, during the deacetylation, the depolymerisation reaction takes place, which influences the chitosan molecular weight [55,57,58].

The chitin deacetylation process occurs through the removal of the acetyl group (C_2H_3O) and the formation of the amino group (NH_2) (Fig. 2). Deacetylation processes start from the chitin amorphous regions and proceed towards the crystalline region [59,60]. The products obtained after the deacetylation process are N–acetylglucosamine and glucosamine copolymer [49]. The obtained copolymer is called chitosan if it shows >50% of N–acetylglucosamine units [55]. Meanwhile, when the obtained copolymer has >50% of glucosamine units, it is called chitin. The DA and degree of deacetylation (DDA) are important parameters that influence the characteristics of these polymers. Because DA and DDA are correlated, the sum of DA and DDA is equal to 100%.

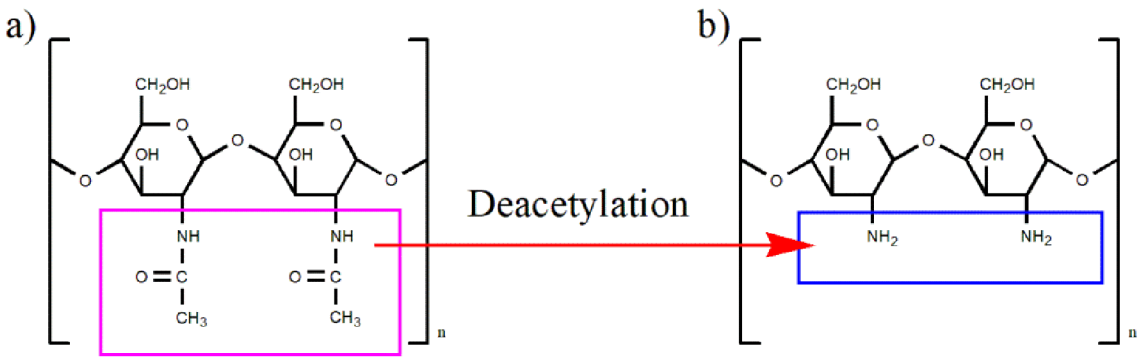

Fig. 2 Deacetylation of a) chitin to b) chitosan (100% of deacetylation).

Several methods are available for chitin deacetylation, however the most used method is by hot alkali treatment which is also used on a commercial scale [58]. The factors that influence the fate of deacetylation are the NaOH concentration, temperature, reaction time, chitin concentration and molecular weight.

The alkali treatment is not the only available deacetylation method used. Enzymatic deacetylation is rousing more and more interest over time [61]. This treatment involves the use of chitin deacetylases from different sources (e.g., from fungi or insects). The deacetylation of chitin by deacetylases shows fascinating characteristics. The obtained chitosan shows more block defined deacetylation pattern and furthermore, the enzymatic treatment is considered eco–friendly [61]. The main problem with this process is the high cost compared to alkali treatment due to the use

of chitin deacetylases. Unfortunately, enzymatic procedures are not really applicable on an industrial scale due to low efficiency, long time reaction and low yield.

Tan et al. [62] recently reported a new treatment for chitin deacetylation. This method is based on steam explosion. The steam applied to the biomass is converted to thermomechanical force under high pressure, which destroys the chitin. The intermolecular interactions of molecules are broken by steam explosion which leads to the formation of free polymer chains. The authors report 42.9% and 43.7% deacetylation from α– and β–chitin, respectively.

Because DDA influences the chitosan properties, such as solubility, its determination is indispensable. DDA determination could be achieved by different methods, such as Fourier transform infrared spectroscopy (FTIR), ^{1}H–NMR, UV spectrophotometric analysis, potentiometric titration, acid–base titration, elemental analysis, capillary zone electrophoresis method and Raman spectroscopy [63–65].

FTIR is one of the most used techniques for DDA determination. This method uses the peak representing the amide group and a reference peak that represents d–glucosamine and N–acetyl–d–glucosamine. Usually, the peaks at 1652 cm^{-1} (amide I) and 3450 cm^{-1} (hydroxyl groups) are the most used for DDA determination. Then, by using Eq. 1, DDA could be easy determined [59,66].

$$DDA\ \% = 100 - \frac{A_{1652}}{A_{3450}} * 115 \quad (1)$$

Where A_{1652} refers to the peak absorbance at 1652 cm^{-1} and A_{3450} to the peak absorbance at 3450 cm^{-1}. With equation 1 it is understandable that the lower the peak of amide I (1652 cm^{-1}), the higher the DDA will be.

DDA determination by FTIR could also be done using different peaks, as reported by Tahtat et al. [67] and Baxter et al. [68]. However, the bands at 1652 cm^{-1} and 3450 cm^{-1} are the most used. DDA determination by FTIR has the advantage of being a cheap and easy technique to use. However, this determination shows some disadvantages which should be considered. One of the main issues is that even a small variation of the peak intensity due to humidity or baseline, for example, dramatically affect DDA determination. Therefore, FTIR is used only for an approximate estimation of DDA value.

Nowadays, ^{1}H–NMR spectroscopy is considered the more accurate method for DDA determination. However, this method shows some disadvantages, such as the cost of the analysis and chemicals.

An additional method that could be used for DDA determination is UV spectrophotometric analysis. This method uses the absorbance at 199–203 nm (N–acetyl glucosamine), which is not uninfluenced by solvents [65]. The UV method is easy and fast to use but is less accurate when compared with other determination methods.

Potentiometric titration methods are reported to be the best choice after the NMR method for DDA determination. Potentiometric titration methods could be divided into pH–titration, two–abrupt–change titration and linear titration [69]. However, all of these procedures show some limitations. pH–titration and linear potentiometric titration methods are limited due to acidic or alkali impurities, which can affect the results. In contrast, two–abrupt–change potentiometric titration shows better results than the previous two. However, chitosan flocculation (at basic pH) can negatively influence the results. Another well–known procedure for DDA calculation is elemental analysis. In this method, DDA can be determined based on C/N ratio [70]. Raman spectroscopy can also be used for DDA determination. This method is a valid alternative to FTIR determination. Raman determination does not require purification or dissolution of the samples, making the determination process easier [71].

DA and DDA are not the only critical parameters for chitosan behaviour, as molecular weight (MW) is a crucial parameter that can influence outcomes, including chitosan bioactivity [58]. Chitosan bioactivity is usually reported to be stronger if the molecular weight is lower than 20 kDa while bioactivity is reduced when the molecular weight is more than 120 kDa [72].

Chitosan is known to possess antibacterial and fungistatic properties [73], yet the precise mechanism of action is not yet fully understood. One of the most accepted mechanisms is that the interaction of a negatively charged bacterial cell wall with chitosan causes cell disruption by modifying cell permeability. This process results in DNA replication inhibition resulting in cell death [74]. However, Divya et al. [75] report another possible mechanism. In this case, the antibacterial properties of chitosan are due to the chelation of the metal by chitosan which could inhibit the

growth of bacteria. Chitosan, under acidic conditions, is able to chelate several metal ions, such as Ni^{2+}, Zn^{2+}, Co^{2+}, Fe^{2+}, Mg^{2+} and Cu^{2+}, which are essential for cell wall stability [73,76,77].

Additional factors could influence the chitosan antibacterial properties, such as positive charge density, molecular weight, and pH.

Several works affirm the importance of chitosan polycationic structure for antibacterial activity. A higher positive charge density leads to strong electrostatic interaction. The positive charge density is influenced by DDA or by substitution degree (DS) as well [78]. Kong et al. [79] report that chitosan microspheres with DDA of 97.5% have a stronger effect against *S. aureus* compared with chitosan microspheres with DDA of 83.7% at pH of 5.5. Another study by Takahashia et al. [80] arrives at the same conclusions. They used chitosan membranes to inhibit the growth of *S. aureus*, with the best results being reached by membranes with higher DDA.

As previously mentioned, DS can also affect the chitosan antibacterial activity. In chitosan derivatives, antibacterial activity is related primarily to the DS of the grafting groups. Yang et al. [81] investigated the antibacterial activity of the N–alkylated disaccharide chitosan derivatives against *E. Coli* and *S. Aureus*. The research team found that both the DS and the disaccharide type influence the antibacterial activity of the chitosan derivatives. Overall, at a pH of 6, chitosan shows better antibacterial activity. Meanwhile, increasing the pH to 7 results in the chitosan derivates working better against both microorganisms.

Another important parameter for chitosan antibacterial properties is MW. Herein the contradictory results could be found. Some studies report that by increasing chitosan MW, the antibacterial activity is reduced against *E. coli*. At the same time, others report that high–MW increases antibacterial properties compared to low–MW [78]. Furthermore, Tikhonov et al. [82] report that chitosan with different MW has the same effect against *E. coli* and *Bacillus subtilis*. Other contradictory results were reported [83] in a study of chitosan with an MW of 9.3 kDa, which resulted in inhibited *E. coli* growth, while chitosan with an MW of 2.2 kDa seemed to promote bacterial growth.

The antimicrobial activity of chitosan also depends on the pH [78]. Under acidic conditions, chitosan is protonated and can easily interact with the cell surface due to the presence of negative charges [81,84]. As mentioned, one of the hypotheses states that the antimicrobial activity of

chitosan against microorganisms, such as bacteria and fungi, is due to polycationic nature of this biopolymer [78,85,86]. However, antimicrobial activity is conditional on poor solubility close to neutral conditions. This happens because, at a pH of 6.5, chitosan loses its cationic character [84,85]. However, contradictory results can be found in the literature [78,81].

Chitosan use

Currently, chitosan is one of the most studied and used biopolymers. Chitosan, due to its properties, can be employed with success in several fields [87–89]. For instance, it is often used as a reducing and capping agent for the synthesis of metal nanoparticles [90–92], enhancing the nanomaterial stability and performance. In addition, several studies reported its use for synthetic bones [93] and skin [94], for the synthesis of bioplastics [95] and in the cosmetics industry [96]. Moreover, chitosan is often coupled with other molecules in order to obtain polymeric conjugates [97].

Use of chitosan in nanomaterial synthesis

The synthesis of TMNPs by reducing metal salts using chitosan is extensively reported, because it not only works as an excellent green reducing agent but can also coat the nanoparticles' surface thus stabilizing them. Even more importantly, it can improve the catalytic performance of TMNPs [98]. These nanoparticles usually show enhanced properties and are safer. Among the most studied metals for catalytic application are noble metals and iron.

The interest of the scientific community in gold nanoparticles and its green production is due to the versatility of these nanoparticles. Gold nanoparticles can be used in various fields, such as catalysis and medicine. However, nanoparticle synthesis often uses chemicals that are hazardous for the environment and human lives. Then, in this context, avoiding the use or at least minimizing use of toxic chemicals in the synthesis procedure is one of the main topics in environmental science.

In 2003, Esumi et al. [98] synthesised gold nanoparticles coated by chitosan *via* the reduction of $HAuCl_4$ by sodium borohydride. The particle size was found to be affected by chitosan concentration and ranged between 6 and 16 nm. The authors reported that nanoparticles were formed by the adsorption of chitosan into gold nanoparticles. These nanoparticles were used as a

catalyst for the elimination of hydroxyl radicals. In 2005, Huang et al. [99] reported a nanocomposite film Cs–Au. The gold nanoparticles show peculiar structures and by varying the chitosan concentration, they obtained branched–like structures and cross–linked needle–like structures. Huang and Yang [90], in 2004, were the first to use chitosan as a reducing/capping agent for the synthesis and stabilisation of gold nanoparticles. The authors demonstrated that by using different chitosan MW and different chitosan concentration, it is possible to tune the size and shape of gold nanoparticles. More recently, other authors worked with chitosan and gold nanoparticles [100] and they stated that by controlling the nucleation and growth phases, gold nanoparticles obtained a uniform size and shape. Sun et al. [101] used different chitosan with different MW and DDA for the synthesis of gold nanoparticles. They report that by varying synthesis conditions, such as temperature, time, and gold precursor concentration, different sizes and shapes of chitosan MW and chitosan DDA were obtained. Additionally, chitosan was successfully used for the production of bimetallic gold nanoparticles, such as Fe_3O_4/Au nanoparticles [102].

Among the noble metals, silver is widely used in nanotechnologies due to its particular physical and chemical characteristics. Thanks to silver's properties, these nanoparticles are used in different fields, such as industry, domesticity and healthcare. Recently, silver nanoparticles have been used in textiles, biomedical devices and keyboards [103].

As with gold, the synthesis of greener silver nanoparticles is also considered a hot topic. Therefore, it is not surprising that several green ways for the production of silver nanoparticles are reported in the literature. Many authors have reported the synthesis of silver nanoparticles using chitosan as a reducing/capping agent furthering investigations of different aspects of this synthesis and uses of these nanoparticles in different applications.

In 2008, Two et al. [104] were the first to demonstrate the possibility of using chitosan as reducing/capping agent for silver nanoparticle production. Ever since, researchers have deeply investigated different aspects and uses of silver nanoparticles capped by chitosan. For instance, Kalaivani et al. [105] reported the synthesis of silver nanoparticles where chitosan acts as reducing and capping agent. In this study, where the produced nanoparticles show high antibacterial and antifungal activity, the authors suggest that the nanoparticles thus produced could be used in

various medical applications. Also, Wei et al. [106] investigated the possibility of using chitosan for the production of silver nanoparticles. The nanoparticles produced strongly bonded with chitosan. The developed material was used by the authors for the catalytic reduction of 4–NP. Several other reports are present in literature about chitosan and silver nanoparticles that were used in different fields of application, such as pressure sensors [107].

Platinum nanoparticles are considered effective catalysts, e.g., in hydrogenation processes. Therefore, their widespread use in catalysis is not surprising. Platinum nanoparticles are used as well in other applications, such as dye degradation, antibacterial and antifungal applications, sensing, anticancer and antioxidant applications [108]. As for the above–mentioned nanoparticles, intensive work was carried out by several research groups to investigate a different aspect of Cs–platinum nanoparticles. Deng et al. [109] investigated the possibility of using chitosan for stabilizing platinum nanoparticles. They report the superiority of chitosan as a capping agent for the synthesis of catalytic platinum nanoparticles. Results clearly show the excellent stabilisation of these nanoparticles and the enhancement of oxidase–like activity of platinum nanoparticles thus synthesised. Meanwhile, Liu et al. [110] used a different synthesis method for chitosan–platinum nanoparticles. They developed a new gas–liquid method for the nanoparticles' synthesis and used the obtained nanoparticles for hydrogen peroxide detection. Nguyen et al. [111] report about the synthesis of platinum nanoparticles by γ–ray irradiation where chitosan was used as a stabilizing agent. The nanoparticles obtained, depending on the conditions used, showed a narrow size distribution of 1.4–1.6 nm.

Chen and co–workers [112] reported on chitosan–supported palladium nanoparticles for hydrolytic dehydrogenation of ammonia borane. The Pd nanoparticles thus produced showed a size in the range of 4–8 nm. Gao et al. [113] investigated the Pd NPs synthesis of encapsulated N–doped carbon nanofibers derivatised from chitosan. They report that the nanofibers produced at 800 °C showed the highest catalytic activity. In environmental applications, one of the most widely used materials is iron in its zero valent form. Therefore, it not surprising that there is a large amount of work reported in literature.

Ferreira et al. [114] synthesised chitosan/Fe^0/Fe_2O_3 and used as an H_2O_2 activator for the removal of a dye. Meanwhile, Caetano et al. [115] reported on chitosan stabilizing nanostructured

iron oxides for the catalytic removal of methylene blue. In addition, Maleki et al. [116] studied Fe_3O_4 NPs supported by chitosan for the catalytic synthesis of 1,2–disubstituted benzimidazole and 1,5–benzodiazepine and derivatives. While, Raji et al. [117] reported on chitosan–coated activated carbon supporting zero valent iron nanoparticles (nZVI) for the treatment of melanoidin wastewater by a heterogeneous Fenton reaction.

Chitosan modification

Polymer conjugates have been successfully used in many applications where their properties have been widely exploited (e.g., in material science, wastewater treatment, drug delivery systems and the synthesis and stabilisation of nanoparticles).

The polymer conjugates or electrolytic complexes with chitosan are feasible because under acidic conditions the chitosan has a positive charge and inter alia, the positive charge can generate conjugates with polymers that have negative charge.

Chitosan shows three main types of functional groups [118], hydroxyl groups (primary in C–2, C–3 and secondary in C–6 positions) and an amino/acetamido group. However, the amino group is considered to be the most important. It is because, by the protonation of the amino group in an acidic medium, chitosan becomes soluble. Consequently, chitosan received broad interest especially for its ability to form a polyelectrolyte complex with molecules that show a positive charge [119]. Furthermore, chitosan shows fascinating physio–chemical properties (non–toxic, biodegradable and biocompatible) which make this polymer interesting for several applications. Unfortunately, chitosan has some limitations, such as insolubility in neutral and alkali pHs.

The chitosan modification due to the presence of amino and hydroxyl functional groups is relatively easy compared with other polymers [120]. One of the most popular modifications is the grafting of hydrophilic functional groups to its backbone to obtain water soluble derivatives of chitosan. For example, carboxymethyl–chitosan is one of the most studied water soluble derivates of chitosan [121,122]. This derivative of chitosan, compared to chitosan, possesses many superior functional properties [121]. Another example of a chitosan derivative is phosphonic chitosan which shows a better metal–chelating ability [123].

Chitosan chemical modification by grafting functional groups is only one of the ways of modifying chitosan. Chitosan conjugates, which are formed by chitosan and another bio–molecule,

have attracted much attention in recent years. Thiolated chitosan is one example of these modifications [124]. The synthesis takes place by binding thiolactic acid to the amino group of chitosan. Thiolated chitosan demonstrated excellent solubility in water and enhanced mucoadhesive properties [125]. Chitosan–based conjugates become a new class of biomaterials with promising potential in several scientific fields (Table 2).

Table 2 Chitosan modification proposed in literature

Substance	Synthesis	Annotations	Application	Ref.
Chitosan and Caffeic acid	Chitosans of different molecular weight were dissolved in acetic acid (1% w/w), then caffeic acid and consequently carbodiimide hydrochloride were added to the solution.	The activity of caffeic acid–chitosan is strongly dependent on the phenolic group	Antioxidant	[126]
Chitosan and Lignin	Film was produced by solvent casting method. Chitosan was dissolved in lactic acid solution (1% w/w, 24 h, 20 °C) while lignin was dissolved in ethanol (24 h, 20 °C). Chitosan and lignin solution were mixed (24 h at 20 °C), then Chitosan–Lignin solution was dyed (24 h, 25 °C, relative humidity 40 %)	The structure of the film is weakened due to the presence of lignin (week interaction between chitosan and lignin and aggregates formation.) Lignin adds scavenging properties to the film (highest result achieved with 20% of lignin).	Antioxidant	[127]
Chitosan and Lignin	Lignin was dissolved in water (48 h, room temperature) then, acetic acid and chitosan were added to lignin solution and stirred (24 h, 20 °C). The Chitosan–Lignin solution was dried in air (Room temperature).	The introduction of lignin shows changes in the morphology of the film's surface. Cell proliferation was facilitated by the film's characteristics (porosity and texture).	Tissue engineering	[128]
Chitosan and Gelatin	The gelatin solution (300 mg/L) was dissolved by heating and then allowed to react with genipin (150 mg/L) for 24 h. Then, the gelatin–genipin solution was added to the chitosan–genipin acid solution (chitosan 300 mg/L, 0.1 M acetic), genipin 150 mg/L) and kept at room temperature.	Chitosan and gelatin were bound by covalent bond to genipin. Chitosan–genipin interaction could be due to nucleophilic ring–opening reaction.	Bio–medical	[129]
Chitosan and Quercetin	Quercetin (150 mg) was dissolved in NaOH (15 mL, 0.33 M), subsequently, H_2O_2 (1 mL, 3.5 %) was added to the solution (2 h, dark). After that, chitosan solution (20 mL, 25 g/L, acetic acid 1%) was added to the solution and stirred for 24 h.	Chitosan is grafted onto quercetin with a functionalisation degree of 0.275 g/g (gram of quercetin / gram of conjugate)	Bio–medical	[130]
Chitosan and quantum–dots	N,N,N–trimethyl–chitosan, was prepared by dissolving chitosan (1 g) in N–methyl–2–pyrrolidone (40 mL) and NaOH (5.5 mL, 20%). Methyl iodide (8 mL) and sodium iodide (2.4 g) were added to the solution.	N,N,N–trimethyl–chitosan shows remarkable effectiveness for the nucleation and stabilisation of CdS–NPs in aqueous solution	Bio–sensor	[131]

	N,N,N–trimethyl–chitosan was produced after 48 h at room temperature.			
Chitosan–Polyhydroxybutyrate	Chitosan solution (26–32 mM, acetic acid–DMSO, 150 mL, 1:14) was add to PHB solution (31–52 mM, DMSO or methylene chloride–DMSO (150 mL, 1:1.5). The mixture was stirred (1–5 days) and then the conjugate was precipitated by acetone	First report of PHB–Chitosan conjugation.	Not mentioned	[132]

Polyhydroxyalkanoates

Polyhydroxyalkanoates (PHA) are natural polyesters produced from renewable resources by several microorganisms [133]. PHA are considered to be biodegradable in nature and this class of substances is also attracting interest as a replacement for petrochemical–based polymers. However, the high production costs limit their use [134].

Because they are considered sustainable and environmentally friendly, PHA are a potential alternative to petrochemical–based plastics [135]. These polymers have several desirable physical properties due to the monomeric units present in the polymer [134,136]. As mentioned above, they are synthesised from sustainable sources and considered environmental friendly unlike synthetic polymers [137]. Additionally, these polymers are biodegradable, making them favourable for use in the chemical and materials industry. For instance, polylactic acid and polybutylene succinate can be used instead of polypropylene and low–density polyethylene as reported previously by Kourmentza et al. [138] PHA applications include drug delivery [139], agricultural fields [140] and tissue engineering [141].

Generally, PHA is produced under certain limited growth conditions, such as the absence of nutrients [142,143]. In this condition, the carbon is diverted towards PHA accumulation. Overall, PHA production can be divided into two steps. In the first one, microorganisms are cultivated until a high cell density culture is obtained. Meanwhile, in the second step, the microorganisms are subjected to a limitation of vital nutrients and an excess of carbon [134]. The unbalanced conditions cause the production and accumulation of PHA in the cells [144]. However, to become commercially attractive, the cost of production needs to be reduced. Nowadays, the main cost is related to the carbon source which corresponds to 40% of the total PHA production [134]. Therefore, in the last decades, several alternatives for PHA production were proposed, such as using different carbon sources (e.g. whey [135], glycerol [145], starch [146] and waste materials

[147]). Other modifications in the PHA synthesis are regarding the use of mixed microbial cultures mainly to reduce the manufacturing cost. In addition, volatile fatty acids have been used as a carbon source for PHA production [148]. The methods reported by Rowaihi et al. [149] are interesting, as PHB is produced by carbon dioxide in a two–step submerged fermentation process.

Polyhydroxybutyrate

At the beginning of the last century, the presence of sudanophilic, lipid–like inclusions in *Azotobacter chroococcum* was observed [150]. Lemoigne was the first to identify this substance as PHB [151]. In a short time, enough information was collected to demonstrate that PHB was used as an intracellular reserve for carbon. PHB is a short–chain–length polymer that shows various properties comparable to polypropylene. In addition, it is easily degraded in aerobic or anaerobic conditions to water and carbon dioxide or methane respectively by microorganisms in sewage, sea, soil, and lake water [152]. PHB has high melting point [153] and shows high crystallinity degree [154], with the crystallinity influencing both physical and mechanical properties (e.g., higher crystallinity affects brittleness). One of the main PHB disadvantages is its thermal instability which influences viscosity and molar mass. In order to address this drawback, PHB properties can be modified by bonding with other polymers or even by adding plasticisers or lubricants. For instance, poly(hydroxybutyrate–valerate) (PHBV), which is produced under certain conditions from bacteria, results in tougher and less stiff PHB.

Several microorganisms are known to be able to accumulate PHB as intracellular storage of carbon sources used as sources of energy. For example, *Ralstonia eutropha* is able to store up to 80% of PHB (the cell dry weight) using different carbon sources, such as carbon dioxide waste, animal waste and methanol [155]. However, limitations for bulk PHB production are related to the high–cost production of synthesis and recovery.

Polyhydroxybutyrate application

PHB has attracted increasing interest over the years. Its applications are numerous (Fig. 3). For example, it has been used in food packaging when coupled with ZnO [156], as well as in antimicrobial applications, such as in PHB–Silver nanoparticle nanocomposites [157,158]. Several studies are using PHB to develop drug carriers [159], bioplastics [160] and bone tissue [161]. In addition, it was successfully used in skin tissue engineering, food packaging [162], agriculture [163]

and for the stabilisation of nanomaterials [164]. Furthermore, PHB is often used to obtain polymeric conjugates. However, in the following section, the use of PHB in synthesis and/or stabilisation of various metal nanoparticles will be considered, while PHB modification will be discussed separately.

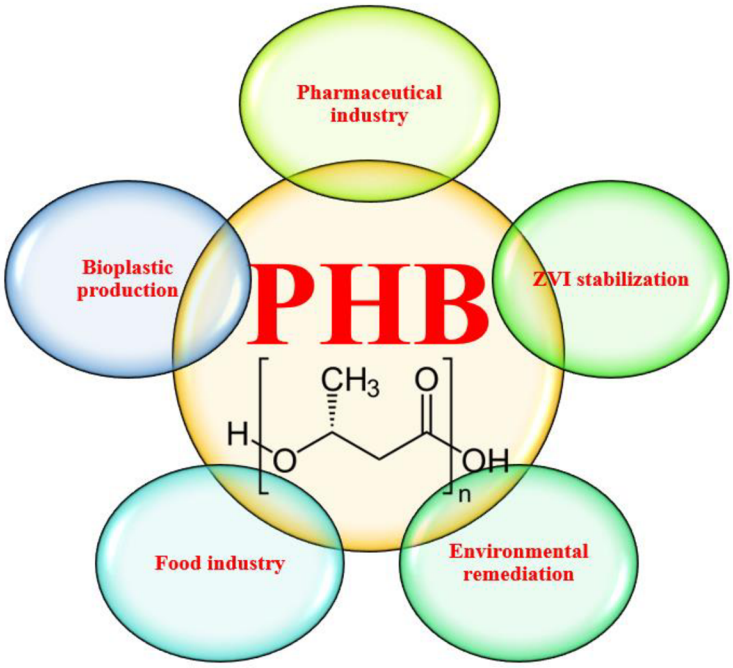

Fig. 3 Main uses of PHB.

Use of polyhydroxybutyrate in nanomaterial synthesis

Several times, PHB has been reported to be a suitable material for metal nanocomposites. Yalcin et al. [159] reported the synthesis and characterisation of PHB–coated magnetic nanoparticles. The authors demonstrated that iron oxide coated by PHB could be used in drug delivery, such as in chemotherapeutics. The authors followed the coprecipitation synthesis procedure in which iron salts were dissolved in the presence of PHB. However, due to the hydrophobicity of the polymer, dichloromethane was used as a solvent, which is toxic to humans and the environment. Additionally, Sruthi et al. [165] reported on the use of PHB coupled with iron oxide nanoparticles. In this work, authors used PHB to encapsulate drug and nanoparticle composites in a core–shell structure. The authors report that these nanoparticles were able to release drugs for more than

165 min. In addition, antimicrobial activity was noted against *Candida albicans* and *Pseudomonas aeruginosa*. Other authors have investigated the use of PHB with other nanomaterials. D'Amico et al. [166] obtained superparamagnetic nanocomposites using iron oxide and PHB. Authors showed that the nanocomposite has a homogeneous optical structure. Furthermore, Castro–Mayorga et al. [158] reported on PHB–AgNP's nanocomposite film synthesis and its use in antimicrobial applications. Authors tested this material against two common food–borne pathogens, *Listeria monocytogenes* and *Salmonella enterica*. They found strong antimicrobial activity in the film and that it bio–disintegrated in 40 days. Meanwhile, Jayakumar et al. [157] have biologically synthesised a PHB–silver nanocomposite using a by–product from cheese whey. The nanocomposite was synthesised *via* one–pot methods and was found to be stable and hydrophobic. Authors report that the nanocomposite shows antibacterial properties against *E. coli* and *Pseudomonas spp*. In addition, Yadav et al. [167] were able to encapsulate gold nanoparticles *via* the coffee ring approach in the PHB matrix. For this purpose, authors used an ink jet printing technique. Díez–Pascual et al. [156] reported about bionanocomposites PHB/ZnO produced *via* a solution casting technique. PHB/ZnO exhibit reduced water uptake and better vapour and gas barrier properties when compared to PHB. Meanwhile, Riaz et al. [168] used PHB to incorporate zinc sulfide nanoparticles in a matrix. The nanomaterials incorporated in the PHB matrix improved the heat resistant properties of the material. The authors reported strong compatibility between PHB and zinc sulfide nanoparticles. Instead, Díez–Pascual [169] used poly(3–hydroxybutyrate–co–3–hydroxyhexanoate), a copolymer of PHB, to incorporate zinc oxide nanoparticles in its net. This nanocomposite was tested for food packaging application. Authors report that material with a 5.0 wt% of nanoparticles could be used instead of synthetic plastics for food and beverage containers. Furthermore, PHB was used by Pope et al. [170] in sensor field. They developed a rGO–PHB composite suitable for biocompatible actuators, biodegradable circuits and wearable sensors. Similarly, Sridhar et al. [171] used PHB to develop a graphene–poly(3–hydroxybutyrate–co–4–hydroxybutyrate) nanocomposite. This material exhibits greater thermal properties due to the presence of graphene. In addition, it was demonstrated that the presence of graphene doesn't interfere with biodegradation. In a recent study, Damasco et al. [172] reported the use of PHB to coat Bismuth nanoparticles and enhance their properties. In this case, nanoparticles were used as

radiopacifiers. PHB has been successfully used in environmental applications as well. Wacławek et al. [164] used PHB for enhancing the stability and reactivity of zero valent iron nanoparticles. The nanoparticles produced show better removal of organic and inorganic compounds, such as perchloroethene and chromium(VI).

Polyhydroxybutyrate modification

Although PHB shows excellent characteristics in several fields, the development of PHB–based biomaterials to improve characteristics, such as stability, mechanical properties and solubility, is one of the main fields related to PHB with several articles published on the topic [173–175]. To modify PHB, several approaches have been proposed, such as blending, copolymerisation and other methods [176].

Biocomposite films were developed using different natural products. Cao et al. [177] reported the production of PHB–chitosan film by mixing both polymers in chloroform (2% v/v) and acetic acid (1% v/v), respectively. The formed emulsion was dried to obtain a film. PHB spherulites were detected in the chitosan polymeric matrix by scanning electron microscopy (SEM). Authors indicate that PHB–chitosan material could have applications in tissue engineering. Recently, Lugoloobi et al. [178] reported the production of PHB–lignin nanocomposites. In this work, lignin nanoparticles were dispersed in a PHB matrix *via* an oil–in–water Pickering emulsion technique. Authors investigated several properties of this composite, concluding that lignin is an efficient nucleating agent, thus increasing the PHB crystallisation rate. In addition, the blends showed higher melt viscosity, higher glass transition temperature and improved UV resistance.

Yeo et al. [179] reported on biopolymers based on poly(lactic acid) and poly(hydroxybutyrate) – rubber copolymer (PLA/PHB–rubber). These materials exhibit good flexibility properties. Authors report an elongation at a break of 73% and Tg of around 30 °C. Due to these characteristics, PLA/PHB–rubber could be used in biomedical applications.

Among various PHB–copolymers poly(3–hydroxybutyrate–co–3–hydroxyvalerate) (PHBV) is one of the most studied and used [180]. Synthesis can be achieved *via* synthetic procedures [180] or by bacterial fermentation [181]. The applications of PHBV are numerous, such as biomedical [182] and packaging applications [183]. For instance, Xia et al. [184] report the use of PHBV as drug delivery for icariin. Under the studied conditions, the proliferation of osteoblast–like cells (MG–63)

and pre–osteoblasts (MC3T3–E1) were enhanced. Authors envision its use in the industrial manufacturing of tissue engineering. In contrast, Meereboer et al. [185] report the use of PHBV combined with cellulose acetate for applications in food packaging. PHB modification are reported in Table 3.

Table 3 modification proposed in literature

Polymers	Material type	Synthesis	Sustainability	Annotations	Application	Ref.
PHB and Glycerol	Film	Film was obtained by thermo–compression method using a hydraulic press at 190 °C and 5 kg cm^{-2}, for 15 min.	Increased water vapor permeability, Decreased barrier property	The effect of different glycerol–based additives on PHB films was investigated	Not reported	[186]
PHB and Epoxidised natural rubber (ENR–50)	Film	Solvent–casting methods [1% (w/w) solution of PHB/ENR–50 in chloroform], Evaporation (24 h at room temperature, dried under vacuum (48 h at 40 °C)	Use of toxic solvent such as chloroform	Melt reaction in PHB/ENR–50 blends occur during isothermal annealing (temperature range 184 to 199°C). The heat of reaction increases as the PHB and ENR–50 content increases	Not reported	[187]
PHB, Chitin and Chitosan	Film	Films were produced by solution–cast method, using Hexafluoro–2–propanol as solvent. PHB, chitin and chitosan were dissolved separately. Once obtained, homogenised solution chitin and chitosan were mixed with PHB solution. Therefore, solutions were kept at room temperature for 10 days and finally dried at 60 °C for 5 days under vacuum.	Use of toxic solvent such a Hexafluoro–2–propanol. Biodegradable polymer blend	The degree of crystallinity of PHB decreased upon blending with polysaccharides. PHB blends with chitosan show significant suppression of PHB crystallisation.	Not reported	[188]
PHB and Soda lignin	Pellets	Lignin and PHB were mixed by Haake minilab twin screw. The temperature was kept at 175 °C for 2 min.	High temperature required, 100 °C for 12 h, 175 °C for 2 min.	Soda lignin improve the PHB overall thermal stability. Intermolecular interactions between soda lignin and PHB were favoured at concentration of 40% of lignin.	Not reported	[189]

PHB and starch	Film	PHB and starch were mixed with hot chloroform and film was produced by solvent–casting method.	Use of toxic solvent, such as chloroform	Films had a single glass transition temperature for all the proportions of PHB:starch tested. The PHB:starch ratio 0.7:0.3, was found to be optimal to enhance the tensile strength.	Bioplastic	[190]
PHB and Polylactic acid	Sheets	PLA and PHB were mixed in a Haake polylab torque rheometer (175 °C 10 min). Then, the material was hot–pressed (180 °C)	Required 20-ton lab press and high temperature	PLA can improve the mechanical properties of PHB. The blend shows improved tensile properties (compared to PLA). The biodegradability of blends correlated this PHB content.	Not reported	[191]
PHB, Polylactic acid and Oligomeric lactic acid	Fibres	The solutions for electrospinning were prepared in a mixture of solvents (chloroform and N,N–dimethyl–formamide ratio 80:20) at 80 °C for 2 h.	Biodegradable fibres. Use of toxic solvents, such as chloroform and N,N–dimethyl–formamide	Oligomeric lactic acid at concentration of 15 wt% and 20 wt% affect the interaction between PLA and PHB by forming uniform crystals.	Agricultural	
PHB and Cellulose nanocrystals	Film	PHB was dissolved in Dimethylformamide at 116°C, and mixed with cellulose nanocrystal solution (2, 4 and 6wt% in Dimethylformamide). Then the mixed solution was kept at 80°C for 12h.	Use of toxic solvent, such as Dimethylformamide	By increasing cellulose nanocrystals concentration, tensile strength and Young's modulus are enhanced. The film showed reduced water vapor permeation compared to pure PHB. Improved UV barrier properties.	Packaging	[192]
PHB and Wood waste fibres	Film	PHB–Wood waste fibres composite was obtained using a Brabender LabStation (165 °C, 8 min). Then the film was obtained using a two–roll mill (130 °C).	Use of a hot press (175 °C, 10 MPa)	The composite showed improved thermal stability, higher crystallinity and a shift in the glass transition to higher temperatures	Not reported	[193]
PHB and Chitin nanocrystals	Film	PHB/Chitin nanocrystals composite was obtained by mixing PHB and Chitin nanocrystals in chloroform (60 °C). The sample was vacuum dried.	Use of toxic solvent, such as chloroform	Pristine chitin nanocrystals was found to be a good nucleation agent for the crystallization of PHB.	Not reported	[194]

PHB and n–hydroxyethyl acrylamide	Scaffolds	Test was performed under vacuum, 0.35 g of PHB were mixed in 2.5 mL of and n–hydroxyethyl acrylamide and dissolved in a solvent. The sample was irradiated by gamma–ray (1.5 kGy/h)	Use of solvent and gamma–ray source (^{60}Co)	High fibroblasts adhesion and survival was promoted by amine group	Medical	[195]
PHB and agave fibre	Sheets	The material was prepared using mixer Haake Rheomix (6 min at 180 °C). The blend was dried in oven (8 h at 60 °C)	Use of waste material (waste of tequila production)	PHB thermal property was not affected (fibre addition). While crystallinity and Tm were enhanced adding fibres	Not reported	[196]

Catalysis

Environmental catalysis plays a vital role in sustainable development through the creation of new catalysts with improved characteristics. By catalysis, it is possible to resolve several environmental problems (e.g., catalysts are used for pollutants degradation [197], carbon dioxide reduction [198] and hydrogen production [199]).

Overall, catalysis can be divided into two big groups named homogeneous and heterogeneous catalysis. As far as homogeneous catalysis is concerned, the catalysts are in the same phase as the reactant, usually in liquid form. Homogeneous catalysts are often soluble transition metal complexes that offer some advantages compared to heterogeneous catalysts (higher selectivity, and more mild reaction conditions). Heterogeneous catalysis involves the use of a solid metal oxide or metal catalyst, while the reactants are in the liquid or gaseous phase. Nowadays, heterogeneous catalysis covers around 80% of all chemicals, with a market size of $34 billion in 2019 with an expected growth of ~4% per year [200].

As the figure shows (Fig. 4), obtaining a new chemical compound (product) from the starting molecule's chemical reaction involves breaking the chemical bond and forming a new one. However, for chemical bond breaking and the formation of new ones to occur, the energy barrier would have to be overcome [200]. Because energy barriers determine the rate of reaction, the use of catalysts can reduce it and then boost the reaction with a faster formation of the product.

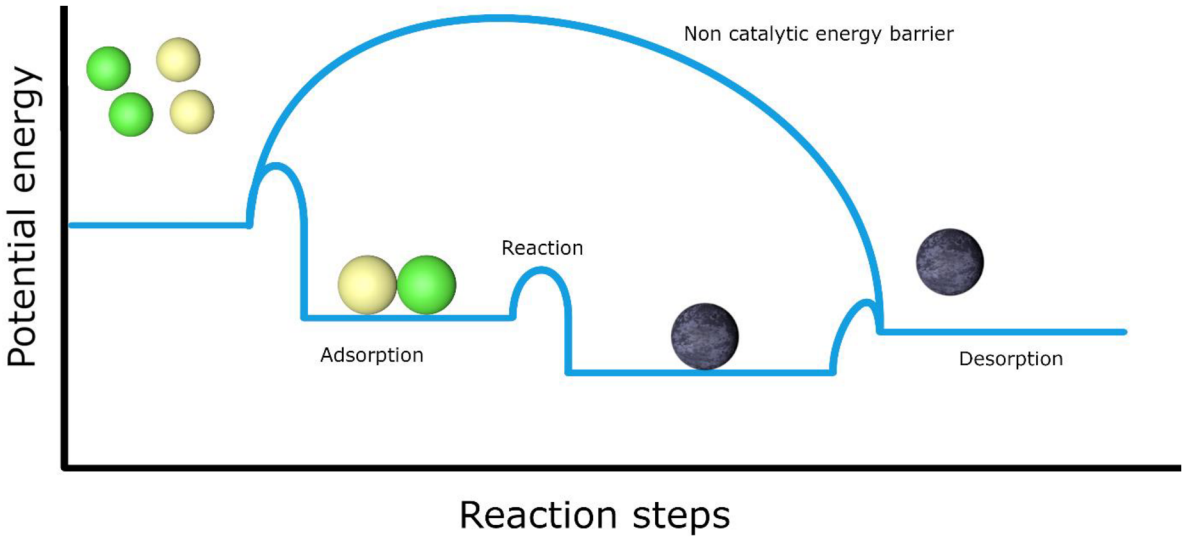

Fig. 4 Simplified representation of a catalytic reaction, with and without catalyst (based on [200]).

The heterogeneous catalytic application covers both reduction and oxidation processes. Several metal nanoparticles can be used in these processes, (e.g., noble metals are employed with great success in hydrogenation processes) [201]. In contrast, iron is often used for the activation of various oxidants, such as hydrogen peroxide (Fenton reaction) and persulfates used for the oxidation of pollutants in water [202]. Several reports in literature show the use of TMNPs as catalysts for the hydrogenation of various compounds, (e.g., gold, silver, platinum and palladium nanoparticles are often used for the catalytic hydrogenation of nitroarenes) [39,203–205].

To the best of my knowledge, Haruta et al. [206] in 1987 were the first to use gold nanoparticles as catalysts. Since then, gold nanoparticles were also considered superb catalysts at low temperatures. Gold nanoparticles are able to catalyse many chemical reactions, from which nitroarenes hydrogenation is one of the most popular [206]. The hydrogenation of one of the most known nitroarene - 4–NP, yields 4–aminophenol (4–AM). 4–AM is an important compound in many applications such as being used as a corrosion inhibitor, photographic developer and drying agent. Furthermore, 4–AM is an intermediate for acetaminophen synthesis [206]. The method frequently used for 4–NP conversion to 4–AM involves $NaBH_4$ as electron donor and TMNPs as a catalyst. However, TMNPs, in some cases, may not work as catalysts. Therefore, the functionalisation of the TMNPs' surface can greatly enhance the activity of the catalyst. The surface functionalisation of TMNPs can be done using several substances, such as enzymes, natural extracts and polymers. For

instance, polyethylene glycol (PEG) is a well know stabiliser of TMNPs. Seo and co–workers [207] used a double hydrophilic block copolymer (polyethylene oxide–block–polyacrylic acid) to enhance the catalytic performance of Au nanoparticles, reporting a turnover frequency of 800 h^{-1} through the hydrogenation of nitroarenes. In addition, Asharani et al. [208] investigated the use of PEG core dendrimer having hydroxyl groups for the production and catalytic use of silver nanoparticles.

Among the biopolymers, chitosan found wide applications in this field. In recent work, Zhu et al. [209] reported the use of chitosan as a reducing/stabilizing agent for the synthesis of gold nanoparticles with different shapes. These nanoparticles were used for the catalytic hydrogenation of 4–NP, showing enhanced properties.

As already mentioned, TMNPs can also be used for the activation of various oxidants, such as hydrogen peroxide [210] and persulfates [37] for the generation of free radicals. The radicals produced this way can be employed for the degradation of water contaminants like dyes and pharmaceuticals. In this scenario, several nanomaterials can be used; however, one of the most studied is nZVI. Indeed, in addition to its surface reactions, nZVI may be used as a slow–releasing supply of ferrous iron. Therefore, the impressive number of works related to nZVI + oxidant is not surprising, especially for the activation of persulfate (PDS). The main reactions involved in the formation of free radicals from PDS are reported in Eqs. (2–8).

$$4Fe^0 + S_2O_8^{2-} + 3O_2 + 12H^+ \rightarrow 4SO_4^{\bullet-} + 6H_2O + 4Fe^{3+} \quad (2)$$

$$Fe^0 + 2S_2O_8^{2-} \rightarrow 2SO_4^{2-} + 2SO_4^{\bullet-} + Fe^{2+} \quad (3)$$

$$Fe^0 + S_2O_8^{2-} \rightarrow Fe^{2+} + 2SO_4^{2-} \quad (4)$$

$$S_2O_8^{2-} + Fe^{2+} \rightarrow SO_4^{\bullet-} + SO_4^{2-} + Fe^{3+} \quad (5)$$

$$H_2O + SO_4^{\bullet-} \rightarrow {}^{\bullet}OH + SO_4^{2-} + H^+ \quad (6)$$

$$Fe^0 \rightarrow Fe^{2+} + 2e^- \quad (7)$$

$$Fe^{3+} + e^- \rightarrow Fe^{2+} \quad (8)$$

However, in this case, surface functionalisation also plays a key role in boosting the activation of, for example, PDS and getting more free radicals. For instance, Toshima [211] points out that proper stabilisation of TMNPs can enhance the catalytic activity and selectivity of the materials.

RESULTS AND DISCUSSION

During my PhD studies, I published a total of **25 articles** of which 3 reviews (in addition, 1 is under review and 5 more are in preparation). Furthermore, I was directly involved in the development of a new method for persulfate determination. This method has been **patented**. From the scientific papers, four were selected for this thesis. All published manuscripts not selected for this thesis are attached for informational purposes.

As mentioned above, polymers are widely used for the stabilisation and synthesis of nanoparticles. Chitosan and PHB are both non–soluble in water, therefore finding a solution to this problem could increase their use. In addition, authors reported enhanced properties of copolymers compared with homopolymers [212]. Furthermore, the development of a polymer conjugate with enhanced properties of each of its constituents could find applications in different fields [212].

Aforementioned, chitosan and PHB have water solubility deficiencies, which limit their use. Therefore, the first part of the work focused on the literature search to find possible ways to conjugate these polymers. From the literature search, it was found that a previous method was reported by Yalpani [132]. In this work, the research team was able to conjugate chitosan and PHB; however, the proposed method uses toxic solvents such as dichloromethane. Once Yalpani's work was found, my research focused on a greener version of this method that avoids use of toxic solvents. In order to reach this goal, several conditions were tested. Different ratios of chitosan to PHB were examined (4.16:1 to 1:1), as well as the influence of the type of acids and their concentration were tested (acetic acid, hydrochloric acid or nitric acid). In addition, the influence of time, temperature and ultrasounds were evaluated. It was found that under optimised conditions [pH 2.3, ratio 4.16:1 (chitosan:PHB), ultrasound 30 min at 80 °C], PHB formed a soluble conjugate with chitosan.

Chitosan–polyhydroxybutyrate conjugate (Cs–PHB) was characterised by several techniques, such as FTIR, ^{1}H NMR, ^{13}C NMR and gel permeation chromatography (GPC), which confirmed the successful conjugation process. Furthermore, a theoretical approach – density functional theory (DFT) model – verified our hypothesis on successful conjugation (Fig. 5). The DFT model shows the presence of C–H (~2930 cm^{-1}) on Cs–PHB spectra, which indicate the increased PHB content as was stated for experimentally obtained FTIR (increase in intensity of the stretching

C–H vibration band). Furthermore, the typical peak of PHB (ester group, 1720 cm^{-1}) was recorded in Cs–PHB spectra obtained by the DFT model (similarly to the experimentally obtained data).

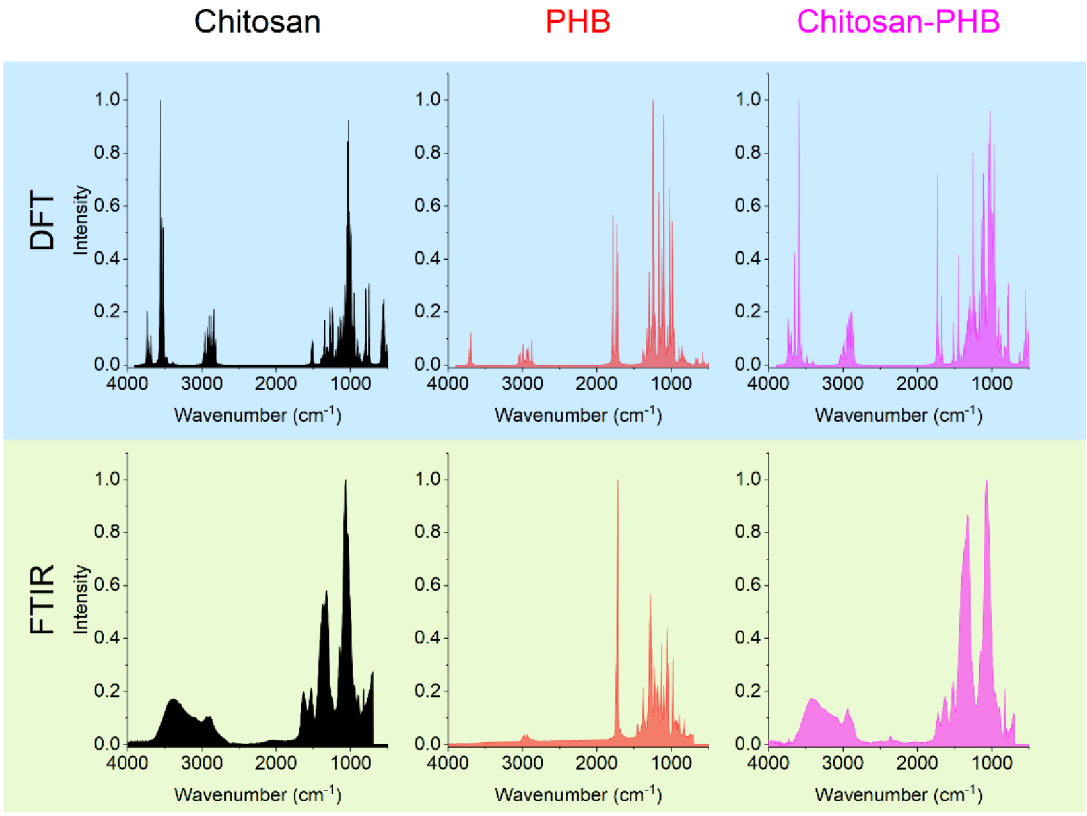

Fig. 5 Density functional theory (blue) and FTIR (green) of Chitosan, PHB and Cs–PHB conjugate. (DFT wavenumbers were shifted by –100 cm^{-1}). The structures/frequencies (example shown in Fig. 6) were examined (with ORCA software [213]) by DFT calculations at the B3LYP/def2SVP level. Data were elaborated by Multiwfn software [214].

The theoretical model is in good agreement with the experimental data and confirms that the amino groups of the chitosan reacted with the ester groups of the PHB forming the amide bond (Fig. 6).

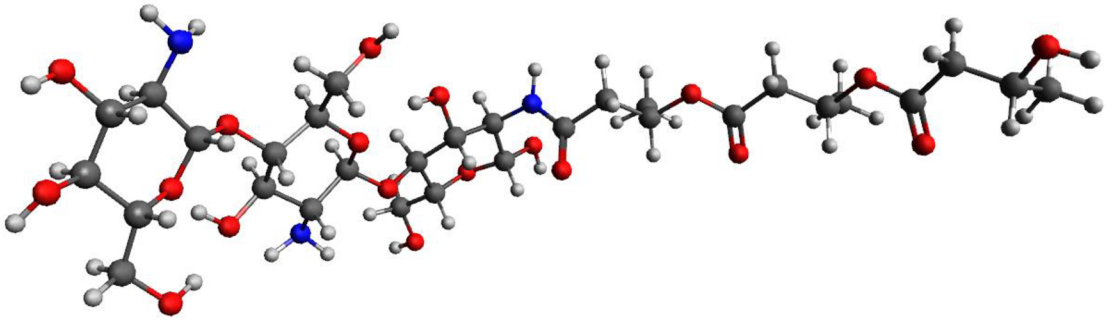

Fig. 6 Cs–PHB conjugate model (structure optimized with the ORCA software [213], at the B3LYP/def2SVP level). Represented are elements C (grey balls), O (red balls), N (blue balls), and H (white balls). The molecule was visualized with the Avogadro program [215].

Once the Cs–PHB conjugate was obtained, it was used for the greener synthesis of several TMNPs, such as gold, silver and bimetallic platinum–palladium. In addition, the bio–conjugate was used to stabilize nZVI.

The obtained nanoparticles were tested for catalytic nitroarene hydrogenation (gold, silver and bimetallic) and for PDS activation (nZVI).

A poly(3–hydroxybutyrate)–chitosan polymer conjugate for the synthesis of safer gold nanoparticles and their applications

Abstract: A facile and eco–friendly approach is developed for the synthesis of a poly(3–hydroxybutyrate)–chitosan (PHB–chit) polymer conjugate, which is an ideal material for the synthesis of safer gold nanoparticles (nAu). The synthesized products are characterized by various electron–based, optical and spectroscopic techniques including the catalytic activity and the stability/toxicity of nAu. In contrast to the conventional synthesis approaches, the use of PHB–chit results in generation of a highly stable and size–controlled nAu material that exhibits important catalytic activity towards the reduction of 4–nitrophenol (4–NP) to 4–aminophenol (4–AM), and at the same time shows no toxicity against living bacterial systems such as *Escherichia coli* or *Staphylococcus aureus*. The synthesis route reported herein would inspire future developments that circumvent toxicity issues of relevance to living systems while performing common catalytic experimentation.

Citation: Silvestri, D.; Wacławek, S.; Sobel, B.; Torres-Mendieta, R.; Novotný, V.; Nguyen, N.H.A.; Ševců, A.; Padil, V.V.T.; Müllerová, J.; Stuchlík, M.; et al. A poly(3-hydroxybutyrate)-chitosan polymer conjugate for the synthesis of safer gold nanoparticles and their applications. *Green Chem*. **2018**, 20, 4975–4982.

Impact Factor: **11** (2021), citations **29** (WOS 25.01.2023)

Green Chemistry

PAPER

View Article Online
View Journal | View Issue

Check for updates

Cite this: *Green Chem.*, 2018, **20**, 4975

A poly(3-hydroxybutyrate)–chitosan polymer conjugate for the synthesis of safer gold nanoparticles and their applications†

Daniele Silvestri,[a] Stanisław Wacławek, *[a] Bartłomiej Sobel,[b] Rafael Torres-Mendieta, [a] Vít Novotný,[a] Nhung H. A. Nguyen,[a] Alena Ševců, [a] Vinod V. T. Padil, [a] Jana Müllerová,[a] Martin Stuchlík,[a] Marco Petrangeli Papini,[c] Miroslav Černík*[a] and Rajender S. Varma *[d]

A facile and eco-friendly approach is developed for the synthesis of a poly(3-hydroxybutyrate)–chitosan (PHB–chit) polymer conjugate, which is an ideal material for the synthesis of safer gold nanoparticles (nAu). The synthesized products are characterized by various electron-based, optical and spectroscopic techniques including the catalytic activity and the stability/toxicity of nAu. In contrast to the conventional synthesis approaches, the use of PHB–chit results in generation of a highly stable and size-controlled nAu material that exhibits important catalytic activity towards the reduction of 4-nitrophenol (4-NP) to 4-aminophenol, and at the same time shows no toxicity against living bacterial systems such as *Escherichia coli* or *Staphylococcus aureus*. The synthesis route reported herein would inspire future developments that circumvent toxicity issues of relevance to living systems while performing common catalytic experimentation.

Received 7th August 2018,
Accepted 24th September 2018
DOI: 10.1039/c8gc02495b
rsc.li/greenchem

Polymers, the macro-molecules that are formed by concatenated sub-units, are present in many materials of daily use and it is not surprising that the development of new technologies is causing their continuous buildup. However, intensive research on the manufacturing of polymers should be accompanied by socially responsible development of clean and sustainable greener processes that should lead to the production of desirable materials devoid of environmentally detrimental effects.[1–3] In this context, two polymers have garnered the attention from the scientific society: chitosan and poly(3-hydroxybutyrate) (PHB).

Chitosan, a linear polymer of α(1 → 4)-linked 2-amino-2-deoxy-β-D-glucopyranose (Fig. 1a), is a naturally occurring abundant cationic polymer mainly extracted from shrimps, crawfish and crabs,[4] and besides being antimicrobial[5] and biocompatible,[6] it has shown a remarkable ability for the removal of chromium,[7] arsenic,[8] copper,[9] lead,[10] and oil from water,[11] including usage in drug delivery[12] and biomedical applications.[13] However, chitosan has a major solubility problem; it is soluble only under acidic pH conditions and not in a neutral/basic medium, thus restricting its use. Additionally, it can only be dissolved in specific organic acids including acetic, citric, formic, lactic, propionic and succinic acids, and in a few inorganic ones, *i.e.* hydrochloric, phosphoric and nitric acids.[14]

PHB, a member of the group of polyhydroxyalkanoates (Fig. 1b), formed as a carbon reserve in a wide variety of bacteria (prokaryotes and eukaryotes),[15] and under suitable growing conditions, can be sustainably extracted on a large scale from waste materials (*e.g.* waste activated sludge);[16–18] it exhibited outstanding potential for *in situ* bioremediation.[19–21] Likewise, due to its compatibility with the blood and tissues of mammals,[22] it has great potential to address current issues in the food packaging industry and pharmacology, micro-capsule manufacturing or in the synthesis of materials for cell and tablet packaging often deployed in therapy or drug delivery. For all the aforementioned applications, it is inevitable to solubilize PHB in water or other eco-friendly solvents. Unfortunately, PHB is completely insoluble

[a]*Institute for Nanomaterials, Advanced Technologies and Innovation, Technical University of Liberec, Studentská 1402/2, 461 17 Liberec, Czech Republic. E-mail: stanislaw.waclawek@tul.cz, miroslav.cernik@tul.cz; Tel: +420 485 353 006*
[b]*Institute of Engineering Materials and Biomaterials, Faculty of Mechanical Engineering, Silesian University of Technology, Konarskiego 18a St., 44-100 Gliwice, Poland*
[c]*Department of Chemistry, University of Rome "La Sapienza", Piazzale Aldo Moro 5, 00185 Rome, Italy.*
[d]*Regional Centre of Advanced Technologies and Materials, Faculty of Science, Palacký University in Olomouc, Šlechtitelů 27, 783 71 Olomouc, Czech Republic. E-mail: Varma.Rajender@epa.gov*
†Electronic supplementary information (ESI) available. See DOI: 10.1039/c8gc02495b

This journal is © The Royal Society of Chemistry 2018

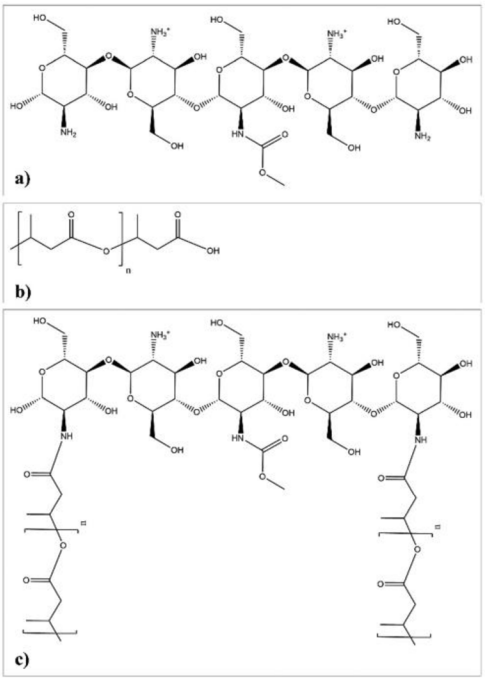

Fig. 1 Structure (in mildly acidic medium) of (a) chitosan, (b) poly(3-hydroxybutyrate) and (c) PHB–chit conjugate.

in water,[23] but soluble in several chlorinated organic solvents such as chloroform,[24,25] dichloromethane, and 1,2-dichloroethane, among others,[26] which are mostly toxic and not environmentally friendly.[27–29]

In the present work, the conjugation of both the polymers is envisioned which addresses both drawbacks at the same time, overlapping the different polymer properties and enabling its use as a non-toxic reducing/stabilizing agent for the synthesis of metal nanoparticles (NPs).

Polymer conjugates have been successfully used in many applications where their properties have been widely exploited, *e.g.* in materials science,[30] waste water treatment,[31] and drug delivery systems[32] and in the synthesis and stabilization of nanoparticles.[33] The polymer conjugates or electrolytic complexes with chitosan are feasible because under acidic conditions, chitosan has a positive charge and *inter alia* the positive charge can generate conjugates with polymers that have a negative charge,[34] which is the case for PHB.

Although the synthesis of gold nanoparticles with chitosan as a reducing[35–39] and stabilizing[40–42] agent is known, hitherto the unprecedented greener synthesis of nanoparticles using a PHB–chit conjugate (Fig. 1c) brings forth interesting properties namely high nanoparticle stability, enhancement of catalytic activity, and importantly products with reduced toxicity.

The as-synthesized nAu were thoroughly characterized using Transmission Electron Microscopy (TEM) images, Energy-Dispersive X-ray spectroscopy (EDX) spectra, size distribution, surface charge, plasmon resonance frequency, conjugate formation kinetics and toxicity to both Gram-negative (*Escherichia coli*) and Gram-positive (*Staphylococcus aureus*) bacteria. Additionally, its catalytic activity was evaluated, the major factors influencing being the size, shape and stability.[43,44] Furthermore, the surface functional groups of the stabilizing agent can also influence the catalytic behaviour.[45,46] Therefore, in our present work, the various sizes of the nAu and the diverse functional groups (chitosan, PHB) were tested for the catalytic reduction of 4-nitrophenol to 4-aminophenol.

Materials and methods

Reagents and solution

Chitosan (physical form 75–85% deacetylated, low molecular weight: 50–190 kDa), $HAuCl_4$ (99.999%), 4-nitrophenol (ReagentPlus >99%) and sodium borohydride (98%) were purchased from the Sigma-Aldrich company. Polyhydroxybutyrate (PHB, Biomer P209) was purchased from Biomer (Krailing, Germany). Nitric acid (65%), acetic acid (98%) and hydrochloric acid (37%) were purchased from Lach-Ner. Deionised water (18.2 MΩ cm, ELGA, Veolia Water, Marlow, UK) was used in all experiments. Bacterial strains of Gram-negative *Escherichia coli* (*E. coli* CCM3954) and Gram-positive *Staphylococcus aureus* (*S. aureus* CCM3953) were obtained from the Czech Collection of Microorganisms (CCM, Masaryk University, Brno, Czech Republic).

Analytical methods

Attenuated total reflection Fourier transform infrared spectroscopy (ATR-FTIR) spectra were acquired at 4000–700 cm^{-1} (with a resolution of 4 cm^{-1}) using a germanium ATR crystal (NICOLET IZ10, Thermo Scientific, USA) equipped with a single reflection angle 45° horizontal ATR accessory. An ultraviolet–visible spectrometer (UV–Vis; Hach Lange DR 3900) with matched 1 cm cuvettes was employed for recording the absorption spectra. Transmission electron microscopy (TEM) investigations were undertaken with a field-emission transmission electron microscope (FEI Titan 80300 TEM/STEM from FEI Company) with a super twin lens operated at 300 kV and equipped with an annular dark-field detector. The energy-dispersive X-ray spectroscopy (EDX) analysis was conducted to determine the presence of various elements in the synthesized nanoparticles, using an EDX system (Oxford Instruments, AZtec) with an X-Max detector attached to a Scanning Electron Microscope (SEM; model UHR FESEM Carl Zeiss ULTRA Plus). The differential centrifugal sedimentation (DCS) technique was used for the particle size distribution analysis (DC24000UHR, CPS Instruments Inc., USA). The DCS measurements were made at a disc rotation speed of 24 000 rpm and in an 8–24% (w/w) sucrose density gradient. Prior to each sample

This journal is © The Royal Society of Chemistry 2018

measurement, the instrument was calibrated using the PVC nanosphere standard (238 nm). The zeta potential was determined in a freshly prepared suspension using a Zetasizer ZS (Malvern Instruments Ltd, UK). Measurements were performed with autocorrelation functions of 10 seconds; each result was the average of triplicate measurements.

Bacterial viability assay ('spot test')

The maintenance and preparation of bacterial strains before the experiment were conducted in accordance with Darwish *et al.*[47] The 'spot test', described in detail, by Aruoja *et al.*[48] was used to evaluate the ability of the toxicant-exposed bacteria to form colonies on agar after 24 h exposure to the nanoparticles. Briefly, 100 µl of the bacterial suspension was added to 100 µl of polymer/nanoparticle solutions with various concentrations in a diluted soya nutrient broth (Sigma Aldrich; 3 g l^{-1}) in 96-well microplates (Immunoplate, SPL Life Sciences). Bacteria exposed to both nAu dispersions were incubated in 96-well microplates for 24 h at 37 °C without shaking. Each bacterial strain was analyzed in each microplate to eliminate cross-contamination. After 24 h of exposure, 5 µl of the cell suspension from each microplate well was pipetted as a 'spot' onto plate count agar (Bio-Rad) and the inoculated agar plates were incubated for 24 h at 37 °C. The minimal inhibitory concentration (MIC) of the tested material was determined as the lowest tested nominal concentration of a material, which completely inhibited the ability of the cells to form visible colonies.

Preparation of reagents and NPs

A chitosan solution was prepared by adding 0.5 g of chitosan in 100 ml of deionized water at pH 2.3 (for solubilization and partial depolymerization of chitosan) and stirred with a magnetic stirrer for one hour; the pH was adjusted with nitric, acetic or hydrochloric acid and the type of acid did not cause any significant changes in the solubility of polymers nor in the conjugation process.

The chitosan stock solution was mixed with PHB in the ratio of 4.16 : 1 (w/w) in a 200 ml volume glass vessel. The conjugation of PHB–chit was achieved by using a modified method for the conjugation of chitosan with folic acid.[49] First, the chitosan solution was stirred for 5 min with a magnetic stirrer and then PHB was introduced. Afterwards, this solution was stirred (in the dark) for 16 hours, being sonicated before and after this period (Autotune 750 W, Bioblock Scientific; equipped with a probe and operating at a frequency of 20 kHz) for 30 min (at 80 °C), to facilitate the synthesis process.[50] The PHB–chit conjugate was completely soluble and after filtration, dialysis (Sigma-Aldrich, MWCO 12 kDa) and lyophilization, it was stored in a refrigerator for further use. The molecular weights of PHB and PHB–chit were determined by gel permeation chromatography (GPC) to be 3 and 260 kDa, respectively (Fig. S1 and S2†).

The nAu were synthesized with chitosan (nAu–chit) in accordance with the procedure described by Huang *et al.*[37] The chitosan solution was added to $HAuCl_4$ in a closed vial at 80 °C and the sample was obtained by performing centrifugation 4 times at 13 500 rcf for one hour. Similarly, nAu were prepared with PHB–chit (nAu–PHB–chit) *via* the addition of the PHB–chit solution to $HAuCl_4$ in a closed glass vial, and at different time intervals, the sample was obtained by centrifugation (4 times, 13 500 rcf for one hour) as reported by Robertson *et al.*;[51] the effects of the synthesis time, the dose of the gold precursor, and the use of the PHB–chit conjugate were then evaluated.

Testing the catalytic effect

The catalytic properties of nAu–PHB–chit were assessed for the reduction of 4-nitrophenol (0.1 mM) to 4-aminophenol by $NaBH_4$ (0.03 M) in 1.5 ml cuvettes (reaction mixture volume: 1 ml). For clarification, the addition of 1 nmol of Au (atoms) corresponds to a Au concentration of 1.97×10^{-4} g l^{-1} in the volume of the reaction mixture; the Au concentration in the samples was determined by ICP-MS (Elan 6000, PerkinElmer, USA). The 4-nitrophenol concentration was determined from the absorbance (UV–Vis) at 401 nm in a continuous measurement. The reaction rate was fitted by the pseudo-first order kinetic model.[52]

Results and discussion

Dissolution of PHB in chitosan under acidic conditions

Due to the insolubility of PHB in water, PHB was dissolved by mixing with chitosan to form the PHB–chit conjugate. To attain the optimal conditions, various chitosan doses (2–5 g l^{-1}), PHB doses (1–2 g l^{-1}), chitosan to PHB ratios (4.16 : 1 to 1 : 1), pH (2.3 to 6.0) and acids used (acetic acid, hydrochloric acid or nitric acid) were evaluated to obtain a transparent solution without any sediment; appropriate amounts of acetic, hydrochloric and nitric acids were chosen in accordance with the literature.[53,54] It was found that under optimized conditions, PHB formed a soluble conjugate with chitosan (1.2 g l^{-1} of PHB and 5 g l^{-1} of chitosan).

Fig. 2 shows PHB sediments due to its insolubility in water (Fig. 2b), in contrast to the sample containing the PHB–chit conjugate in which the precipitates were not observed (Fig. 2c). These conditions were used in the entire study.

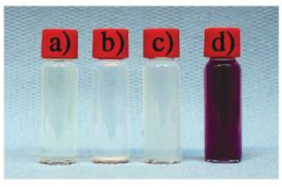

Fig. 2 (a) Chitosan solution (5 g l^{-1}), (b) sedimented PHB (1.2 g l^{-1}), (c) PHB–chit conjugate solution (1.6 g l^{-1}), and (d) nAu synthesized and stabilized with the PHB–chit conjugate.

Optimal parameters for nAu–PHB–chit preparation

One of the main goals of this research work was to assess the PHB–chit conjugate as a reducing agent for the preparation of gold NPs. The nAu have remarkable optical properties (Fig. S3†) due to their typical surface plasmon resonance (SPR) frequency. The absorption (determined by UV–Vis spectroscopy) and the evaluation of the NP size (determined with DCS, Fig. S4†) were used to determine the influence of several parameters on the synthetic performance. The synthesis time was varied from 1 to 90 min and the amount of PHB–chit conjugate from 0.2 to 3.0 g l^{-1} at two concentrations of $HAuCl_4$ (either 0.25 or 0.50 mM).

The increase in the absorption of light at 530 nm confirmed the formation of nAu; the enhancement of the absorption value occurs with the reaction time increments indicating the nAu concentration. In the case of $HAuCl_4$ with an initial concentration of 0.25 mM, the absorption increases almost linearly with time, but for the more concentrated precursor, the curve has an S-shape, a sigmoidal curve, exhibiting the degree of functionalization on the material's surface.[55] In this context, from 0 to 35 min, there is no evidence of attachment of molecules to the NP surface, and from 45 min and beyond, the NP surface is saturated with molecules.

Based on the UV–Vis and DCS results, an optimum synthesis time of 45 min was selected for further experiments, because of a narrow size distribution of ensued small NPs (below 25 nm), which could be synthesized on a larger scale. The concentrations of PHB–chit and the $HAuCl_4$ precursor (Fig. S5 and S6†) were chosen to be 1.6 g l^{-1} and 0.25 mM, respectively, for the ideal outcome.

nAu–PHB–chit characterization

To ascertain the functional groups, present in chitosan, PHB, PHB–chit conjugate and the composite, nAu–PHB–chit, a detailed ATR-FTIR analysis was carried out (Fig. 3).

In the PHB spectrum, the band at 1724 cm^{-1} was determined as the most relevant peak ascribable to the ester group (O–C═O) of PHB. The spectrum of chitosan showed various bands: the first one can be seen at ~3300 cm^{-1}, representing O–H and N–H bonds, the band at ~2900 cm^{-1} is compatible with symmetric or asymmetric $–CH_2–$ stretching vibrations, the band at ~1600 cm^{-1} represents the NH_2 group, and the band at 1100 cm^{-1} represents the –C–O–C– glycosidic linkage.

This analysis agrees with the literature documentation.[56,57] The spectra of the PHB–chit conjugate showed a decrease in the characteristic absorption peak at *ca.* 1600 cm^{-1} (NH_2) while the absorption peak (amide type II) at 1555 cm^{-1} increased in intensity, confirming that the amino groups on chitosan reacted with the ester groups of PHB to form the amide bond (Fig. 3 and S7A†).[58]

Moreover, an increase in the intensity of the C–H stretching vibration band at 2930 cm^{-1} can further affirm an increased PHB content when compared to the chitosan alone. These results are in accordance with recent reports concerning chitosan derivatives[58,59] and ^1H NMR and ^{13}C NMR analyses have provided additional proof of PHB–chit conjugation (Fig. S8 and S9,† respectively).[60]

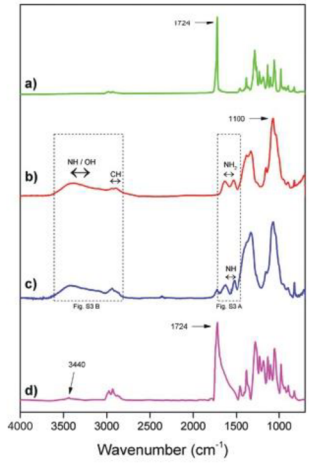

Fig. 3 ATR-FTIR analysis of (a) PHB, (b) chitosan, (c) PHB–chit conjugate, and (d) nAu–PHB–chit (the areas marked by dashed squares are shown in Fig. S7†).

On the other hand, the spectrum of the organics found on the surface of nAu–PHB–chit shows significant changes, when compared to the precursor materials. The peak at 3440 cm^{-1} probably corresponds to the secondary amide stretching. As can also be observed, the ester group of PHB (1724 cm^{-1}) has significantly changed. Moreover, the varying weak intensity of chitosan bands in the fingerprint (<1500 cm^{-1}) region may be explained in view of its small amount on the nAu surface. It can be discerned that the hydroxyl groups of the PHB–chit conjugate are most likely used in the process of gold salt reduction as stated previously[36,39,61] and the chitosan part of the conjugate is consumed. This hypothesis was further validated as it was found that formic acid is generated during the nAu synthesis corroborating previous reports by Pestov *et al.*[62] and Nazirov *et al.*[63]

The micrographs from TEM and energy-dispersive X-ray spectroscopy show spherical and aspherical NPs with relatively homogeneous sizes (Fig. 4).

Moreover, the selected area electron diffraction (SAED) patterns, acquired for nAu–PHB–chit, exhibit a ring structure, which is typical of polycrystalline gold nanoparticles. According to the data sheets of the Joint Committee on Powder Diffraction Standards (JCPDS) for face centered cubic (fcc) Au crystals (JCPDS: 04-0784), the rings were indexed to [111], [200], [220] and [311] as reflections of fcc Au for the corresponding *d*-spacings of 0.235 nm, 0.203 nm, 0.144 nm and 0.123 nm.

The particle size distributions obtained by TEM and DCS were found to be very similar, which confirms the high pre-

This journal is © The Royal Society of Chemistry 2018

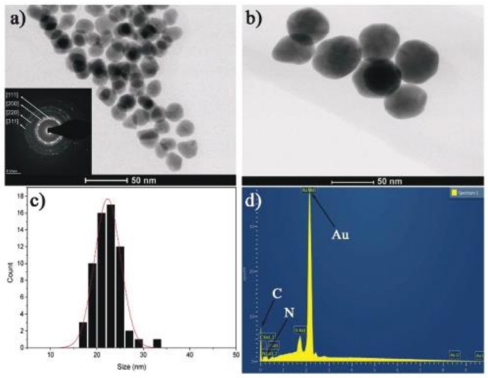

Fig. 4 (a) and (b) TEM images of nAu–PHB–chit with the median particle sizes of 23 and 41 nm (synthesized by two different approaches), (c) size distribution of nAu–PHB–chit (with the median particle size of 23 nm) and (d) EDX analysis of nAu–PHB–chit; the inset of (a) shows the selected area electron diffraction (SAED) pattern for nAu–PHB–chit.

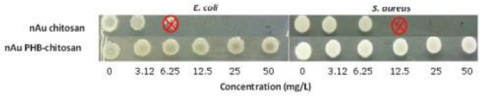

Fig. 5 Toxicity of nAu–chit and nAu–PHB–chit conjugate to bacteria, *Escherichia coli* and *Staphylococcus aureus*. Toxicity was assessed by the colony-forming ability of the bacteria after contact with the nanoparticles for 24 h. The red circle with crosses shows the minimum inhibitory concentration (MIC).

Table 1 The effects of chit, PHB, PHB–chit, nAu–chit and nAu–PHB–chit on the growth of *E. coli* and *S. aureus*[a]

Sample	Tested concentration (mg l^{-1})	*E. coli* MIC (mg l^{-1})	*S. aureus* MIC (mg l^{-1})
Chit	3.12–50	25	—
PHB	3.12–50	—	—
PHB–chit	3.12–50	—	—
nAu–chit	3.12–50	6.25	12.5
nAu–PHB–chit	3.12–50	—	—

[a] The tested concentration was chosen in the application range. '–': no effect of bacterial growth. The different observed effect is in accordance with the results from Regiel-Futyra *et al.*[67]

cision measurement using the DCS instrument (Fig. S4†). Furthermore, the EDX analysis (Fig. 4d) shows the presence of gold, carbon, oxygen and nitrogen which confirms the presence of protective PHB–NH– layers on the surface of nAu–PHB–chit. The bond between the amino group of chitosan and the carboxyl terminal of PHB was previously observed by Yalpani *et al.*[60] However, herein, this conjugate was exploited to utilize chitosan as a reducing agent and PHB as a stabilizer which is normally difficult to achieve due to the insolubility of PHB in nontoxic solvents. The amide groups comprising PHB–chit molecules can coordinate with Au ions *via* a weak covalent linkage as reported by Leff *et al.*[64] and Priyadarshini *et al.*[65] The creation of the nAu–NH– bond can impart electrostatic stabilization to the synthesized particles.[65] Additionally, the negatively charged PHB can provide stronger electrostatic repulsion, thus stabilizing the particles and preventing their agglomeration.

Colloidal stability of nAu–PHB–chit

The zeta potential is an important parameter characterizing *inter alia* the stability of colloids and can be used to assess the NP aggregation capability. In accordance with Honary *et al.*,[66] the zeta potential above ±30 mV produces good stability, while that around ±20 mV gives only short-term stability and a value smaller than ±5 mV indicates fast aggregation. In our case, the analysis of NP zeta potential revealed a large difference between NPs synthesized with chitosan alone and with PHB–chit conjugates; the zeta potential of nAu synthesized with chitosan is −4.4 ± 0.5 mV, whereas the zeta potential of nAu–PHB–chit is −27.4 ± 0.1 mV. Therefore, the nAu–chit tends to agglomerate rather quickly, while nAu–PHB–chit presents this tendency in a much slower manner.

Testing for toxicity

The 24 h 'spot' assay clearly showed that nAu–chit inhibited the growth of *E. coli* and *S. aureus* at a very low concentration, 6.25 and 12.5 mg l^{-1}, respectively, whereas the nAu–PHB–chit conjugate instigated no such effect against bacteria at concentrations up to 50 mg l^{-1} (Fig. 5 and Table 1). Our study agrees with the previous report showing that nAu synthesized with chitosan inhibited *S. aureus* ATCC 25923 and *P. aeruginosa* ATCC 27853 when the Au precursor concentration was 10 mM.[67] Engineered particles are designed to meet a wide range of desired properties for varied applications in diverse fields. If they are toxic by design, they can be modified again to be safer in terms of environmental or health hazard or can be used as biocide or additive materials; nAu are generally considered safe for many applications,[68,69] although our results clearly point out the importance of the stabilization agent in terms of toxicity. In this respect, herein, we report for the first time that the stabilization of nAu with PHB–chit can generate a safer and biodegradable material with no negative effects against the Gram-positive and Gram-negative bacteria; several applications namely the detection of hormones and proteins in the blood, bone implants, drug or vaccine delivery, and tumor therapy can be envisioned, among others.

Catalytic effect of nAu towards the reduction of 4-NP

Both samples, nAu–chit and nAu–PHB–chit, were evaluated for the catalytic reduction of 4-nitrophenol to 4-aminophenol by catalytic hydrogenation (using $NaBH_4$ as the hydrogen donor). The determined rate constants of the 1st order kinetics (k) are different for both types of nAu exhibiting a linear behavior over time (Fig. 6a); while k is 0.57 min^{-1} for nAu–chit, it is

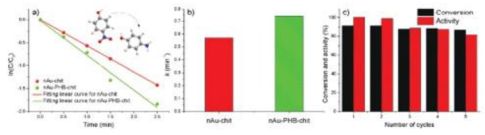

Fig. 6 (a) Pseudo-first-order model (solid lines) for the catalytic reduction of 4-nitrophenol to 4-aminophenol using nAu–PHB–chit and nAu–chit catalysts, (b) comparison of the rate constants of 4-nitrophenol reduction with catalysts synthesized using nAu–PHB–chit and nAu–chit, and (c) the change in the activity and conversion of nAu–PHB–chit (data taken after 5 min of the reaction time) with 5 repeated cycles. The concentrations of nAu (nAu–PHB–chit and nAu–chit) and 4-NP are the same in all experiments – 2.74×10^{-2} g l^{-1} (139 nmol) and 0.1 mM, respectively; the standard deviation between the measurements is less than <5%.

about 20% higher for nAu–PHB–chit (0.739 min^{-1}). The evaluation of nAu–PHB–chit was also conducted for various sizes of nAu to seek the correlation between their size and the rate constants, the highest being exhibited for the smallest sized particles in the tested range of ~23 nm (Fig. S10a†). Fig. 6b shows a comparison between k constants for both samples at their highest performance level, and nAu–PHB–chit shows the highest values; the influence of the nAu–PHB–chit dose on k can be found in Fig. S10b.† Based on this, it can be concluded that the use of the conjugate plays a key role in the catalytic reduction of 4-nitrophenol.

Since the concentration and the particle size distribution of both catalysts were the same, it could be safely concluded that the enhanced reaction kinetics (of 4-NP reduction) could be rationalized in terms of different functional groups on the surfaces of these particles.[70] The activity and reusability are both of significant value for an effective catalyst. With the intention of examining nAu–PHB–chit reusability, the same material was used repeatedly up to 5 times for the reduction of 4-nitrophenol. As can be seen in Fig. 6c, the conversion % stayed roughly unaffected, while the catalyst's activity reduced to 81% with the 5th use. The NP activity was determined based on the reduction of the reaction rate constants in comparison with the initial one. The decline in the catalytic efficacy could be due to the loss of smaller nAu–PHB–chit during the retrieval of the catalysts by centrifugation.

Conclusions

The current research presents a prospect of conjugating two green polymers (PHB and chitosan) and their application in the synthesis and stabilization of gold nanoparticles. The insolubility of both polymers (especially PHB) in water could be circumvented as their conjugate under determined optimum conditions is readily soluble and can be used for the reduction of the gold salt and the stabilization of the ensuing nanoparticles. Gold nanoparticles were synthesized from the precursor salt, $HAuCl_4$, and the optimal synthetic conditions (synthesis time of 45 min, precursor concentration of 0.25 mM, PHB–chit conjugate of 1.6 g l^{-1}) were chosen based on UV–Vis and size distribution (DCS) analyses.

Furthermore, the high stability of nAu–PHB–chit was confirmed by zeta potential analysis. A 24 h 'spot' assay clearly showed that nAu–chit inhibited the growth of *E. coli* and *S. aureus* at very low concentrations of 6.25 and 12.5 mg l^{-1}, respectively, while nAu–PHB–chit caused no harm to these bacteria at the tested concentrations up to 50 mg l^{-1}. Moreover, both nAu–chit and nAu–PHB–chit were assessed for the catalytic reduction of 4-nitrophenol by $NaBH_4$. The determined rate constants of the 1st order kinetics showed that the use of the conjugate improves the catalysis by 20%. The results reported herein provide newer perspectives for the greener synthetic approaches applicable to other nanoparticles that may improve conventional catalysis *via* the creation of biodegradable and recyclable catalysts, which are not harmful to the living systems in the environment.

Author contributions

D. S. and S. W. conceived and designed the experiments; D. S., S. W., B. S., V. N., N. H.A. N., J. M. and M. S. performed the experimental work; A. Š., M. P. P., R. S. V. and M. Č. analyzed the data; D. S., S. W., R. T.-M., V. T.P. P., M. Č. and R. S. V. wrote the paper.

Conflicts of interest

There are no conflicts to declare.

Acknowledgements

The research presented in this article was supported by the Ministry of Education, Youth and Sports in the framework of the targeted support of the "National Programme for Sustainability I" LO 1201 and the OPR & DI project "Extension of CxI facilities" (CZ.1.05/2.1.00/19.0386). The authors also acknowledge the assistance provided by the Research Infrastructure NanoEnviCz, supported by the Ministry of Education, Youth and Sports of the Czech Republic under Project no. LM2015073 and the European FP7 FutureNanoNeeds project (no. 604602). This work was supported by the Ministry of Education, Youth and Sports of the Czech Republic and the European Union – European Structural and Investment Funds in the frames of Operational Program Research, Development and Education – project Hybrid Materials for Hierarchical Structures (HyHi, Reg. No. CZ.02.1.01/0.0/0.0/16_019/0000843).

References

1 R. S. Varma, *Green Chem.*, 1999, **1**, 43–55.

This journal is © The Royal Society of Chemistry 2018

2 R. S. Varma, *ACS Sustainable Chem. Eng.*, 2016, **4**, 5866–5878.
3 V. Polshettiwar and R. S. Varma, *Curr. Opin. Drug Discovery Dev.*, 2007, **10**, 723–737.
4 R. B. Nasir Baig, B. R. Vaddula, M. A. Gonzalez and R. S. Varma, *RSC Adv.*, 2014, **4**, 9103–9106.
5 J. A. M. Delezuk, D. E. Ramírez-Herrera, B. Esteban-Fernández de Ávila and J. Wang, *Nanoscale*, 2017, **9**, 2195–2200.
6 G. Ma, D. Yang, K. Wang, J. Han, S. Ding, G. Song and J. Nie, *J. Appl. Polym. Sci.*, 2010, **118**, 3619–3624.
7 H. Zhang, F. Wang, X. Jin, Y. Zhu, X. Li and H. Zhou, *Water Sci. Technol.*, 2013, **67**, 2768–2775.
8 C. C. Chen and Y. C. Chung, *J. Environ. Sci. Health, Part A: Toxic/Hazard. Subst. Environ. Eng.*, 2006, **41**, 645–658.
9 W. S. Wan Ngah, C. S. Endud and R. Mayanar, *React. Funct. Polym.*, 2002, **50**, 181–190.
10 N. Van Suc and H. T. Y. Ly, *J. Chem. Technol. Biotechnol.*, 2013, **88**, 1641–1649.
11 I. C. da S. Grem, B. N. B. Lima, W. F. Carneiro, Y. G. de C. Queirós and C. R. E. Mansur, *Polim.: Cienc. Tecnol.*, 2013, **23**, 705–711.
12 N. Islam and V. Ferro, *Nanoscale*, 2016, **8**, 14341–14358.
13 F. Ding, H. Deng, Y. Du, X. Shi and Q. Wang, *Nanoscale*, 2014, **6**, 9477–9493.
14 T. Wang, M. Turhan and S. Gunasekaran, *Polym. Int.*, 2004, **53**, 911–918.
15 R. Huang and R. N. Reusch, *J. Biol. Chem.*, 1996, **271**, 22196–22202.
16 F. Valentino, F. Morgan-Sagastume, S. Campanari, M. Villano, A. Werker and M. Majone, *Nat. Biotechnol.*, 2017, **37**, 9–23.
17 F. Silva, S. Campanari, S. Matteo, F. Valentino, M. Majone and M. Villano, *Nat. Biotechnol.*, 2017, **37**, 90–98.
18 L. Hilliou, D. Machado, C. S. S. Oliveira, A. R. Gouveia, M. A. M. Reis, S. Campanari, M. Villano and M. Majone, *J. Appl. Polym. Sci.*, 2016, **133**, 42818.
19 M. Petrangeli, M. Majone, F. Arjmand, D. Silvestri, M. Sagliaschi, S. Sucato, E. Alesi, E. Barstch and L. Pierro, *Chem. Eng. Trans.*, 2016, **49**, 91–96.
20 M. Baric, L. Pierro, B. Pietrangeli and M. P. Papini, *Nat. Biotechnol.*, 2014, **31**, 377–382.
21 M. Baric, M. Majone, M. Beccari and M. P. Papini, *Chem. Eng. J.*, 2012, **195–196**, 22–30.
22 A. Shrivastav, H.-Y. Kim and Y.-R. Kim, *Biomed. Res. Int.*, 2013, **2013**, 1–12, DOI: 10.1155/2013/581684.
23 R. N. Reusch, *Int. J. Mol. Sci.*, 2013, **14**, 10727–10748.
24 L. Chronopoulou, C. Palocci, F. Valentino, I. Pettiti, S. Wacławek, M. Černík and M. Petrangeli Papini, *Appl. Sci.*, 2016, **6**, 417.
25 T. Fei, S. Cazeneuve, Z. Wen, L. Wu and T. Wang, *Biotechnol. Prog.*, 2016, **32**, 678–685.
26 N. Jacquel, C.-W. Lo, H.-S. Wu, Y.-H. Wei and S. S. Wang, *AIChE J.*, 2007, **53**, 2704–2714.
27 T. R. Torkelson, F. Oyen and V. K. Rowe, *Am. Ind. Hyg. Assoc. J.*, 1976, **37**, 697–705.
28 U. Rannug, *Mutat. Res., Rev. Genet. Toxicol.*, 1980, **76**, 269–295.
29 M. Manno, M. Rugge and V. Cocheo, *Hum. Exp. Toxicol.*, 1992, **11**, 540–545.
30 J. G. Fernandez and D. E. Ingber, *Macromol. Mater. Eng.*, 2014, **299**, 932–938.
31 Y. Huang, J. Li, X. Chen and X. Wang, *RSC Adv.*, 2014, **4**, 62160–62178.
32 S. Kitano, Y. Koyama, K. Kataoka, T. Okano and Y. Sakurai, *J. Controlled Release*, 1992, **19**, 161–170.
33 V. T. P. Vinod, S. Wacławek and M. Černík, *Ecol. Chem. Eng. S*, 2016, **23**, 533–557.
34 T. Galo Cárdenas, L. Johana Sanzana and H. Inoccentini Mei Lucia, *Bol. Soc. Chil. Quim.*, 2002, **47**, 529–535.
35 Y. Du, X. L. Luo, J. J. Xu and H. Y. Chen, *Bioelectrochemistry*, 2007, **70**, 342–347.
36 Y. Qiu, Z. Ma and P. Hu, *J. Mater. Chem. A*, 2014, **2**, 13471–13478.
37 H. Huang and X. Yang, *Biomacromolecules*, 2004, **5**, 2340–2346.
38 G. Zhang, X. Sun, J. Jasinski, D. Patel and A. M. Gobin, *J. Nanomater.*, 2012, **2012**, 1–9.
39 K. Dang Nguyen VÔ, C. Kowandy, L. Dupont and X. Coqueret, *Chem. Commun.*, 2015, **51**, 4017–4020.
40 D. G. de Oliveira, L. P. F. Peixoto, S. Sánchez-Cortés and G. F. S. Andrade, *Vib. Spectrosc.*, 2016, **87**, 8–13.
41 K. D. N. Vo, C. Kowandy, L. Dupont, X. Coqueret and N. Q. Hien, *Radiat. Phys. Chem.*, 2014, **94**, 84–87.
42 H.-H. Deng, X.-L. Lin, Y.-H. Liu, K.-L. Li, Q.-Q. Zhuang, H.-P. Peng, A.-L. Liu, X.-H. Xia and W. Chen, *Nanoscale*, 2017, **9**, 10292–10300.
43 J. Fang, B. Zhang, Q. Yao, Y. Yang, J. Xie and N. Yan, *Coord. Chem. Rev.*, 2016, **322**, 1–29.
44 T. Ma, W. Yang, S. Liu, H. Zhang and F. Liang, *Catalysts*, 2017, **7**, 38.
45 R. Ciganda, N. Li, C. Deraedt, S. Gatard, P. Zhao, L. Salmon, R. Hernández, J. Ruiz and D. Astruc, *Chem. Commun.*, 2014, **50**, 10126–10129.
46 J. Virkutyte and R. S. Varma, *Chem. Sci.*, 2011, **2**, 837–846.
47 M. S. A. Darwish, N. H. A. Nguyen, A. Ševců, I. Stibor and S. K. Smoukov, *Mater. Sci. Eng., C*, 2016, **63**, 88–95.
48 V. Aruoja, S. Pokhrel, M. Sihtmäe, M. Mortimer, L. Mädler and A. Kahru, *Environ. Sci.: Nano*, 2015, **2**, 630–644.
49 J. Ji, D. Wu, L. Liu, J. Chen and Y. Xu, *Polym. Bull.*, 2012, **68**, 1707–1720.
50 P. Kruus, M. O'Neill and D. Robertson, *Ultrasonics*, 1990, **28**, 304–309.
51 J. D. Robertson, L. Rizzello, M. Avila-Olias, J. Gaitzsch, C. Contini, M. S. MagoÅ, S. A. Renshaw and G. Battaglia, *Sci. Rep.*, 2016, **6**, 27494.
52 W. Stumm and J. J. Morgan, *Aquatic Chemistry: Chemical Equilibria and Rates in Natural Waters*, Wiley, 2012.
53 W. Cao, A. Wang, D. Jing, Y. Gong, N. Zhao and X. Zhang, *J. Biomater. Sci., Polym. Ed.*, 2005, **16**, 1379–1394.
54 T. T. B. Nguyen, S. Hein, C. H. Ng and W. F. Stevens, *J. Appl. Polym. Sci.*, 2008, **107**, 2588–2593.

55 K. Fujiwara, H. Watarai, H. Itoh, E. Nakahama and N. Ogawa, *Anal. Bioanal. Chem.*, 2006, **386**, 639–644.
56 V. Kumar, A. K. Tiwary and G. Kaur, *Int. J. Drug Delivery*, 2010, **2**, 242–250.
57 A. Pawlak and M. Mucha, in *Thermochimica Acta*, 2003, vol. 396, pp. 153–166.
58 J. C. C. Santos, P. M. D. Moreno, A. A. P. Mansur, V. Leiro, H. S. Mansur and A. P. Pêgo, *Soft Matter*, 2015, **11**, 8113–8125.
59 X. Huang, X. Bao, Y. Liu, Z. Wang and Q. Hu, *Sci. Rep.*, 2017, **7**, 1860.
60 M. Yalpani, R. H. Marchessault, F. G. Morin and C. J. Monasteries, *Macromolecules*, 1991, **24**, 6046–6049.
61 L. Au, B. Lim, P. Colletti, Y. S. Jun and Y. Xia, *Chem. – Asian J.*, 2010, **5**, 123–129.
62 A. Pestov, A. Nazirov, E. Modin, A. Mironenko and S. Bratskaya, *Carbohydr. Polym.*, 2015, **117**, 70–77.
63 A. Nazirov, A. Pestov, Y. Privar, A. Ustinov, E. Modin and S. Bratskaya, *Carbohydr. Polym.*, 2016, **151**, 649–655.
64 D. V. Leff, L. Brandt and J. R. Heath, *Langmuir*, 1996, **12**, 4723–4730.
65 E. Priyadarshini and N. Pradhan, *Sci. Rep.*, 2017, **7**, 9278.
66 S. Honary and F. Zahir, *Trop. J. Pharm. Res.*, 2013, **12**, 255–264.
67 A. Regiel-Futyra, M. Kus-Liśkiewicz, V. Sebastian, S. Irusta, M. Arruebo, G. Stochel and A. Kyzioł, *ACS Appl. Mater. Interfaces*, 2015, **7**, 1087–1099.
68 P. Ghosh, G. Han, M. De, C. K. Kim and V. M. Rotello, *Adv. Drug. Delivery Rev.*, 2008, **60**, 1307–1315.
69 W. Eck, A. I. Nicholson, H. Zentgraf, W. Semmler and S. S. Bartling, *Nano Lett.*, 2010, **10**, 2318–2322.
70 P. Zhao, X. Feng, D. Huang, G. Yang and D. Astruc, *Coord. Chem. Rev.*, 2015, **287**, 114–136.

This journal is © The Royal Society of Chemistry 2018

The use of a biopolymer conjugate for an eco-friendly one-pot synthesis of palladium-platinum alloys

Abstract: Raising health and environmental concerns over the nanoparticles synthesized from hazardous chemicals have urged researchers to focus on safer, environmentally friendlier and cheaper alternatives as well as prompted the development of green synthesis. Apart from many advantages, green synthesis is often not selective enough (among other issues) to create shape–specific nanoparticle structures. Herein, we have used a biopolymer conjugate and Pd and Pt precursors to prepare sustainable bimetallic nanoparticles with various morphology types. The nanoparticles were synthesized by a novel green approach using a bio–conjugate of chitosan and polyhydroxybutyrate (Cs–PHB). The bio–conjugate plays the simultaneous roles of a reducing and a capping agent, which was confirmed by attenuated total reflection Fourier transform infrared spectroscopy (ATR–FTIR) and energy dispersive X–ray spectrometry (EDS) analysis, proving the presence of a Cs–PHB layer on the surface of the prepared nanoparticles. The EDS profile also revealed the elemental structure of these nanoparticles and confirmed the formation of a Pd/Pt alloy. TEM morphological analysis showed the formation of star–like, octahedron or decahedron Pd/Pt nanoparticles, depending on the synthesis conditions. The bimetallic Pd/Pt nanoparticles synthesized with various Pd/Pt molar ratios were successfully applied for the catalytic reduction of 4–nitrophenol to 4–aminophenol by borohydride. The calculated κc values (ratio of kapp to the concentration of the catalyst) revealed that the decahedron nanoparticles (size of 15 ± 4 nm), synthesized at the molar ratio of 2:1 (Pd/Pt), temperature of 130 °C, 10 g/L of Cs–PHB conjugate and time of 30 min, exhibited excellent catalytic activity compared to other bimetallic nanoparticles reported in the literature.

Citation: Silvestri, D.; Wacławek, S.; Ramakrishnan, R. K.; Venkateshaiah, A.; Krawczyk, K.; Padil, V.V.; Sobel, B.; Černík, M. The Use of a Biopolymer Conjugate for an Eco-Friendly One-Pot Synthesis of Palladium-Platinum Alloys. *Polymers* **2019**, 11, 1948.
Impact Factor: **4.9** (2021), citations **6** (WOS 25.01.2023)

polymers

MDPI

Article

The Use of a Biopolymer Conjugate for an Eco-Friendly One-Pot Synthesis of Palladium-Platinum Alloys

Daniele Silvestri [1], Stanisław Wacławek [1,*], Rohith K. Ramakrishnan [1], Abhilash Venkateshaiah [1], Kamil Krawczyk [1], Vinod V. T. Padil [1], Bartłomiej Sobel [2] and Miroslav Černík [1,*]

[1] Institute for Nanomaterials, Advanced Technologies and Innovation, Technical University of Liberec, 46117 Liberec, Czech Republic; daniele.silvestri@tul.cz (D.S.); rohith.kunjiparambil.ramakrishnan@tul.cz (R.K.R.); abhilash.venkateshaiah@tul.cz (A.V.); kamil.krawczyk@tul.cz (K.K.); vinod.padil@tul.cz (V.V.T.P.)

[2] Institute of Engineering Materials and Biomaterials, Faculty of Mechanical Engineering, Silesian University of Technology, 44–100 Gliwice, Poland; bartlomiej.sobel@gmail.com

* Correspondence: stanislaw.waclawek@tul.cz (S.W.); miroslav.cernik@tul.cz (M.Č.)

Received: 6 November 2019; Accepted: 25 November 2019; Published: 27 November 2019

Abstract: Raising health and environmental concerns over the nanoparticles synthesized from hazardous chemicals have urged researchers to focus on safer, environmentally friendlier and cheaper alternatives as well as prompted the development of green synthesis. Apart from many advantages, green synthesis is often not selective enough (among other issues) to create shape-specific nanoparticle structures. Herein, we have used a biopolymer conjugate and Pd and Pt precursors to prepare sustainable bimetallic nanoparticles with various morphology types. The nanoparticles were synthesized by a novel green approach using a bio-conjugate of chitosan and polyhydroxybutyrate (Cs-PHB). The bio-conjugate plays the simultaneous roles of a reducing and a capping agent, which was confirmed by attenuated total reflection Fourier transform infrared spectroscopy (ATR-FTIR) and energy dispersive X-ray spectrometry (EDS) analysis, proving the presence of a Cs-PHB layer on the surface of the prepared nanoparticles. The EDS profile also revealed the elemental structure of these nanoparticles and confirmed the formation of a Pd/Pt alloy. TEM morphological analysis showed the formation of star-like, octahedron or decahedron Pd/Pt nanoparticles, depending on the synthesis conditions. The bimetallic Pd/Pt nanoparticles synthesized with various Pd/Pt molar ratios were successfully applied for the catalytic reduction of 4-nitrophenol to 4-aminophenol by borohydride. The calculated κc values (ratio of k_{app} to the concentration of the catalyst) revealed that the decahedron nanoparticles (size of 15 ± 4 nm), synthesized at the molar ratio of 2:1 (Pd/Pt), temperature of 130 °C, 10 g/L of Cs-PHB conjugate and time of 30 min, exhibited excellent catalytic activity compared to other bimetallic nanoparticles reported in the literature.

Keywords: green synthesis; biopolymers; bimetallic nanoparticles; catalytic reduction; 4-nitrophenol

1. Introduction

The raising health and environmental concerns over nanoparticles synthesized from hazardous chemicals, which are also often economically unfeasible, have urged researchers to focus on safer, environmentally-friendlier and cheaper alternatives. These reasons have prompted the development of green nanoparticle syntheses, which are safe and adhere to the green chemistry approach [1]. Biopolymers, which are abundantly available and easily biodegradable, are promising materials for providing an environmentally-benign synthesis of nanomaterials. These natural polymers have been

successfully used as reducing, stabilizing and capping agents in the synthesis of nanoparticles [2–4], allowing alterations in the nanoparticle size [5] and shape [6]. Furthermore, the different functional groups present in these biopolymers can actively contribute to the improvement of metallic nanoparticle catalytic reactions [7,8]. A typical example of a simple monometallic and bimetallic nanoparticle synthesis is the one-step reduction and stabilization of Au and Ag nanoparticles [9,10].

Chitosan is considered one of the most studied biopolymers in the literature, and has been successfully used in different applications such as the synthesis and stabilization of various different nanoparticles [11–13], bio-medical applications [14], drug delivery [15], water treatment [16] and many other uses [17–19]. Chitosan is obtained from chitin, which is mainly extracted from crustacean shell wastes [20]. While its non-toxicity for mammals and biodegradability make it popular, its insolubility in water is one of its drawbacks.

Another biopolymer that is starting to gain interest in different scientific fields is poly(3-hydroxybutyrate) (PHB), which can be produced by different bacteria [21] and also from waste materials [22,23]. It is usually used as a carbon source in *in-situ* bioremediation [24], a drug delivery carrier [25], a biodegradable bioplastic [26], and a stabilizing agent for nanoparticles [27]. However, difficulties such as the solubility of PHB in only organic solvents, which are toxic to both humans and the environment [28,29], need to be addressed to achieve good dispersions for synthesis.

Motivated by the above situation, our group developed a water-soluble conjugate of chitosan and PHB, which was successfully applied to control not only the growth and aggregation of the Au nanoparticles but also their surface properties [30].

Due to interactions between two metals and their unique and more flexible surface structures in comparison to monometallic nanoparticles, bimetallic nanoparticles have gained precedence over traditional heterogeneous catalysts due to their excellent catalytic activity [31]. The nanoparticle surface area plays a key role in heterogeneous catalysis because it is directly correlated to the catalyst active sites on which the catalytic reactions are taking place. Moreover, the nanoparticles are often easily recovered from the reaction medium, and they possess steric environments within their active sites, both features that can positively influence the catalytic activity [32]. Among the noble metals, both palladium (Pd) and platinum (Pt) are well known for their unique characteristics, and both are used successfully in different scientific fields, including catalysis [33–38]. Due to the fact they have similar face-centred cubic (fcc) crystal structures and a high lattice match (lattice mismatch of 0.77%), palladium and platinum are highly miscible [39,40].

We propose a one-pot, quick and green synthesis of decahedral Pd/Pt using solely Pd and Pt precursors and a Cs-PHB bio-conjugate as a reducing reagent. Based on our previous studies, we hypothesize that Cs-PHB cannot only help to control the growth and aggregation of the nanoparticles but also to tailor their catalytic activity. To the best of our knowledge, this is the first report to use Cs-PHB for the green synthesis of bimetallic nanoparticles. In addition, we believe in the simplicity of this procedure for obtaining decahedron Pd/Pt bimetallic nanoparticles. The synthesized nanoparticles were characterized by ATR-FTIR, TEM, and EDS, and successfully tested on the standard reduction reaction of the 4-nitrophenol (4-NP) to 4-aminophenol (4-AP).

2. Materials and Methods

2.1. Reagents and Solutions

Chitosan (low M_w of 50–190 kDa, 75%–85% deacetylated), sodium borohydride (98%), 4-nitrophenol (ReagentPlus, >99%), K_2PdCl_4 (98%), $PtCl_4$ (96%) were purchased from Sigma–Aldrich (Saint Louis, MO, USA); polyhydroxybutyrate (PHB, Biomer P209) from Biomer (Krailing, Germany); nitric acid (65%) from Lach-ner (Neratovice, Czech Republic). Deionized water (DI; 18.2 MΩ·cm^{-1}, ELGA, Veolia Water, Marlow, UK) was used in all of the experiments.

2.2. Analytical Methods

ATR-FTIR spectra were recorded at a resolution of 4 cm^{-1} over the 4000–700 cm^{-1} range using a NICOLET IZ10 spectrometer (Thermo Scientific, Waltham, MA, USA) equipped with a germanium ATR crystal and a single reflection angle 45° horizontal ATR accessory. The UV-Vis spectroscopic analysis was performed using a DR 3900 UV-Vis spectrophotometer (Hach Lange, Loveland, CO, USA) equipped with 1 cm quartz cuvettes. High-resolution transmission electron microscopy (HR-TEM) analysis was carried out using transmission electron microscopy/scanning transmission electron microscopy (TEM/STEM) system (Titan 80-300, FEI, city, state abbrev if USA, country) with a super twin-lens operated at 300 kV and equipped with an annular dark field detector. The presence of various elements in the obtained nanoparticles was analysed using energy-dispersive X-ray spectroscopy (EDX, Aztec, Oxford Instruments, Abingdon, UK). ICP-MS (Elan 6000, Perkin Elmer, Waltham, MA, USA) was used to determine the Pd/Pt concentration.

2.3. Preparation of Cs-PHB Conjugate

The conjugate was prepared following the procedure reported previously by our group [30]. Briefly, a chitosan solution was made by adding chitosan (0.5 g) to acidified deionized water (100 mL) and stirring to obtain a homogeneous solution. Subsequently, PHB (0.12 g) was added to the mixture and stirred overnight at 80 °C. The resulting solution was sonicated for 30 min at 80 °C, purified by a dialysis tube, and finally freeze-dried.

2.4. Synthesis of Bimetallic Nanoparticles

Pd/Pt bimetallic nanoparticles were synthesized following a modified co-reduction method of Lim et al. [41]. Briefly, K_2PdCl_4 and $PtCl_4$ were dissolved in DI to get two (Pd and Pt) stock solutions with a concentration of 10 mM each. Both solutions were stirred for 5 minutes in order to dissolve the salts. Cs-PHB was dissolved in DI to get a stock solution of 20 g/L. Subsequently, a certain amount of palladium and platinum precursor stock solutions (0.5 mL of Pd and 0.5 mL of Pt precursor stock solution for the Pd:Pt ratio of 1:1; 0.25 mL of Pd and 0.5 mL of Pt precursor stock solution for the Pd:Pt ratio of 1:2; 0.5 mL of Pd and 0.25 mL of Pt precursor stock solution for the Pd:Pt ratio 2:1) were added to the Cs-PHB solution (2.5 mL), the volume was raised to 5 mL by adding DI. The reactor was heated (130–150 °C) for 30 min following the procedure reported by Venkateshaiah et al. [42]. The reaction was stopped by cooling down the samples in cold water. The obtained nanoparticles were washed three times with deionized water and stored in a refrigerator (4 °C) for future use.

2.5. Catalytic Test

The catalytic test of 4-NP reduction to 4-AP by $NaBH_4$ was carried out in a standard 1 cm path length quartz cuvette. The procedure was reported previously by Baruah et al. [43]. A typical test involves the mixing of 24 µL of 4-NP (5 mM), and an excess of $NaBH_4$ (120 µL of 0.1 M) in an Eppendorf tube (1.5 mL). A certain amount of nanoparticles was added, and the volume was adjusted to 1 mL using DI water. Then the solution was immediately transferred into a quartz cuvette and the absorbance was recorded by UV-Vis at regular intervals. All of the tests were carried out at room temperature (25 °C) in triplicate. An excess of $NaBH_4$ (12 mM of $NaBH_4$ and 0.12 mM of 4-NP) was used in the reduction process.

3. Results and Discussion

Pd/Pt nanoparticles were synthesized under different conditions (temperature from 130 to 150 °C) and using different ratios of Pd and Pt precursors (from 1:2 to 2:1). The resulting particles were characterised by ATR-FTIR, HR-TEM and EDS. Three types of nanoparticles synthetized at a constant temperature but at different metallic ratio were also compared for their catalytic activity.

3.1. Characterization of the Nanoparticles

3.1.1. ATR-FTIR

An ATR-FTIR analysis was performed to examine the functional groups located on the Pd/Pt bimetallic nanoparticles (Figure 1). The peak observable at ~1724 cm^{-1} in the PHB spectrum (Figure 1a) may be attributed to the ester group present in the PHB. The chitosan spectrum shows a peak at ~3300 cm^{-1} due to the O–H and N–H bonds, whereas the peak at ~2900 cm^{-1} may be ascribed to the symmetric or asymmetric CH_2 stretching vibrations. The peak at ~1600 cm^{-1} may be assigned to the NH_2 groups, while at ~1380 cm^{-1} the peak may be ascribed to CH_3 symmetrical deformations [44]. The last representative peak at ~1100 cm^{-1} may be attributed to C–O–C glycosidic linkage. The conjugate spectrum (Figure 1c) shows differences when comparing the PHB (Figure 1a) to the chitosan (Figure 1b) spectra. A decrease in the intensity of the NH_2 group at ~1600 cm^{-1} [30] was observed, while an increase in the intensity at ~1555 cm^{-1} was observed, which may correspond to the amide type II bond formation [30]. This suggests that the amino group of chitosan reacts with the C–O–C group of PHB to form the amide bond.

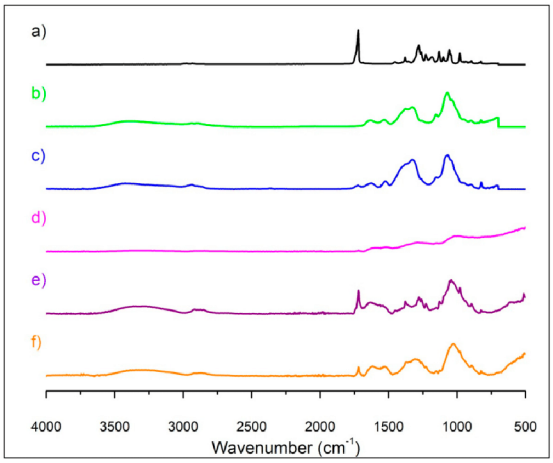

Figure 1. ATR-FTIR analysis of (**a**) PHB, (**b**) chitosan, (**c**) Cs-PHB, (**d**) Pd/Pt ratio 1:1 (zoom on the region of the 4000–1500 cm^{-1} spectrum part is available in Figure S1 in Supplementary Materials), (**e**) Pd/Pt ratio 1:2 and (**f**) Pd/Pt ratio 2:1 (synthesis temperature of Pd/Pt: 130 °C).

The ATR-FTIR spectra of Pd/Pt nanoparticles (Figure 1d–f) showed several bands. The first one (~3330 cm^{-1}) may be attributed to the NH/OH bond, whereas the one at ~2926 cm^{-1} is compatible with asymmetric or symmetric CH_2 stretching vibration. The peak at 1724 cm^{-1} may be related to the ester group, while the one at ~1555 cm^{-1} to the amide type II bond. The hydroxyl groups present in the conjugate may assist in the reduction of the precursor as reported by Dang et al. [45] and by Dorjnamjin et al. [46], while the rest of the polymer may coat the nanoparticles. The differences in intensity between the variously synthesized Pd/Pt nanoparticles may indicate different amounts of organic and inorganic material that could be found in samples. For example, Pd/Pt = 1:1 nanoparticles were synthesized with the highest ratio of metal precursors concentration (2 mM overall) to the polymer conjugate concentration, and in the low frequencies (<1500 cm^{-1}) their spectrum exhibits a (high absorbance) baseline sloping down to the left (typical for some metal nanoparticles; similar phenomena could be observed e.g. in the work of Hu et al. [47]).

3.1.2. HR-TEM

In order to obtain more information about the morphology of the synthesized Pd/Pt nanoparticles, a HR-TEM analysis was performed. Figure 2 shows the different shapes obtained by altering the synthesis temperature (from 130 to 150 °C) and Pd/Pt molar ratio (1:1, 1:2 and 2:1).

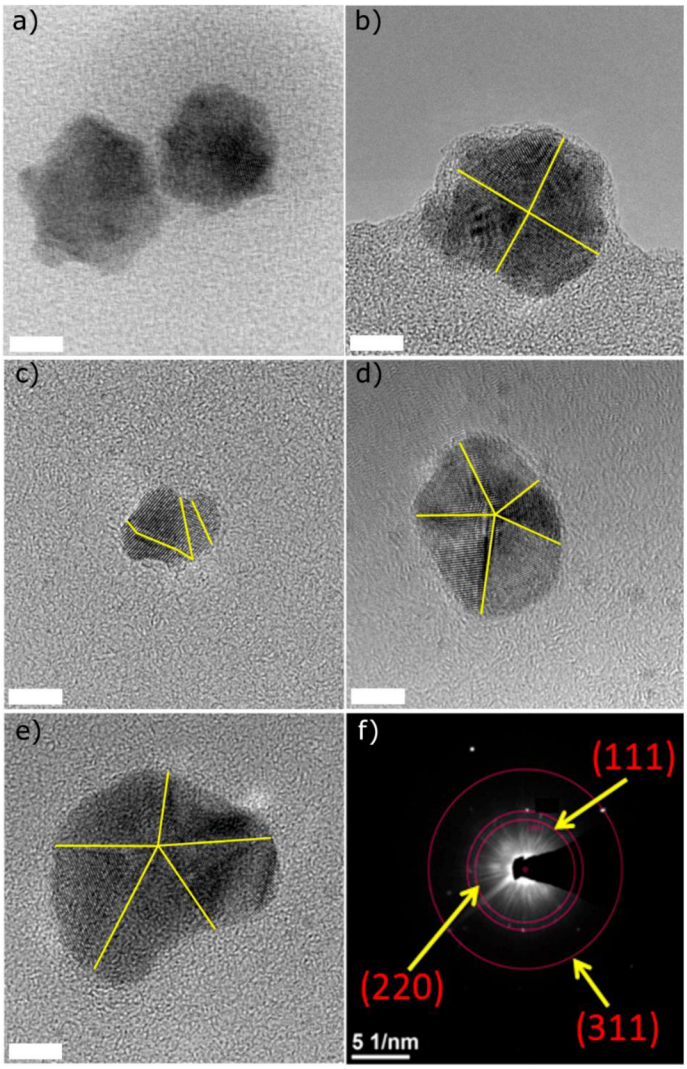

Figure 2. HR-TEM images of characteristic Pd/Pt nanoparticles synthesized with different molar ratios and temperatures (**a**) Pd/Pt 1:1 at 150 °C, (**b**) 1:1 at 140 °C, (**c**) 1:1 at 130 °C, and (**d**) 2:1 at 130 °C; (**e**) 1:2 at 130 °C and (**f**) SAED pattern of Pd/Pt (2:1). For all of the samples, the scale bar stands for 5 nm.

The sample synthesized at 150 °C and with a molar ratio 1:1 (Pd/Pt) (Figure 2a) shows a star-like structure, while lowering the temperature of synthesis to 140 °C (Figure 2b) changed the morphology of the nanoparticles to an octahedron. An additional decrease of temperature to 130 °C (Figure 2c) caused a synthesis of smaller nanoparticles with a surface characterized by different, randomly-orientated faces. Moreover, when the molar ratio changed to 2:1 and 1:2 (Pd/Pt) at the remaining temperature (130 °C), nanoparticles with decahedral morphology were observed (Figure 2d,e). The decahedral shape of the nanoparticles occurs only under strict conditions [48]. When certain conditions are applied, the ions specifically interact to form a Cs-PHB/precursor complex, which determines the formation of decahedron shapes upon reduction. However, when the conditions and the ratios vary, other shapes are formed. Zhang et al. [49] reported that hydroxyl groups may affect the shape of the nanoparticles. Ghosh et al. [50] showed the possibility of obtaining flower-shaped zero-valent iron by controlling the amount of hydroxyl groups during the synthesis process, which suggests that the presence of hydroxyl groups may influence the formation of decahedral morphology. The SAED pattern for a Pd/Pt ratio of 2:1 indicates the polycrystalline nature of an as-synthesized Pd/Pt bimetallic alloy (Figure 2f). The SAED analysis identified (111), (220) and (311) planes of fcc. For this sample, the nanoparticle size distribution was calculated from TEM micrographs, and the mean size of these nanoparticles was found to be 15 ± 4 nm (Figure S2 in Supplementary Materials).

The various synthesis strategies used to obtain bimetallic Pd/Pt nanoparticles with varying morphologies are shown in Table 1. As stated earlier, changes to the synthesis procedure may result in the formation of structurally different nanoparticles, e.g. nanocubes are obtained by reduction with poly(vinylpyrrolidone) (PVP) while nanotetrahedra are formed when $Na_2C_2O_4$ and formaldehyde are used [39]. Conventionally for these kind of reactions, high temperatures [51] and prolonged synthesis times [52,53] are required. Very often the reducing agents used are hazardous, e.g. sodium borohydride [44,45].

Table 1. Synthesis procedures reported in the literature for obtaining Pd/Pt nanoparticles with different shapes.

Shape	Solvent	Precursors	Molar Pd/Pt Ratio	Reducing Agent	Temperature (°C)	Synthesis Time (min)	Reference
Cube	DMF	Na_2PdCl_4 K_2PtCl_6	1:1	-	130	300	[54]
Nanosponges	Water	H_2PdCl_4 K_2PtCl_6	1:1	$NaBH_4$	Room temperature	~5	[55]
Tetrahedron	Water	Na_2PdCl_4 K_2PtCl_6	1:1	HCHO	180	120	[56]
Octahedron	Water	Na_2PdCl_4 H_2PtCl_6	1:1	Glycerol	100	180	[57]
Corallite-like structure	Water	K_2PdCl_4 $K_2Pt(CN)_4$	2.05:1	$NaBH_4$	Room temperature	120	[58]
Branched Dandelion-like	Water	Na_2PdCl_4 K_2PtCl_6	1:7	Ascorbic acid	Room temperature	30	[55]
Nanocages	Water	K_2PdBr_4 Na_2PtBr_6	1:2	Ascorbic acid	Room temperature	480	[40]
Irregular polyhedron	Water	K_2PdCl_4 $PtCl_4$	1:1	Cs-PHB	130	30	This work
Decahedron	Water	K_2PdCl_4 $PtCl_4$	1:2	Cs-PHB	130	30	This work
Decahedron	Water	K_2PdCl_4 $PtCl_4$	2:1	Cs-PHB	130	30	This work

Wang et al. [59] reported the possibility to synthesize decahedral Pd/Pt, wherein the synthesis procedure can be divided into two steps: the first is to obtain Pd decahedraln structures, followed by

the platinum deposition. Nano star-shaped Pd/Pt particles were reported by Lim et al. [41] using a co-reduction method involving Na_2PdCl_4 and K_2PtCl_4 in a PVP aqueous medium at 80 °C for 18 h. Another example of shape-specific synthesis of Pd/Pt was a seeded growth method using palladium truncated octahedral seeds for the synthesis of Pd/Pt nanodendrites [60].

3.1.3. EDS, Mapping and Profile

The EDS analysis of the bimetallic nanoparticles shows that all of the samples contain both palladium and platinum metals (Figure 3). Moreover, carbon and oxygen were also present in all of the analysed samples. The presence of both C and O may be attributed to the existence of a conjugate on the surface of these nanoparticles, which may act as a stabilizing agent.

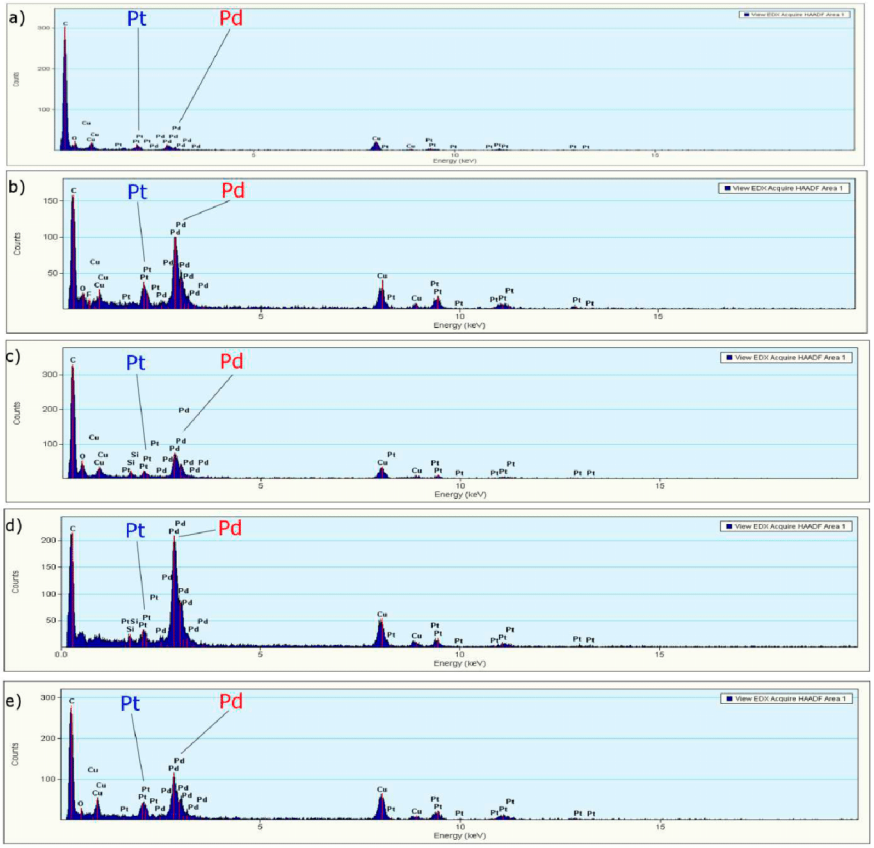

Figure 3. EDS analysis of Pd/Pt nanoparticles synthesized at different temperatures and molar ratios (**a**) 150 °C and 1:1, (**b**) 140 °C and 1:1, (**c**) 130 °C and 1:1, (**d**) 130 °C and 2:1, and (**e**) 130 °C and 1:2.

The EDS mapping analysis of the bimetallic nanoparticles (molar ratio of Pd/Pt of 2:1 and temperature of 130 °C) clearly shows the presence of both metals ubiquitously on the surface of the nanoparticle (Figure 4a,b). The EDS mapping also determined the presence of Pd/Pt alloy. The EDS profile analysis (Figure 4c) shows the presence of carbon (due to the presence of the conjugate), and

it is in accordance with the previous ATR-FTIR analysis (see above). The profile also confirmed the predominant presence of Pd in almost all of the particle regions due to the initial Pd/Pt ratio of 2:1.

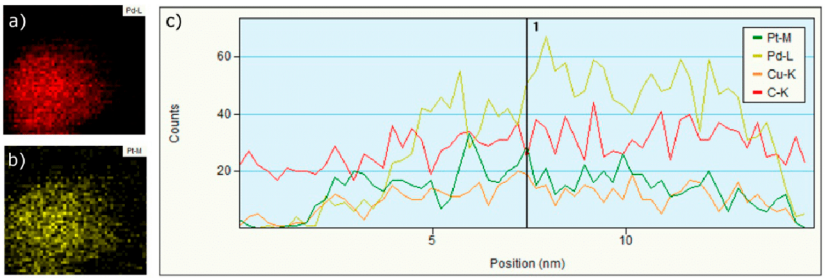

Figure 4. EDS mapping of (**a**) Pd and (**b**) Pt, and (**c**) EDS profile analysis of Pd/Pt nanoparticles (synthesis condition: Pd/Pt ratio 2:1, 10 g/L of Cs-PHB and temperature of 130 °C).

3.2. *Catalysis*

The catalytic performance of the Pd/Pt nanoparticles was proven by employing the reduction of 4-NP to 4-AP by $NaBH_4$ as a model [61]. The aqueous 4-NP solution shows a maximum absorption at ~317 nm, which upon addition of sodium borohydride shifts to 401 nm, indicating the formation of 4-nitrophenolate, and the solution turns from pale yellow to bright yellow. The reduction does not take place in the absence of a catalyst (kinetic barrier), which was verified by the unchanged intensity of the maximum absorption at 401 nm in the absence of the catalysts for 40 min (data not shown).

When the Pd/Pt nanoparticles were added to the solution, the intensity at 401 nm gradually decreased until it disappeared. Because an excess of $NaBH_4$ was used, the pseudo first-order kinetics model was applied to evaluate the catalytic performance of the Pd/Pt nanoparticles [62]. Due to the fact that the absorbance at 401 nm was linearly dependent on the 4-NP concentration (through 4-nitrophenolate), the rate constant k of the reaction can be calculated from the linear plot of $\ln(A_t/A_0)$ versus the reaction time t(min) [63–67]:

$$\ln(A_t/A_0) = -k_{app}t \quad (1)$$

where A_t and A_0 is absorbance at time t and 0, respectively. The pseudo-first-order kinetic rate constants (k_{app}) of the 4-NP reduction calculated based on Equation (1) for the various concentrations of nanoparticles synthesized with different molar (Pd/Pt) ratios of 1:1, 1:2 and 2:1, respectively are summarized in Table 2.

The reduction of 4-NP to 4-AP with borohydride catalysed by Pd/Pt nanoparticles may be explained by an electrochemical reaction, where the nanoparticles facilitate the electron transfer from BH_4^- to 4-NP. The mechanism is divided into the following steps: first both borohydride and 4-NP are adsorbed on the surface of the Pd/Pt nanoparticles, then electrons are transferred from BH_4^- to the nanoparticles with the formation of a negatively charged layer on their surface, later the electrons are transferred to 4-NP with a consequent formation of reduced products (Figure 5).

Table 2. The pseudo-first-order kinetic rate constants (k_{app}) of Pd/Pt synthesized in different ratios and κ_c value obtained by linear approximation of k_{app} (s^{-1}) vs concentration of catalysts (g/L).

Catalysts	Synthesis Temperature (°C)	Concentration (mg/L)	k_{app} (min^{-1})	κ_c (L s^{-1} g^{-1})
Pd/Pt (1:1)	130	0.379	0.038	12 ± 4
		0.757	0.546	
		1.515	0.897	
Pd/Pt (1:2)	130	0.147	0.066	9 ± 1
		0.293	0.152	
		0.586	0.305	
Pd/Pt (2:1)	130	0.202	0.198	51 ± 11
		0.404	0.424	
		0.809	1.967	

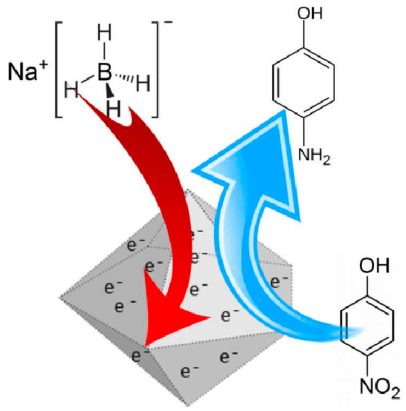

Figure 5. Electron transfer mechanism for reduction of 4-NP to 4-AP.

4-NP is often used for testing the catalytic activities of nanoparticles; nevertheless, catalytic performance comparisons are not easy. Most studies report only the k_{app}, but the k_{app} is strongly dependent on the concentration of reactants and the catalyst used for the reaction. Increasing the amount of catalyst in the reactor increases the total surface area available for the reaction, which means that a higher reaction rate is facilitated, and the time needed for reduction is shortened. Also, it was not possible in our study to add the same amounts of catalysts at different Pd/Pt ratios during the experiments. To overcome this, the activity parameter (κ_c) was employed to compare the efficiencies. This was determined by calculation of the slope of k_{app} (s^{-1}) as a function of the catalyst concentration (g/L) [65].

To the best of our knowledge, κ_c is the most appropriate parameter for comparing the catalytic activity of catalysts reported in the literature [65,67]. The κ_c values were calculated for these three different Pd/Pt ratios and, therefore, different morphologies. While for the same Pd/Pt ratio (1:1) and excess of Pt (1:2), the κ_c value is approximately 10, for the excess of Pd (2:1), the κ_c value of 51 is significantly higher. This is probably caused by a higher Pd ratio and not by morphology, since both excesses of one of the metals (1:2 and 2:1) have the same morphology of a decahedron, but significantly different κ_c values (Figure 6).

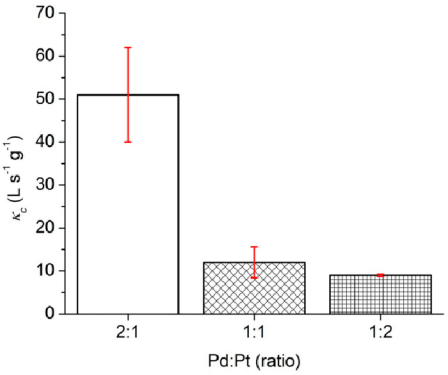

Figure 6. Comparison between the κ_c values of nanoparticles obtained by different ratios of Pd and Pt precursors (the red error bars represent the slope error).

Table 3 shows a comparison of the κ_c values obtained by different bimetallic catalysts for the reduction of 4-NP. The value determined by this study for a Pd/Pt ratio of 2:1 is one of the highest known to-date.

Table 3. Comparison of different bimetallic catalysts on the reduction of 4-NP reported in the literature.

Catalysts	Catalyst Concentration (mg/L)	4-NP Concentration (mM)	$NaBH_4$ Concentration (mM)	k_{app} (s^{-1})	κ_c (L s^{-1} g^{-1})	Ref.
Pd/Au	8	0.07	21	0.258	32	[68]
$Au_{53}Pd_{47}$/graphene nanosheets	0.06	0.05	5	0.014	240	[69]
Cu/Ag	0.48	0.096	11.2	0.0003	7.18	[70]
PdCuY	20	0.72	1.5	0.002	0.12	[71]
Pd/Pt nanotubes	3.4	0.09	100	0.008	25	[72]
Pd/Pt (2:1)	0.809	0.12	12	0.033	51 ± 11	This work
Pd/Pt (1:1)	0.757	0.12	12	0.009	12 ± 4	This work
Pd/Pt (1:2)	0.586	0.12	12	0.005	9 ± 1	This work

4. Conclusions

The present research describes a facile mediated green synthesis of bimetallic Pd/Pt nanoparticles of various morphologies. The nanoparticles were synthesized from K_2PdCl_4 and $PtCl_4$ precursor salts by a co-reduction with a Cs-PHB conjugate. Depending on the temperature and metal ratio, nanoparticles with a star-like structure, and octahedral or decahedral morphology were formed. The optimal conditions to obtain a decahedral shape were found to be: (Pd/Pt) molar ratio of 2:1, synthesis temperature of 130 °C, 10 g/L of Cs-PHB conjugate and time of 30 min. While ATR-FTIR and EDS confirmed the presence of a Cs-PHB layer on the surface of the nanoparticles, EDS verified the formation of a Pd/Pt alloy. TEM analysis confirmed the different shapes and sizes of the nanoparticles by changing the temperature and molar metal ratio. The decahedral bimetallic nanoparticles prepared at a molar ratio of 2:1 show an excellent catalytic performance for the catalytic reduction of 4-NP by borohydride. The pseudo-first-order kinetic constant for the nanoparticles synthesized with molar ratios (Pd/Pt) of 1:1, 1:2 and 2:1 were found to be 0.898 min^{-1} (catalyst concentration: 1.515 mg/L), 0.305 min^{-1} (0.586 mg/L) and 1.968 min^{-1} (0.809 mg/L), respectively. Compared with the other bimetallic nanoparticles, the (2:1) decahedral Pd/Pt nanoparticles exhibit excellent catalytic performance, which is demonstrated by the high κ_c value (51 ± 11 L s^{-1} g^{-1}).

Supplementary Materials: The following are available online at http://www.mdpi.com/2073-4360/11/12/1948/s1, Figure S1 FTIR analysis of Pd/Pt ratio 1:1, Figure S2: Size distribution of Pd/Pt synthesized at 130 °C and molar ratio 2:1 (Pd:Pt), Figure S3: pseudo-first-order kinetics of sample synthesized with molar ratio of 1:1 with differet concentration of nanoparticles (a) 0.379 mg/L (R^2 0.993), (b) 0.757 mg/L (R^2 0.992), (c) 1.515 mg/L (R^2 0.982) and (d) HRTEM image of Pd/Pt decahedron nanoparticle (molar ratio 1:1 (Pd/Pt) 130 °C), Figure S4: pseudo-first-order kinetics of sample synthesized with molar ratio of 1:2 with differet concentration of nanoparticles (a) 0.147 mg/L (R^2 0.992), (b) 0.293 mg/L (R^2 0.998), (c) 0.586 mg/L (R^2 0.984) and (d) HRTEM image of Pd/Pt decahedron nanoparticle (molar ratio 1:2 (Pd/Pt) 130 °C), Figure S5: pseudo-first-order kinetics of sample synthesized with molar ratio of 2:1 with different concentration of nanoparticles (a) 0.202 mg/L (R^2 0.997) (b) 0.404 mg/L (R^2 0.986) (c) 0.809 g/L (R^2 0.979) and d) HRTEM image of Pd/Pt decahedron nanoparticle (molar ratio 2:1 (Pd/Pt) 130 °C).

Author Contributions: Conceptualization, D.S. and S.W.; Funding acquisition, M.Č.; Investigation, D.S. and R.K.R.; Methodology, R.K.R., A.V. and B.S.; Supervision, S.W.; Writing—original draft, D.S.; Writing—review & editing, S.W., K.K., V.V.T.P., B.S. and M.Č.

Funding: This work was supported by the Student Grant Scheme 2019 project of the Technical University of Liberec. The authors would also like to acknowledge the assistance provided by the Research Infrastructure NanoEnviCz, supported by the Ministry of Education, Youth and Sports of the Czech Republic in the framework of Project No. LM2015073, and the project Pro-NanoEnviCz (Reg. No. CZ.02.1.01/0.0/0.0/16_013/0001821) supported by the Ministry of Education, Youth and Sports of the Czech Republic and the European Union - European Structural and Investments Funds in the frame of Operational Programme Research Development and Education.

Conflicts of Interest: The authors declare no conflict of interest.

References

1. Virkutyte, J.; Varma, R.S. Green synthesis of metal nanoparticles: Biodegradable polymers and enzymes in stabilization and surface functionalization. *Chem. Sci.* **2011**, *2*, 837–846. [CrossRef]
2. Moulton, M.C.; Braydich-Stolle, L.K.; Nadagouda, M.N.; Kunzelman, S.; Hussain, S.M.; Varma, R.S. Synthesis, characterization and biocompatibility of "green" synthesized silver nanoparticles using tea polyphenols. *Nanoscale* **2010**, *2*, 763–770. [CrossRef] [PubMed]
3. Vinod, V.T.P.; Saravanan, P.; Sreedhar, B.; Devi, D.K.; Sashidhar, R.B. A facile synthesis and characterization of Ag, Au and Pt nanoparticles using a natural hydrocolloid gum kondagogu (Cochlospermum gossypium). *Colloids Surf. B Biointerfaces* **2011**, *83*, 291–298. [CrossRef] [PubMed]
4. Padil, V.V.T.; Černík, M.; Thekkae Padil, V.V.; Černík, M. Green synthesis of copper oxide nanoparticles using gum karaya as a biotemplate and their antibacterial application. *Int. J. Nanomed.* **2013**, *8*, 889–898. [CrossRef]
5. Nadagouda, M.N.; Speth, T.F.; Varma, R.S. Microwave-assisted green synthesis of silver nanostructures. *Acc. Chem. Res.* **2011**, *44*, 469–478. [CrossRef]
6. Hebbalalu, D.; Lalley, J.; Nadagouda, M.N.; Varma, R.S. Greener techniques for the synthesis of silver nanoparticles using plant extracts, enzymes, bacteria, biodegradable polymers, and microwaves. *ACS Sustain. Chem. Eng.* **2013**, *1*, 703–712. [CrossRef]
7. Seo, E.; Kim, J.; Hong, Y.; Kim, Y.S.; Lee, D.; Kim, B.S. Double hydrophilic block copolymer templated au nanoparticles with enhanced catalytic activity toward nitroarene reduction. *J. Phys. Chem. C* **2013**, *117*, 11686–11693. [CrossRef]
8. Machmudah, S.; Sato, T.; Wahyudiono; Sasaki, M.; Goto, M. Silver nanoparticles generated by pulsed laser ablation in supercritical CO_2 medium. *High Press. Res.* **2012**, *32*, 60–66. [CrossRef]
9. Zhao, L.; Song, J.; Xue, Y.; Zhao, X.; Deng, Y.; Li, Q.; Xia, Y. Green synthesis of Ag–Au bimetallic nanoparticles with alginate for sensitive detection of H_2O_2. *Catal. Lett.* **2018**, *148*, 3248–3256. [CrossRef]
10. Padil, V.V.T.; Wacławek, S.; Černík, M. Green Synthesis: Nanoparticles and Nanofibres Based on Tree Gums for Environmental Applications. *Ecol. Chem. Eng. S* **2016**, *23*, 533–557. [CrossRef]
11. Sun, L.; Li, J.; Cai, J.; Zhong, L.; Ren, G.; Ma, Q. One pot synthesis of gold nanoparticles using chitosan with varying degree of deacetylation and molecular weight. *Carbohydr. Polym.* **2017**, *178*, 105–114. [CrossRef] [PubMed]
12. Chen, X.; Xu, X.J.; Zheng, X.C.; Guan, X.X.; Liu, P. Chitosan supported palladium nanoparticles: The novel catalysts for hydrogen generation from hydrolysis of ammonia borane. *Mater. Res. Bull.* **2018**, *103*, 89–95. [CrossRef]

13. Oliveira, Â.A.S.; Medeiros, R.L.B.A.; Figueredo, G.P.; Macedo, H.P.; Braga, R.M.; Maziviero, F.V.; Melo, M.A.F.; Melo, D.M.A.; Vieira, M.M. One-step synthesis of $LaNiO_3$ with chitosan for dry reforming of methane. *Int. J. Hydrogen Energy* **2018**, *43*, 9696–9704. [CrossRef]
14. Anitha, A.; Sowmya, S.; Kumar, P.T.S.; Deepthi, S.; Chennazhi, K.P.; Ehrlich, H.; Tsurkan, M.; Jayakumar, R. Chitin and chitosan in selected biomedical applications. *Prog. Polym. Sci.* **2014**, *39*, 1644–1667. [CrossRef]
15. Ali, A.; Ahmed, S. A review on chitosan and its nanocomposites in drug delivery. *Int. J. Biol. Macromol.* **2018**, *109*, 273–286. [CrossRef]
16. Hahn, T.; Zibek, S. Sewage Polluted Water Treatment via Chitosan: A Review. In *Chitin-Chitosan—Myriad Functionalities in Science and Technology*; InTechOpen: London, UK, 2018.
17. Logithkumar, R.; Keshavnarayan, A.; Dhivya, S.; Chawla, A.; Saravanan, S.; Selvamurugan, N. A review of chitosan and its derivatives in bone tissue engineering. *Carbohydr. Polym.* **2016**, *151*, 172–188. [CrossRef]
18. Baig, R.B.N.; Varma, R.S. Copper on chitosan: A recyclable heterogeneous catalyst for azide-alkyne cycloaddition reactions in water. *Green Chem.* **2013**, *15*, 1839. [CrossRef]
19. Sedghi, R.; Heidari, B.; Shahmohamadi, H.; Zarshenas, P.; Varma, R.S. Pd Nanocatalyst Adorned on Magnetic Chitosan@N-Heterocyclic Carbene: Eco-Compatible Suzuki Cross-Coupling Reaction. *Molecules* **2019**, *24*, 3048. [CrossRef]
20. Devi, R.; Dhamodharan, R. Pretreatment in Hot Glycerol for Facile and Green Separation of Chitin from Prawn Shell Waste. *ACS Sustain. Chem. Eng.* **2018**, *6*, 846–853. [CrossRef]
21. Al Rowaihi, I.S.; Paillier, A.; Rasul, S.; Karan, R.; Grötzinger, S.W.; Takanabe, K.; Eppinger, J. Poly(3-hydroxybutyrate) production in an integrated electromicrobial setup: Investigation under stress-inducing conditions. *PLoS ONE* **2018**, *13*, e0196079. [CrossRef]
22. Silva, F.; Campanari, S.; Matteo, S.; Valentino, F.; Majone, M.; Villano, M. Impact of nitrogen feeding regulation on polyhydroxyalkanoates production by mixed microbial cultures. *New Biotechnol.* **2017**, *37*, 90–98. [CrossRef] [PubMed]
23. Valentino, F.; Morgan-Sagastume, F.; Campanari, S.; Villano, M.; Werker, A.; Majone, M. Carbon recovery from wastewater through bioconversion into biodegradable polymers. *New Biotechnol.* **2017**, *37*, 9–23. [CrossRef] [PubMed]
24. Baric, M.; Pierro, L.; Pietrangeli, B.; Papini, M.P. Polyhydroxyalkanoate (PHB) as a slow-release electron donor for advanced in situ bioremediation of chlorinated solvent-contaminated aquifers. *New Biotechnol.* **2014**, *31*, 377–382. [CrossRef] [PubMed]
25. Michalak, M.; Marek, A.A.; Zawadiak, J.; Kawalec, M.; Kurcok, P. Synthesis of PHB-based carrier for drug delivery systems with pH-controlled release. *Eur. Polym. J.* **2013**, *49*, 4149–4156. [CrossRef]
26. Getachew, A.; Woldesenbet, F. Production of biodegradable plastic by polyhydroxybutyrate (PHB) accumulating bacteria using low cost agricultural waste material. *BMC Res. Notes* **2016**, *9*, 1–9. [CrossRef] [PubMed]
27. Wacławek, S.; Chronopoulou, L.; Petrangeli Papini, M.; Vtp, V.; Palocci, C.; Kupčík, J.; Černík, M. Enhancement of stability and reactivity of nanosized zero-valent iron with polyhydroxybutyrate. *Desalin. Water Treat.* **2017**, *69*. [CrossRef]
28. Torkelson, T.R.; Oyen, F.; Rowe, V.K. The toxicity of chloroform as determined by single and repeated exposure of laboratory animals. *Am. Ind. Hyg. Assoc. J.* **1976**, *37*, 697–705. [CrossRef]
29. Rannug, U. Genotoxic effects of 1,2-dibromoethane and 1,2-dichloroethane. *Mutat. Res. Rev. Genet. Toxicol.* **1980**, *76*, 269–295. [CrossRef]
30. Silvestri, D.; Wacławek, S.; Sobel, B.; Torres-Mendieta, R.; Novotný, V.; Nguyen, N.H.A.; Ševců, A.; Padil, V.V.T.; Müllerová, J.; Stuchlík, M.; et al. A poly(3-hydroxybutyrate)-chitosan polymer conjugate for the synthesis of safer gold nanoparticles and their applications. *Green Chem.* **2018**, *20*, 4975–4982. [CrossRef]
31. Sharma, G.; Kumar, A.; Sharma, S.; Naushad, M.; Prakash Dwivedi, R.; ALOthman, Z.A.; Mola, G.T. Novel development of nanoparticles to bimetallic nanoparticles and their composites: A review. *J. King Saud Univ. Sci.* **2019**, *31*, 257–269. [CrossRef]
32. Shifrina, Z.B.; Matveeva, V.G.; Bronstein, L.M. Role of polymer structures in catalysis by transition metal and metal oxide Nanoparticle Composites. *Chem. Rev.* **2019**. [CrossRef] [PubMed]
33. Mei, Y.; Lu, Y.; Polzer, F.; Ballauff, M.; Drechsler, M. Catalytic activity of palladium nanoparticles encapsulated in spherical poly electrolyte brushes and core-shell microgels. *Chem. Mater.* **2007**, *19*, 1062–1069. [CrossRef]

34. Mei, Y.; Sharma, G.; Lu, Y.; Ballauff, M.; Drechsler, M.; Irrgang, T.; Kempe, R. High catalytic activity of platinum nanoparticles immobilized on spherical polyelectrolyte brushes. *Langmuir* **2005**, *21*, 12229–12234. [CrossRef] [PubMed]
35. Li, Z.; Yao, C.; Wang, Y.C.; Mikael, S.; Gunasekaran, S.; Ma, Z.; Cai, Z.; Wang, X. High-density platinum nanoparticle-decorated titanium dioxide nanofiber networks for efficient capillary photocatalytic hydrogen generation. *J. Mater. Chem. A* **2016**, *4*, 11672–11679. [CrossRef]
36. Wu, M.C.; Hsiao, K.C.; Chang, Y.H.; Chan, S.H. Photocatalytic hydrogen evolution of palladium nanoparticles decorated black TiO_2 calcined in argon atmosphere. *Appl. Surf. Sci.* **2018**, *430*, 407–414. [CrossRef]
37. Elsey, J.; Bubley, J.A.; Zhu, L.; Rao, S.; Sasaki, M.; Pollack, B.P.; Yang, L.; Arbiser, J.L. Palladium based nanoparticles for the treatment of advanced melanoma. *Sci. Rep.* **2019**, *9*, 3255. [CrossRef] [PubMed]
38. Samadi, A.; Klingberg, H.; Jauffred, L.; Kjær, A.; Bendix, P.M.; Oddershede, L.B. Platinum nanoparticles: A non-toxic, effective and thermally stable alternative plasmonic material for cancer therapy and bioengineering. *Nanoscale* **2018**, *10*, 9097–9107. [CrossRef]
39. Lai, J.; Luque, R.; Xu, G. Recent Advances in the Synthesis and Electrocatalytic Applications of Platinum-Based Bimetallic Alloy Nanostructures. *ChemCatChem* **2015**, *7*, 3206–3228. [CrossRef]
40. Wang, L.; Yamauchi, Y. Metallic nanocages: Synthesis of bimetallic Pt-Pd hollow nanoparticles with dendritic shells by selective chemical etching. *J. Am. Chem. Soc.* **2013**, *135*, 16762–16765. [CrossRef]
41. Lim, B.; Wang, J.; Camargo, P.H.C.; Cobley, C.M.; Kim, M.J.; Xia, Y. Twin-induced growth of palladium-platinum alloy nanocrystals. *Angew. Chem. Int. Ed.* **2009**, *48*, 6304–6308. [CrossRef]
42. Venkateshaiah, A.; Silvestri, D.; Ramakrishnan, R.K.; Wacławek, S.; Padil, V.V.T.; Černík, M.; Varma, R.S. Gum Kondagogu/Reduced Graphene Oxide Framed Platinum Nanoparticles and Their Catalytic Role. *Molecules* **2019**, *24*, 3643. [CrossRef] [PubMed]
43. Baruah, B.; Gabriel, G.J.; Akbashev, M.J.; Booher, M.E. Facile synthesis of silver nanoparticles stabilized by cationic polynorbornenes and their catalytic activity in 4-nitrophenol reduction. *Langmuir* **2013**, *29*, 4225–4234. [CrossRef] [PubMed]
44. Queiroz, M.F.; Melo, K.R.T.; Sabry, D.A.; Sassaki, G.L.; Rocha, H.A.O. Does the use of chitosan contribute to oxalate kidney stone formation? *Mar. Drugs* **2015**, *13*, 141–158. [CrossRef] [PubMed]
45. Dang Nguyen Vô, K.; Kowandy, C.; Dupont, L.; Coqueret, X. Evidence of chitosan-mediated reduction of Au(III) to Au(0) nanoparticles under electron beam by using OH and e-aq scavengers. *Chem. Commun.* **2015**, *51*, 4017–4020. [CrossRef]
46. Dorjnamjin, D.; Ariunaa, M.; Shim, Y.K. Synthesis of silver nanoparticles using hydroxyl functionalized ionic liquids and their antimicrobial activity. *Int. J. Mol. Sci.* **2008**, *9*, 807–820. [CrossRef]
47. Hu, P.; Song, Y.; Rojas-Andrade, M.D.; Chen, S. Platinum Nanoparticles Functionalized with Ethynylphenylboronic Acid Derivatives: Selective Manipulation of Nanoparticle Photoluminescence by Fluoride Ions. *Langmuir* **2014**, *30*, 5224–5229. [CrossRef]
48. Mendoza-Pérez, R.; Guisbiers, G. Bimetallic Pt-Pd nano-catalyst: Size, shape and composition matter. *Nanotechnology* **2019**, *30*, 305702. [CrossRef]
49. Zhang, Q.; Li, N.; Goebl, J.; Lu, Z.; Yin, Y. A systematic study of the synthesis of silver nanoplates: Is citrate a "magic" reagent? *J. Am. Chem. Soc.* **2011**, *133*, 18931–18939. [CrossRef]
50. Ghosh, A.; Dutta, S.; Mukherjee, I.; Biswas, S.; Chatterjee, S.; Saha, R. Template-free synthesis of flower-shaped zero-valent iron nanoparticle: Role of hydroxyl group in controlling morphology and nitrate reduction. *Adv. Powder Technol.* **2017**, *28*, 2256–2264. [CrossRef]
51. Long, N.V.; Hien, T.D.; Asaka, T.; Ohtaki, M.; Nogami, M. Synthesis and characterization of Pt–Pd nanoparticles with core-shell morphology: Nucleation and overgrowth of the Pd shells on the as-prepared and defined Pt seeds. *J. Alloys Compd.* **2011**, *509*, 7702–7709. [CrossRef]
52. Tuo, Y.; Liu, G.; Dong, B.; Yu, H.; Zhou, J.; Wang, J.; Jin, R. Microbial synthesis of bimetallic PdPt nanoparticles for catalytic reduction of 4-nitrophenol. *Environ. Sci. Pollut. Res.* **2017**, *24*, 5249–5258. [CrossRef]
53. Li, H.; Han, L.; Cooper-White, J.; Kim, I. Palladium nanoparticles decorated carbon nanotubes: Facile synthesis and their applications as highly efficient catalysts for the reduction of 4-nitrophenol. *Green Chem.* **2012**, *14*, 586. [CrossRef]
54. Huang, X.; Li, Y.; Li, Y.; Zhou, H.; Duan, X.; Huang, Y. Synthesis of PtPd bimetal nanocrystals with controllable shape, composition, and their tunable catalytic properties. *Nano Lett.* **2012**, *12*, 4265–4270. [CrossRef] [PubMed]

55. Zhu, C.; Guo, S.; Dong, S. Rapid, general synthesis of pdpt bimetallic alloy nanosponges and their enhanced catalytic performance for ethanol/methanol electrooxidation in an alkaline medium. *Chem. A Eur. J.* **2013**, *19*, 1104–1111. [CrossRef] [PubMed]
56. Yin, A.X.; Min, X.Q.; Zhang, Y.W.; Yan, C.H. Shape-selective synthesis and facet-dependent enhanced electrocatalytic activity and durability of monodisperse Sub-10 nm Pt-Pd tetrahedrons and cubes. *J. Am. Chem. Soc.* **2011**, *133*, 3816–3819. [CrossRef] [PubMed]
57. Lee, Y.W.; Ko, A.R.; Han, S.B.; Kim, H.S.; Park, K.W. Synthesis of octahedral Pt–Pd alloy nanoparticles for improved catalytic activity and stability in methanol electrooxidation. *Phys. Chem. Chem. Phys.* **2011**, *13*, 5569. [CrossRef]
58. Liu, X.Y.; Zhang, Y.; Gong, M.X.; Tang, Y.W.; Lu, T.H.; Chen, Y.; Lee, J.M. Facile synthesis of corallite-like Pt-Pd alloy nanostructures and their enhanced catalytic activity and stability for ethanol oxidation. *J. Mater. Chem. A* **2014**, *2*, 13840–13844. [CrossRef]
59. Scott, R.W.J.; Datye, A.K.; Crooks, R.M. Bimetallic Palladium-Platinum Dendrimer-Encapsulated Catalysts. *J. Am. Chem. Soc.* **2003**, *125*, 3708–3709. [CrossRef]
60. Datta, K.J.; Datta, K.K.R.; Gawande, M.B.; Ranc, V.; Čépe, K.; Malgras, V.; Yamauchi, Y.; Varma, R.S.; Zboril, R. Pd@Pt Core-Shell Nanoparticles with Branched Dandelion-like Morphology as Highly Efficient Catalysts for Olefin Reduction. *Chem. A Eur. J.* **2016**, *22*, 1577–1581. [CrossRef]
61. Wang, X.; Vara, M.; Luo, M.; Huang, H.; Ruditskiy, A.; Park, J.; Bao, S.; Liu, J.; Howe, J.; Chi, M.; et al. Pd@Pt Core—Shell Concave Decahedra: A Class of Catalysts for the Oxygen Reduction Reaction with Enhanced Activity and Durability. *J. Am. Chem. Soc.* **2015**, *137*, 15036–15042. [CrossRef]
62. Lim, B.; Jiang, M.; Camargo, P.H.C.; Cho, E.C.; Tao, J.; Lu, X.; Zhu, Y.; Xia, Y. Pd-Pt bimetallic nanodendrites with high activity for oxygen reduction. *Science* **2009**, *324*, 1302–1305. [CrossRef]
63. Wacławek, S.; Gončuková, Z.; Adach, K.; Fijałkowski, M.; Černík, M. Green synthesis of gold nanoparticles using Artemisia dracunculus extract: Control of the shape and size by varying synthesis conditions. *Environ. Sci. Pollut. Res.* **2018**, *25*, 24210–24219. [CrossRef] [PubMed]
64. Stumm, W.; Morgan, J.J. *Aquatic Chemistry: Chemical Equilibria and Rates in Natural Waters*; Wiley: Hoboken, NJ, USA, 2012; ISBN 1118591488.
65. Kästner, C.; Thünemann, A.F. Catalytic Reduction of 4-Nitrophenol Using Silver Nanoparticles with Adjustable Activity. *Langmuir* **2016**, *32*, 7383–7391. [CrossRef] [PubMed]
66. Gangula, A.; Podila, R.; Karanam, L.; Janardhana, C.; Rao, A.M. Catalytic reduction of 4-nitrophenol using biogenic gold and silver nanoparticles derived from breynia rhamnoides. *Langmuir* **2011**, *27*, 15268–15274. [CrossRef] [PubMed]
67. Lara, L.R.S.; Zottis, A.D.; Elias, W.C.; Faggion, D.; Maduro De Campos, C.E.; Acuña, J.J.S.; Domingos, J.B. The catalytic evaluation of in situ grown Pd nanoparticles on the surface of Fe3O4@dextran particles in the p-nitrophenol reduction reaction. *RSC Adv.* **2015**, *5*, 8289–8296. [CrossRef]
68. Ma, T.; Liang, F.; Chen, R.; Liu, S.; Zhang, H. Synthesis of Au-Pd bimetallic nanoflowers for catalytic reduction of 4-nitrophenol. *Nanomaterials* **2017**, *7*, 239. [CrossRef]
69. Chen, X.; Cai, Z.; Chen, X.; Oyama, M. AuPd bimetallic nanoparticles decorated on graphene nanosheets: Their green synthesis, growth mechanism and high catalytic ability in 4-nitrophenol reduction. *J. Mater. Chem. A* **2014**, *2*, 5668–5674. [CrossRef]
70. Wu, W.; Lei, M.; Yang, S.; Zhou, L.; Liu, L.; Xiao, X.; Jiang, C.; Roy, V.A.L. A one-pot route to the synthesis of alloyed Cu/Ag bimetallic nanoparticles with different mass ratios for catalytic reduction of 4-nitrophenol. *J. Mater. Chem. A* **2015**, *3*, 3450–3455. [CrossRef]
71. El-Bahy, Z.M.; Hanafy, A.I.; El-Bahy, S.M. Preparation of Pt, Pd and Cu nano single and bimetallic systems-supported NaY zeolite and test their activity in p-nitrophenol reduction and as anticancer agents. *J. Environ. Chem. Eng.* **2019**, *7*, 103117. [CrossRef]
72. Wang, Y.; Li, Q.; Zhang, P.; O'Connor, D.; Varma, R.S.; Yu, M.; Hou, D. One-pot green synthesis of bimetallic hollow palladium-platinum nanotubes for enhanced catalytic reduction of p-nitrophenol. *J. Colloid Interf. Sci.* **2019**, *539*, 161–167. [CrossRef]

© 2019 by the authors. Licensee MDPI, Basel, Switzerland. This article is an open access article distributed under the terms and conditions of the Creative Commons Attribution (CC BY) license (http://creativecommons.org/licenses/by/4.0/).

Synthesis of Ag nanoparticles by a chitosan-poly(3-hydroxybutyrate) polymer conjugate and their superb catalytic activity

Abstract: This work describes an eco–friendly and sustainable technique for the synthesis of silver nanoparticles (nAg), where chitosan–poly(3–hydroxybutyrate) polymer conjugate (Chit–PHB) acts as a reducing and stabilizing material. The ensuing nanoparticles show an exceptional catalytic activity in the reduction of 4–nitrophenol to 4–aminophenol. nAg were characterized by several techniques, SEM and TEM–EDX, to confirm their production, size and morphology. Furthermore, infrared spectroscopy analysis proved the presence of a Chit–PHB coating on the nAg. The excellent catalytic properties of the nAg–Chit–PHB was discernible when the activity parameter (κ_c) normalized by the specific surface area (SSA) of the nanoparticles was taken into consideration; normalization of κ_c by the SSA is a vital parameter for the assessment of the accessibility to the surface area of particles. Herein synthesized Ag nanoparticles, as far as we know, exhibited the fastest reaction kinetics of 4–nitrophenol reduction compared to the silver nanoparticles reported in the literature.

Citation: Silvestri, D.; Wacławek, S.; Venkateshaiah, A.; Krawczyk, K.; Sobel, B.; Padil, V.V.T.; Černík, M.; Varma, R.S. Synthesis of Ag nanoparticles by a chitosan-poly(3-hydroxybutyrate) polymer conjugate and their superb catalytic activity. *Carbohydr. Polym.* **2020**, *232*, 115806
Impact Factor: **10.7** (2021), citations **19** (WOS 25.01.2023)

Carbohydrate Polymers 232 (2020) 115806

Contents lists available at ScienceDirect

Carbohydrate Polymers

journal homepage: www.elsevier.com/locate/carbpol

Synthesis of Ag nanoparticles by a chitosan-poly(3-hydroxybutyrate) polymer conjugate and their superb catalytic activity

Daniele Silvestri[a], Stanisław Wacławek[a,*], Abhilash Venkateshaiah[a], Kamil Krawczyk[a], Bartłomiej Sobel[b], Vinod V.T. Padil[a], Miroslav Černík[a,*], Rajender S. Varma[c,*]

[a] Institute for Nanomaterials, Advanced Technologies and Innovation, Technical University of Liberec, Studentská 1402/2, 46117 Liberec 1, Czech Republic
[b] Institute of Engineering Materials and Biomaterials, Faculty of Mechanical Engineering, Silesian University of Technology, Konarskiego 18a St., 44–100 Gliwice, Poland
[c] Regional Centre of Advanced Technologies and Materials, Faculty of Science, Palacký University in Olomouc, Šlechtitelů 27, 783 71 Olomouc, Czech Republic

ARTICLE INFO

Keywords:
Green synthesis
Biopolymers
Silver nanoparticles
Catalytic reduction
4-nitrophenol

ABSTRACT

This work describes an eco-friendly and sustainable technique for the synthesis of silver nanoparticles (nAg), where chitosan-poly(3-hydroxybutyrate) polymer conjugate (Chit-PHB) acts as a reducing and stabilizing material. The ensuing nanoparticles show an exceptional catalytic activity in the reduction of 4-nitrophenol to 4-aminophenol. nAg were characterized by several techniques, i.e. SEM and TEM-EDX, to confirm their production, size and morphology. Furthermore, infrared spectroscopy analysis proved the presence of a Chit-PHB coating on the nAg. The excellent catalytic properties of the nAg-Chit-PHB was discernible when the activity parameter (κ_c) normalized by the specific surface area (SSA) of the nanoparticles was taken into consideration; normalization of κ_c by the SSA is a vital parameter for the assessment of the accessibility to the surface area of particles. Herein synthesized Ag nanoparticles, as far as we know, exhibited the fastest reaction kinetics of 4-nitrophenol reduction compared to the silver nanoparticles reported in the literature.

1. Introduction

Over the past twenty years, the green synthesis of nanomaterials has attracted enormous attention within the scientific community. The main reason behind this is the need to reduce or at least minimize the use of materials/substances and methods that present a potential threat to humans and the environment, e.g. the use of aqueous media instead toxic solvents (Rafique, Sadaf, Rafique, & Tahir, 2017).

Due to their remarkable properties, silver nanoparticles (nAg) are used in several scientific fields such as catalysis (Dong, Gao, Yang, Zhang, & Xu, 2015), medicine (Burdușel et al., 2018) and surface-enhanced Raman scattering (SERS) (Zhang, Li, Sun, & Li, 2005). In the medical field, nAg have garnered considerable interest owing to their inherent antimicrobial properties (Rai, Yadav, & Gade, 2009) on a wide range of microorganisms (Jadhav et al., 2018). The mechanism of reaction involves an interaction between the nanoparticles and the cell walls. After uptake, the nanoparticles can interact with DNA and proteins (Woo et al., 2008). Therefore, it is not surprising to see their major applications in medical devices (Marassi et al., 2018), dental materials (Noronha et al., 2017), textile fabrics (Tang et al., 2012), plastics and food packaging (Carbone, Donia, Sabbatella, & Antiochia, 2016). Their efficacy to induce apoptosis in cancer cells has also been reported (Sanpui, Chattopadhyay, & Ghosh, 2011).

Catalysts, classified as being either heterogeneous, homogeneous or biological (Wang, Li, & Zhang, 2018), are frequently used in a wide range of industrial processes to increase the rate of reactions. In order to be effective as a heterogeneous catalyst, the used material has to be stable at high temperatures and pressures (nAg meet both of these conditions) and presents active sites on the surface. Therefore, the surface area and accessibility to such active sites is a key point in heterogeneous catalysis. Moreover, to be suitable for full-scale applications, the catalyst must be affordable, which favours nAg over other precious catalysts [e.g., palladium, platinum, gold, and rhodium (Akbayrak, Gençtürk, Morkan, & Özkar, 2014; Stephen, Rees, Mikheenko, & Macaskie, 2019)].

Many studies have reported the synthesis of silver nanoparticles by assorted approaches such as chemical reduction (Wang, Qiao, Chen, & Ding, 2005), sonochemical (Li, Qin, Li, & Cui, 2018), photochemical (Giocondi & Rohrer, 2001), electrochemical (Rodríguez-Sánchez, Blanco, & Rodrı, 2000), microwave irradiation (Hebbalalu, Lalley,

* Corresponding authors.
E-mail addresses: daniele.silvestri@tul.cz (D. Silvestri), stanislaw.waclawek@tul.cz (S. Wacławek), abhilash.venkateshaiah@tul.cz (A. Venkateshaiah), kamil.krawczyk@tul.cz (K. Krawczyk), bartlomiej.sobel@polsl.pl (B. Sobel), vinod.padil@tul.cz (V.V.T. Padil), miroslav.cernik@tul.cz (M. Černík), Varma.Rajender@epa.gov (R.S. Varma).

https://doi.org/10.1016/j.carbpol.2019.115806
Received 14 November 2019; Received in revised form 28 December 2019; Accepted 29 December 2019
Available online 30 December 2019
0144-8617/ © 2019 Elsevier Ltd. All rights reserved.

Nadagouda, & Varma, 2013; Nadagouda, Speth, & Varma, 2011), physical methods [pulsed laser ablation (Machmudah, Sato, Wahyudiono, Sasaki, & Goto, 2012), spray pyrolysis (Brayner et al., 2010), ball milling (Khayati & Janghorban, 2012) and others (Lee & Jun, 2019)] and by biological approaches deploying fungi (Mukherjee et al., 2001), bacteria (Hebbalalu et al., 2013), plant extracts (Moulton et al., 2010; Nadagouda & Varma, 2008; Nadagouda et al., 2014), enzymes or biopolymers (Virkutyte & Varma, 2011). Of the reported approaches to obtaining silver nanoparticles, chemical reduction by sodium borohydride is one of the most sought-after owing to its versatility (Van Hyning & Zukoski, 1998) although it is considered a hazardous material for both the environment and humans. To overcome the threat posed by such harmful chemicals and to obtain nanoparticles with high catalytic activity, researchers have turned their focus to their greener synthesis. The use of sustainably synthesized nanoparticles in reduction is often hindered by their low efficiency arising from the less available surface area and consequently lower catalytic performance due to a limitation in the number of active sites present on the catalysts surface.

Since nanoparticles tend to agglomerate, polymers can be grafted onto their surface in order to improve their dispersion. Homogeneous dispersion leads to a narrow particle size distribution and as the size decreases the specific surface area of the particles increases, which improves their reactivity and makes them better catalysts material (Kango et al., 2013; Sharma, Yngard, & Lin, 2009). Particle size, reactivity, stability and solubility also depend on the concentration and type of polymer deployed (Jin et al., 2001; Tolaymat et al., 2010). Another important point in the synthesis of nanoparticles concerns the synthesis time. Furthermore, as a reduction in the synthesis time is associated with lower production costs, finding the appropriate synthesis conditions can render the whole process more economically feasible and sustainable (Cinelli et al., 2015).

Chitosan is one of the most abundant biopolymers in nature and can be produced primarily via deacetylation of chitin from the shells of crustaceans. It is used in several different fields, including medicine (Logithkumar et al., 2016), food packaging (de Moraes Crizel et al., 2018), synthesis and stabilization of nanomaterials (Tiwari, Mishra, Mishra, Arotiba, & Mamba, 2011) and others (Xu, Hein, Loo, & Wang, 2008). The main reason for chitosan being very popular and useful among biopolymers is its low-toxicity towards mammals (Landriscina, Rosen, & Friedman, 2015), as well as its good antibacterial properties (Kong, Chen, Xing, & Park, 2010). It is also considered as a biodegradable polymer and is, therefore, also used as a biopesticide (Masood, Randhawa, Butt, & Asghar, 2016), drug delivery material (Bernkop-Schnürch & Dünnhaupt, 2012), scaffold for cell proliferation (Cai, Li, Weihs, & Wang, 2017) and for bone implants (Ho et al., 2015). The main limitations of chitosan polymers are related to their low solubility in water at neutral or basic pH values. Therefore, in order to solubilize chitosan, the pH value of the solution needs to the substantially decreased or non-sustainable and hazardous solvents are required.

Polyhydroxybutyrate (PHB) is one of the most popular and widely used members of the polyhydroxyalkanoates family. It is synthesized by various bacterial strains (Huang & Reusch, 1996; Poirier, Somerville, Schechtman, Satkowski, & Noda, 1995) and can be accessed from waste material (Hilliou et al., 2016; Nielsen, Rahman, Rehman, Walsh, & Miller, 2017; Rodriguez-Perez, Serrano, Pantión, & Alonso-Fariñas, 2018; Silva et al., 2017; Valentino et al., 2017). Owing to its properties, PHB has been used as a drug delivery agent (Michalak, Marek, Zawadiak, Kawalec, & Kurcok, 2013), stabilizing agent (Wacławek et al., 2017), bioplastic (Getachew & Woldesenbet, 2016), and as a carbon source/electron donor in *in-situ* bioremediation (Baric, Pierro, Pietrangeli, & Papini, 2014; Petrangeli et al., 2016). PHB is hydrophobic and soluble only in few organic solvents (e.g. chloroform), which are toxic to humans or the environment (Rannug, 1980; Torkelson, Oyen, & Rowe, 1976).

To overcome the aforementioned solubility problems, chitosan (basic) and PHB (acidic) were simply admixed to generate a polymer conjugate (Chit-PHB) with enhanced solubility in water at a neutral pH; its use has been demonstrated for the successful green synthesis of safer gold nanoparticles (Silvestri et al., 2018).

The synthesis of nAg using chitosan as a reducing agent has been documented in the literature (Cinteza et al., 2018; Praveenkumar, Rabinal, Kalasad, Sankarappa, & Bedre, 2013) and a typical preparation requires around 10 − 12 h (Kalaivani et al., 2018; Regiel-Futyra et al., 2017). Twu et al. reported a fast synthesis of nAg by using chitosan; however, the temperatures employed during the reaction were extremely high (600 °C) (Twu, Chen, & Shih, 2008).

The present work investigates the possibility of producing nAg with enhanced catalytic activities by an eco-friendly and facile method. The use of the Chit-PHB conjugate was explored for the synthesis and stabilization of silver nanoparticles by this conjugate (nAg-Chit-PHB) with high catalytic activity. These synthesized nAg were then carefully characterized and tested for their catalytic prowess for the reduction of 4-nitrophenol (4-NP) to 4-aminophenol (4-AP). To the best of our knowledge, this is the first time a Chit-PHB conjugate has been employed to obtain stable nAg colloidal solutions.

2. Material and methods

2.1. Reagents and solution

Silver nitrate (≥99 %), sodium borohydride (≥96 %), 4-nitrophenol (≥99 %) and chitosan (low MW 50–190 kilo dalton, 75–85 % deacetylated) were purchased from Sigma-Aldrich. Nitric acid (65 %) was purchased from Lach ner. Polyhydroxybutyrate (Biomer® P209, PHB) was bought from Krailing, Germany. Deionised water [ELGA, Veolia Water (UK); 18.2 MΩ·cm^{-1}] was used in all of the tests.

2.2. Analytical

Absorption spectra were analysed in a UV–vis spectrophotometer (Hach Lange DR 3900) with matched 1 cm quartz cuvettes.

Fourier-transform infrared spectroscopy (FTIR) spectra (resolution of 4 cm^{-1} at 4000–700 cm^{-1}) were acquired with a germanium ATR crystal (NICOLET IZ10, Thermo Scientific, USA) equipped with a single reflection angle 45° horizontal ATR accessory.

Transmission electron microscope [field emission; Titan 80–300 TEM/STEM, (FEI Company)] was used for transmission electron microscope (TEM) analyses, equipped with a super twin lens (operated at 300 kV) and an annular dark-field detector. A scanning electron microscope (UHR FE-SEM Carl Zeiss ULTRA Plus, Germany) working at an acceleration V of 0.5–2.5 kV was used to observe the nanoparticle's structure. Energy-dispersive X-ray spectroscopy (EDX, Oxford Instruments AZtec) analyses were performed to observe the occurrence of different elements.

A Zetasizer ZS (Malvern Instruments Ltd, UK) was operated for the zeta potential measurements prepared in a fresh suspension. The analyses were performed with ten-second autocorrelation functions. Triplicate measurements were made, and each result is the average of the three.

2.3. Preparation of the conjugate

The conjugate was prepared employing the method described previously by us (Silvestri et al., 2018). Briefly, the solution of chitosan was made by adding 1 g of chitosan in 200 mL of acidified water and was stirred to obtain a homogeneous solution. A total of 0.24 g of PHB was added to this solution and was kept overnight at 80 °C under continuous stirring. Subsequently, the obtained solution was sonicated for 30 min at 80 °C. After sonication, the solution was purified by a dialysis tube and then freeze-dried.

2.4. Preparation of nanoparticles

nAg-Chit-PHB was synthesized by adding 0.1 g of Chit-PHB conjugate to a closed vial containing 9 mL of DI water and stirring at 90 °C to obtain a homogeneous solution. A total of 1 mL of silver nitrate solution was added (dropwise) to the Chit-PHB mixture at 90 °C under dynamic stirring. Subsequently, the vial was tightly closed and stirred continuously until the end of the reaction. To find optimal parameters for the synthesis, preparation of nAg-Chit-PHB was also carried out under various conditions such as: different Chit-PHB concentration (from 1 to 30 g/L), silver precursor concentration (from 0.25 to 4 mM) and reaction time (from 30 − 300 min).

2.5. Catalytic test

The catalytic test for the reduction of 4-NP to 4-AP by $NaBH_4$ was performed in a standard quartz cuvette (1 cm path length) and was adapted from previously reported work by Baruah, Gabriel, Akbashev, & Booher (2013). Briefly, the test was conducted by adding 24 µL of 4-NP (5 mM) into Eppendorf tube (1.5 mL) and mixed with 12 µL of nAg-Chit-PHB. This was followed by the addition of 120 µL of $NaBH_4$ (0.1 M) as a reducing agent and the volume was raised to 1 mL by adding DI water. After mixing, the solution was immediately transferred to a quartz cell, and the absorbance was recorded by UV–vis (Hach Lange DR 3900) at regular intervals. All of the tests were performed at room temperature (25 °C).

3. Results and discussion

3.1. nAg preparation

The main aim of this work was to use the Chit-PHB conjugate as a reducing and stabilizing agent for the greener synthesis of monodisperse nAg, and to study their activity in the catalytic reduction of 4-NP. It is well recognised that some metal nanoparticles show special optical properties; nAg in particular can be easily detected by UV–vis due to their characteristic plasmon resonance frequency (around 415 nm). Therefore, UV–vis was used to determine the influence of different parameters on the performance of synthesis (Fig. 1).

The absorption peak at 415 nm found in all of the samples confirmed the formation of nAg. The intensity of this absorption peak was observed to be proportional to the reaction time (Fig. 1a and b). This suggests that there is a linear relationship among the concentration and the reaction time of nAg. From the results obtained by UV–vis analysis (highest intensity/narrowest peak without visible nanoparticles aggregation; aggregation was observed for samples reacting more than 240 min), it was deduced that 240 min is the optimum reaction time and was maintained in all of the subsequent experiments.

After obtaining the optimum reaction time, we then varied the Chit-PHB conjugate concentration from 1 to 30 g/L to determine the ideal concentration of the polymer conjugate (Fig. 1c). The UV–vis spectra of nAg-Chit-PHB suggest the formation of nAg for all of the studied concentrations of the conjugate. In addition to obtaining the nanoparticles, it was observed that at lower conjugate concentration of 1, 2 and 5 g/L, the concentration of the obtained particles was also lower. Besides the main peak in the UV–vis spectra, another peak at ~535 nm was obtained for these low concentrations of conjugates which can be ascribed to the lack or overdose of conjugate resulting in particle agglomeration (Dang, Dang, & Fribourg-Blanc, 2014; Ziegler, Klose, Voitekhovich, Gaponik, & Eychmüller, 2011), e.g. a lack of the stabilizing agent; the nanoparticles aggregation was also confirmed based on the TEM particle size distribution (data not shown). In the samples made at a conjugate concentration of 10 g/L, this peak disappeared, indicating no (or low) agglomeration. For the highest conjugate concentrations (20 and 30 g/L), the spectra dramatically changed, which indicated probable agglomeration (moreover, a sediment on the bottom of the reactor was visible). Subsequently, a conjugate concentration of 10 g/L was selected as being ideal for obtaining large amounts of nanoparticles without their aggregation.

The influence of the precursor ($AgNO_3$) concentration confirmed that nanoparticles were formed in all of the precursor concentrations (from 0.25 to 4 mM) (Fig. 1d). At the lowest concentration (0.25 mM), the UV–vis spectrum showed a broad peak with low intensity, suggesting minimum nanoparticle formation. However, when the

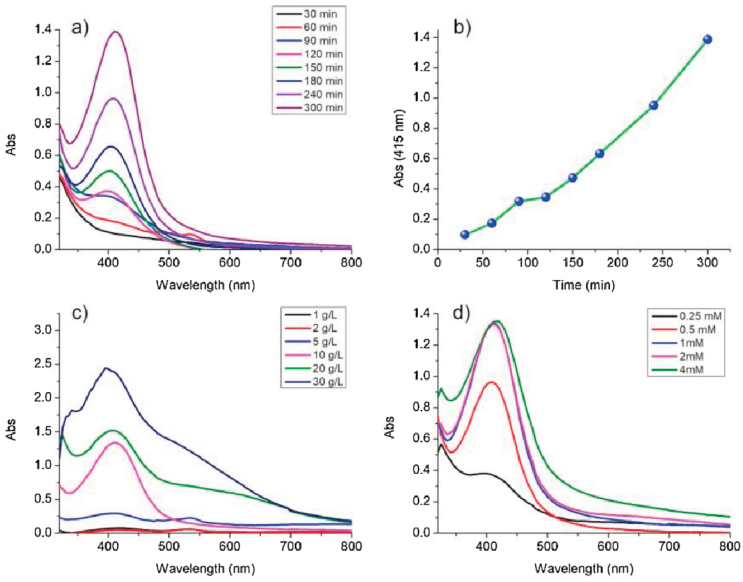

Fig. 1. UV–vis spectra determined by various conditions a) influence of the synthesis time, b) relationship between the absorbance at 415 nm and time of reaction, c) influence of the conjugate concentration ($AgNO_3$: 1 mM) and d) influence of the precursor concentration for the nAg production (general conditions: Chit-PHB: 10 g/L, $AgNO_3$: 0.5 mM, temperature: 90 °C).

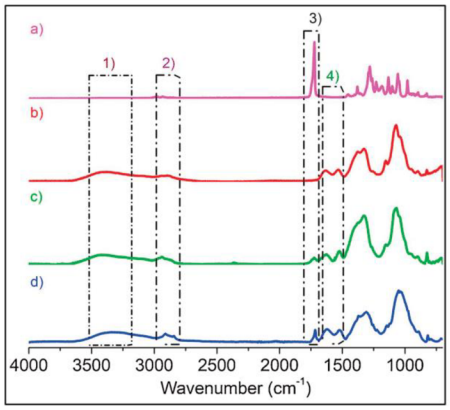

Fig. 2. FTIR analyses of a) PHB, b) chitosan, c) Chit-PHB conjugate, d) nAg-Chit-PHB. The dashed rectangles identify the regions of the spectra where 1) peaks of O—H and N—H bonds, 2) symmetric or asymmetric CH_2 stretching, 3) ester groups, 4) amide type II and amine functional groups could be identified.

concentration increased to 0.5 mM, the absorption peak narrowed down indicating successful synthesis of nanoparticles without extensive agglomeration.

The optimum synthesis conditions were: a synthesis time of 240 min, Chit-PHB conjugate concentration of 10 g/L, and initial precursor concentration of 0.5 mM.

3.2. FTIR analysis

An FTIR analysis was conducted in order to obtain more information about the functional groups present on the surface of nAg-Chit-PHB. The PHB spectrum in Fig. 2a shows a peak at $\sim 1724\ cm^{-1}$ corresponding to the ester group. On the other hand, the chitosan spectrum in Fig. 2b exhibits a band at $\sim 3300\ cm^{-1}$, which could be linked to the N—H and O—H bonds. The peak at $\sim 2900\ cm^{-1}$ is ascribable to the symmetric or asymmetric CH_2 stretching vibration, while the peak at $\sim 1600\ cm^{-1}$ is present due to the NH_2 group. The last representative peak at $\sim 1100\ cm^{-1}$ can be ascribed to C—O—C glycosidic linkage. The conjugate spectrum in Fig. 2c shows significant differences compared to PHB and chitosan spectra alone, the NH_2 group at $\sim 1600\ cm^{-1}$ has a lower intensity than the chitosan sample, but the peak intensity assigned to the amide type II ($\sim 1555\ cm^{-1}$) is higher, indicating a reaction between the amino group of chitosan with the ester group of PHB and the formation of an amide linkage (Santos et al., 2015). On the other hand, the FTIR spectrum of nAg (stabilized by conjugate) (Fig. 2d) shows several bands. The first one ($\sim 3330\ cm^{-1}$) can be ascribed to NH / OH functional groups, the one at $\sim 2926\ cm^{-1}$ to the asymmetric or symmetric CH_2 stretching vibration, while the NH_2 and secondary amide functional groups can be found at $\sim 1620\ cm^{-1}$ and $\sim 1558\ cm^{-1}$, respectively. The hydroxyl groups present on the conjugate may reduce the silver ions as reported by Dang Nguyen Vô, Kowandy, Dupont, and Coqueret (2015) and Dorjnamjin, Ariunaa, and Shim (2008). Due to the high concentration of conjugate (10 g/L) used in the synthesis process, an excess of the hydroxyl groups was clearly

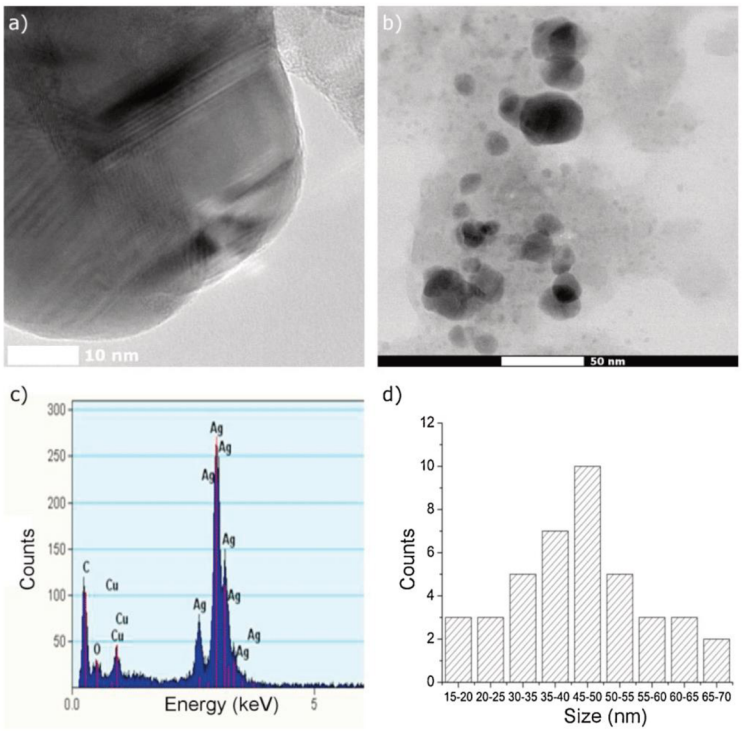

Fig. 3. a) HRTEM, b) TEM, c) EDX and d) particle size distribution of nAg-Chit-PHB (Chit-PHB: 10 g/L, $AgNO_3$: 0.5 mM, temperature: 90 °C).

visible in the FTIR analysis. Moreover, FTIR showed the presence of the conjugate layer on the surface of the nAg [ester group ~1724 cm^{-1} (Fig. 2: dashed rectangle 3) and amide type II ~1555 cm^{-1} (Fig. 2: dashed rectangle 4)]. The presence of the conjugate on the surface of the nanoparticles is slightly different than for gold nanoparticles (Silvestri et al., 2018), which can be assigned to the different reaction pathways of silver and gold with the conjugate. One possible explanation of this phenomenon could be that the gold precursor is more prone to be reduced due to a higher standard reduction potential [vs standard hydrogen electrode (E° = +1.4 V)] than the silver precursor (E° = +0.8 V). For example, recently Chit-PHB was used for the synthesis of bimetallic Pd/Pt nanoparticles (standard reduction potentials of platinum and palladium precursors are similar to the silver one and range from 0.726 to 0.915 V) and the organic functional groups on their surface were similar to the ones reported herein, suggesting the presence of the conjugate on the surface (Silvestri et al., 2019).

3.3. TEM/EDX analysis

Morphological analysis is fundamental for studying the structure and state of nanomaterials. Fig. 3a and b show HRTEM and TEM images of nAg-Chit-PHB, respectively. The analyses demonstrated a quasi-spherical shape of nAg. Moreover, based on the TEM micrographs, the particle size distribution oscillated around 45 nm with a relatively narrow distribution (Fig. 3d). EDX analysis (Fig. 3c) confirmed the presence of nAg, carbon and oxygen atoms on their surface, which is in accordance with the FTIR analysis, and it confirmed the existence of the conjugate layer on the nAg surface.

3.4. Catalytic tests

Nitroaromatics are often used in the synthesis of drugs, dyes and pesticides; however, they are reported to manifest toxicity for bacteria, plants, oceanic fauna and humans (Albukhari, Ismail, Akhtar, & Danish, 2019). Consequently, we explored the use of prepared nAg as a catalyst for the reduction of 4-NP to 4-AP (Fig. 4). The highest absorption peak of the 4-NP solution was shown at 317 nm. By adding sodium borohydride to the solution, the absorption peak shifted from ~317 nm to 401 nm due to the generation of 4-nitrophenolate; the colour of the suspension changed to bright yellow. In the absence of catalysts, the absorption at 401 nm remained stable for 40 min (data not shown). This implies that the reduction to 4-AP did not proceed without the catalyst due to a high kinetic barrier. The nAg catalyst acts by borohydride anions and 4-NP being adsorbed on the surface of the nAg. The zeta potential of +17.2 ± 0.6 mV of the nAg-Chit-PHB surface can help speed up the reaction due to the attraction of a negative charge of BH_4^-. Then, BH_4^- transfers an electron to nAg, forming a negative charge layer on the surface of the nAg. Nanoparticles serve as an electron relay, transferring the received electron to the 4-NP, whereby reducing it (Silvestri et al., 2019).

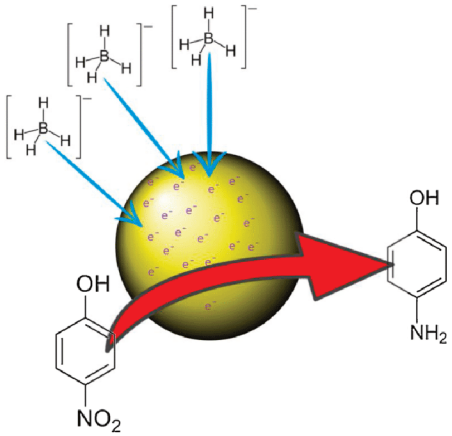

Fig. 4. Reduction of 4-NP to 4-AP by the electron transfer mechanism.

The reductive reaction in the presence of the catalyst (nAg-Chit-PHB) can be monitored by measuring the decrease in 4-nitrophenolate (the absorbance at 401 nm). The reaction kinetics were fitted using the pseudo-first-order kinetic model to reveal the catalytic performance of nAg (Stumm & Morgan, 2012). The absorbance is equivalent to the concentration of 4-NP in the solution. Eq. (1) was used to calculate the kinetic rate constants:

$$\ln\left(\frac{A_t}{A_0}\right) = -k_{app}t \quad (1)$$

where A_0 and A_t are the initial measured absorbance (t = 0) and at time t (proportional to the 4-NP concentration), respectively, and k_{app} is an apparent rate constant of the first order. The concentration of the nanoparticles used affects their catalytic activity. By increasing the concentration of the nanoparticles, k_{app} also increases due to an increase in the total surface area, resulting in more active sites available for the reaction. The k_{app} of the 4-NP reduction was determined to be 0.041 min^{-1}, 0.147 min^{-1}, 0.206 min^{-1} and 0.921 min^{-1}, for the concentrations of nAg-Chit-PHB of 0.021, 0.028, 0.042 and 0.088 mg/L, respectively (Fig. 5).

Because previous authors, e.g. Lara et al. (2015) or Kästner and Thünemann (2016) have already reported the linear correlation between k_{app} and the catalyst concentration, we have also used the slope of the linear regression line between k_{app} and the nanoparticles concentration to determine the activity parameter (κ_c). The value determined for our study (151 ± 17 L g^{-1} s^{-1} with R^2 = 0.93) was compared to other reported values (Table 1).

For a better understanding of the catalytic activities of nanoparticles, it is not possible to ignore the specific surface area and accessibility. In our opinion, to obtain nanoparticles with enhanced catalytic activity, it is mandatory to have high accessibility to active sites on the surface of the nanoparticles. For this reason, normalizing the κ_c values with the specific surface area (SSA) can provide important information on the reactivity of the nanoparticles. Based on the fact that the nanoparticles have the same density as a bulk material (Kästner & Thünemann, 2016), the SSA of nanoparticles was estimated [basing on the equation: SSA = $6000/d\rho$; Where d is the diameter (nm) and ρ is the

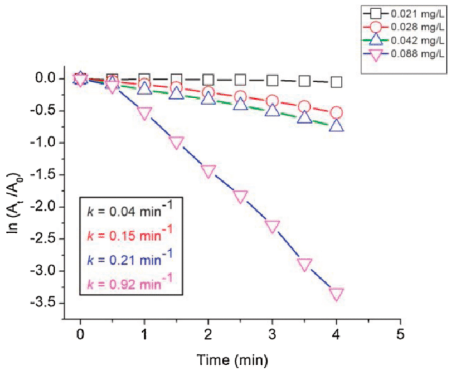

Fig. 5. Kinetic of 4-NP reduction for different nAg-Chit-PHB catalyst concentrations [conditions: 25 °C, 4-NP: 0.12 mM and $NaBH_4$: 1.2 mM; the standard deviation between the measurements is less than < 5 % (n = 3)].

Table 1
Comparison of different nanocatalysts reported in the literature for the reduction of 4-NP.

Catalyst	Catalyst concentration (10^{-3} g/L)	k_{app} (10^{-3} sec^{-1})	κ_c (sec^{-1} : g/L)	Diameter (nm)	SSA ($m^2 g^{-1}$)	κ_c/SSA (L m^{-2} s^{-1})	Reference
nAg-Chit-PHB	0.021–0.088	0.7–15	151 ± 17	45	13	11.6 ± 1.3	This work
Ag-PAA	0.035	15	436	6	95	4.58	(Kästner & Thünemann, 2016)
AgNP-PG-5K	4	5.5	1.4	18	31	0.044	(Baruah, Gabriel, Akbashev, & Booher, 2013)
AgNP@PGMA-SH	0.9	3.9	4.4	19	30	0.146	(Zhang, Sun, & Zhang, 2015)
nAg-hydroxyapatite	2	7.3	3.6	15	38	0.096	(Das, Ganguly, Bhawal, Mondal, & Das, 2018)
AuNBCs	1.989	2.8	1.4	5	62	0.022	(Das, Dickinson, Lafir, Brougham, & Marsili, 2012)
TAC-Ag	1.33	5.2	3.9	–	–	–	(Rashid & Mandal, 2007)
AgNPs@MWCNTs	0.84	7.9	9.4	3	191	0.049	(Alshehri et al., 2016)

density of nanoparticles (g cm^{-3})] to be 13 $m^2 g^{-1}$ and then the specific surface area normalized κ_c value (κ_c / SSA) was calculated to be 11.6 ± 1.3 L m^{-2} s^{-1}. With respect to the above values, the nanoparticles synthesized using the Chit-PHB conjugate are more than two-times more active as the most efficient nanoparticles (used for catalysis) reported in the literature (Kästner & Thünemann, 2016). Such outstanding catalytic properties of nAg-Chit-PHB can be due to a positive zeta potential and the specific functional groups present on the surface of the particles. Also, the *N*-functional groups present on the nAg-Chit-PHB can affect the kinetics of the reaction. In example, Xiong et al. (2018) reported the possibility of enhancing the catalytic activities of Mo_2C-C by incorporating *N*-functional groups.

4. Conclusion

The present work describes the use of Chit-PHB to enhance the catalytic properties of silver nanoparticles. Compared to chitosan, the conjugate had better properties for the synthesis of nAg, especially exhibited dramatic shortening of the synthesis time (by several hours); optimum synthesis time determined for the nAg being four hours with the optimum synthesis temperature of 90 °C. By applying the data obtained from the UV–vis analysis, further optimum synthesis conditions were Chit-PHB concentration of 10 g/L and $AgNO_3$ of 0.5 mM. The obtained nanoparticles were analysed with FTIR to understand the functional groups present on them, which affirmed the presence of a Chit-PHB layer on the surface of the nAg. TEM analysis made it possible to appreciate the quasi-spherical shape of the nanoparticles with a mean size of approximately 45 nm.

Furthermore, the produced nanoparticles showed incredible catalytic activity in the reduction of 4-NP. The enhanced catalytic activity was due to the existence of *N*-functional groups present on the surface of these nanoparticles and a positive zeta potential (+17.2 ± 0.6 mV), which helped the electron transfer process.

The nAg-Chit-PHB were tested as catalyst for the reduction of 4-NP to 4-AP. The apparent first-order kinetic constant k_{app} was estimated to be 0.921 min^{-1} for a nAg-Chit-PHB concentration of 0.088 mg/L. The activity parameter κ_c was calculated in order to compare with other nanomaterials reported in the literature. The κ_c value was found to be 151 L g^{-1} s^{-1}, which is significantly higher than for other silver nanoparticles. To further analyse the catalytic performance of nAg-Chit-PHB, the κ_c value was normalized by SSA. To the best of our knowledge, a value of 11.6 L m^{-2} s^{-1} is the highest value reported for silver nanoparticles.

Declaration of Competing Interest

The authors declare that they have no conflict of interest.

Acknowledgements

This research was supported by the SGS (Student Grant Competition) project at the Technical University of Liberec in 2019. Moreover, we also acknowledge the assistance provided by the Ministry of Education, Youth and Sports in the framework of the targeted support of the OPR&DI project "Extension of CXI facilities" (CZ.1.05/2.1.00/19.0386), the Research Infrastructures NanoEnviCz (Project No. LM2015073) and the project Pro-NanoEnviCz (Reg. No. CZ.02.1.01/0.0/0.0/16_013/0001821) supported also by the European Union - European Structural and Investments Funds in the frame of Operational Programme Research Development and Education.

References

Akbayrak, S., Gençtürk, S., Morkan, İ., & Özkar, S. (2014). Rhodium(0) nanoparticles supported on nanotitania as highly active catalyst in hydrogen generation from the hydrolysis of ammonia borane. *RSC Advances, 4*(26), 13742–13748. https://doi.org/10.1039/C4RA00469H.

Albukhari, S. M., Ismail, M., Akhtar, K., & Danish, E. Y. (2019). Catalytic reduction of nitrophenols and dyes using silver nanoparticles @ cellulose polymer paper for the resolution of waste water treatment challenges. *Colloids and Surfaces A, Physicochemical and Engineering Aspects, 577*, 548–561. https://doi.org/10.1016/j.colsurfa.2019.05.058.

Alshehri, S. M., Almuqati, T., Almuqati, N., Al-Farraj, E., Alhokbany, N., & Ahamad, T. (2016). Chitosan based polymer matrix with silver nanoparticles decorated multi-walled carbon nanotubes for catalytic reduction of 4-nitrophenol. *Carbohydrate Polymers, 151*, 135–143. https://doi.org/10.1016/j.carbpol.2016.05.018.

Baric, M., Pierro, L., Pietrangeli, B., & Papini, M. P. (2014). Polyhydroxyalkanoate (PHB) as a slow-release electron donor for advanced in situ bioremediation of chlorinated solvent-contaminated aquifers. *New Biotechnology, 31*(4), 377–382. https://doi.org/10.1016/j.nbt.2013.10.008.

Baruah, B., Gabriel, G. J., Akbashev, M. J., & Booher, M. E. (2013). Facile synthesis of silver nanoparticles stabilized by cationic polynorbornenes and their catalytic activity in 4-nitrophenol reduction. *Langmuir, 29*(13), 4225–4234. https://doi.org/10.1021/la305068p.

Bernkop-Schnürch, A., & Dünnhaupt, S. (2012). Chitosan-based drug delivery systems. *European Journal of Pharmaceutics and Biopharmaceutics, 81*(3), 463–469. https://doi.org/10.1016/j.ejpb.2012.04.007.

Brayner, R., Iglesias, R., Truong, S., Beji, Z., Felidj, N., Fiévet, F., ... Aubard, J. (2010). Surface-enhanced raman scattering on silver nanostructured films prepared by spray-deposition. *Langmuir, 26*(22), 17465–17469. https://doi.org/10.1021/la102722v.

Burduşel, A.-C., Gherasim, O., Grumezescu, A. M., Mogoantă, L., Ficai, A., Andronescu, E., ... Andronescu, E. (2018). Biomedical applications of silver nanoparticles: An up-to-date overview. *Nanomaterials, 8*(9), 681. https://doi.org/10.3390/nano8090681.

Cai, S.-J., Li, C.-W., Weihs, D., & Wang, G.-J. (2017). Control of cell proliferation by a porous chitosan scaffold with multiple releasing capabilities. *Science and Technology of Advanced Materials, 18*(1), 987–996. https://doi.org/10.1080/14686996.2017.1406287.

Carbone, M., Donia, D. T., Sabbatella, G., & Antiochia, R. (2016). Silver nanoparticles in polymeric matrices for fresh food packaging. *Journal of King Saud University - Science, 28*(4), 273–279. https://doi.org/10.1016/J.JKSUS.2016.05.004.

Cinelli, M., Coles, S. R., Nadagouda, M. N., Błaszczyński, J., Słowiński, R., Varma, R. S., ... Kirwan, K. (2015). A green chemistry-based classification model for the synthesis of silver nanoparticles. *Green Chemistry, 17*(5), 2825–2839. https://doi.org/10.1039/C4GC02088J.

Cinteza, L. O., Scomoroscenco, C., Voicu, S. N., Nistor, C. L., Nitu, S. G., Trica, B., ... Petcu, C. (2018). Chitosan-stabilized ag nanoparticles with superior biocompatibility and their synergistic antibacterial effect in mixtures with essential oils. *Nanomaterials, 8*(10), https://doi.org/10.3390/nano8100826.

Dang, M. C., Dang, T. M. D., & Fribourg-Blanc, E. (2014). Silver nanoparticles ink

synthesis for conductive patterns fabrication using inkjet printing technology. *Advances in Natural Sciences Nanoscience and Nanotechnology, 6*(1), 015003. https://doi.org/10.1088/2043-6262/6/1/015003.

Dang Nguyen Vô, K., Kowandy, C., Dupont, L., & Coqueret, X. (2015). Evidence of chitosan-mediated reduction of Au(III) to Au(0) nanoparticles under electron beam by using OH and e-aq scavengers. *Chemical Communications, 51*(19), 4017–4020. https://doi.org/10.1039/c4cc09346a.

Das, S. K., Dickinson, C., Lafir, F., Brougham, D. F., & Marsili, E. (2012). Synthesis, characterization and catalytic activity of gold nanoparticles biosynthesized with Rhizopus oryzae protein extract. *Green Chemistry, 14*(5), 1322. https://doi.org/10.1039/c2gc16676c.

Das, T. K., Ganguly, S., Bhawal, P., Mondal, S., & Das, N. C. (2018). A facile green synthesis of silver nanoparticle-decorated hydroxyapatite for efficient catalytic activity towards 4-nitrophenol reduction. *Research on Chemical Intermediates, 44*(2), 1189–1208. https://doi.org/10.1007/s11164-017-3161-7.

de Moraes Crizel, T., de Oliveira Rios, A., Alves, V. D., Bandarra, N., Moldão-Martins, M., & Hickmann Flôres, S. (2018). Active food packaging prepared with chitosan and olive pomace. *Food Hydrocolloids, 74*, 139–150. https://doi.org/10.1016/j.foodhyd.2017.08.007.

Dong, X.-Y., Gao, Z.-W., Yang, K.-F., Zhang, W.-Q., & Xu, L.-W. (2015). Nanosilver as a new generation of silver catalysts in organic transformations for efficient synthesis of fine chemicals. *Catalysis Science & Technology, 5*(5), 2554–2574. https://doi.org/10.1039/C5CY00285K.

Dorjnamjin, D., Ariunaa, M., & Shim, Y. K. (2008). Synthesis of silver nanoparticles using hydroxyl functionalized ionic liquids and their antimicrobial activity. *International Journal of Molecular Sciences, 9*(5), 807–820. https://doi.org/10.3390/ijms9050807.

Getachew, A., & Woldesenbet, F. (2016). Production of biodegradable plastic by polyhydroxybutyrate (PHB) accumulating bacteria using low cost agricultural waste material. *BMC Research Notes, 9*(1), 1–9. https://doi.org/10.1186/s13104-016-2321-y.

Giocondi, J. L., & Rohrer, G. S. (2001). Spatially selective photochemical reduction of silver on the surface of ferroelectric barium titanate. *Chemistry of Materials, 13*(2), 241–242. https://doi.org/10.1021/cm000890h.

Hebbalalu, D., Lalley, J., Nadagouda, M. N., & Varma, R. S. (2013). Greener techniques for the synthesis of silver nanoparticles using plant extracts, enzymes, bacteria, biodegradable polymers, and microwaves. *ACS Sustainable Chemistry & Engineering, 1*(7), 703–712. https://doi.org/10.1021/sc4000362.

Hilliou, L., Machado, D., Oliveira, C. S. S., Gouveia, A. R., Reis, M. A. M., Campanari, S., ... Majone, M. (2016). Impact of fermentation residues on the thermal, structural, and rheological properties of polyhydroxy(butyrate-co-valerate) produced from cheese whey and olive oil mill wastewater. *Journal of Applied Polymer Science, 133*(2), https://doi.org/10.1002/app.42818.

Ho, M. H., Yao, C. J., Liao, M. H., Lin, P. I., Liu, S. H., & Chen, R. M. (2015). Chitosan nanofiber scaffold improves bone healing via stimulating trabecular bone production due to upregulation of the Runx2/osteocalcin/alkaline phosphatase signaling pathway. *International Journal of Nanomedicine, 10*, 5941–5954. https://doi.org/10.2147/IJN.S90669.

Huang, R., & Reusch, R. N. (1996). Poly(3-hydroxybutyrate) is associated with specific proteins in the cytoplasm and membranes of *Escherichia coli*. *The Journal of Biological Chemistry, 271*(36), 22196–22202. https://doi.org/10.1074/jbc.271.36.22196.

Jadhav, K., Deore, S., Dhamecha, D., H R, R., Jagwani, S., Jalalpure, S., ... Bohara, R. (2018). Phytosynthesis of silver nanoparticles: Characterization, biocompatibility studies, and anticancer activity. *ACS Biomaterials Science & Engineering, 4*(3), 892–899. https://doi.org/10.1021/acsbiomaterials.7b00707.

Jin, R., Cao, Y., Mirkin, C. A., Kelly, K. L., Schatz, G. C., & Zheng, J. G. (2001). Photoinduced conversion of silver nanospheres to nanoprisms. *Science, 294*(5548), 1901–1903. https://doi.org/10.1126/science.1066541.

Kalaivani, R., Maruthupandy, M., Muneeswaran, T., Hameedha Beevi, A., Anand, M., Ramakritinan, C. M., ... Kumaraguru, A. K. (2018). Synthesis of chitosan mediated silver nanoparticles (Ag NPs) for potential antimicrobial applications. *Frontiers in Laboratory Medicine, 2*(1), 30–35. https://doi.org/10.1016/j.flm.2018.04.002.

Kango, S., Kalia, S., Celli, A., Njuguna, J., Habibi, Y., & Kumar, R. (2013). Surface modification of inorganic nanoparticles for development of organic–inorganic nanocomposites—A review. *Progress in Polymer Science, 38*(8), 1232–1261. https://doi.org/10.1016/j.progpolymsci.2013.02.003.

Kästner, C., & Thünemann, A. F. (2016). Catalytic reduction of 4-nitrophenol using silver nanoparticles with adjustable activity. *Langmuir, 32*(29), 7383–7391. https://doi.org/10.1021/acs.langmuir.6b01477.

Khayati, G. R., & Janghorban, K. (2012). The nanostructure evolution of Ag powder synthesized by high energy ball milling. *Advanced Powder Technology, 23*(3), 393–397. https://doi.org/10.1016/J.APT.2011.05.005.

Kong, M., Chen, X. G., Xing, K., & Park, H. J. (2010). Antimicrobial properties of chitosan and mode of action: A state of the art review. *International Journal of Food Microbiology, 144*(1), 51–63. https://doi.org/10.1016/j.ijfoodmicro.2010.09.012.

Landriscina, A., Rosen, J., & Friedman, A. J. (2015). Biodegradable chitosan nanoparticles in drug delivery for infectious disease. *Nanomedicine, 10*(10), 1609–1619. https://doi.org/10.2217/nnm.15.7.

Lara, L. R. S., Zottis, A. D., Elias, W. C., Faggion, D., Maduro De Campos, C. E., Acuña, J. J. S., ... Domingos, J. B. (2015). The catalytic evaluation of in situ grown Pd nanoparticles on the surface of Fe_3O_4@dextran particles in the p-nitrophenol reduction reaction. *RSC Advances, 5*(11), 8289–8296. https://doi.org/10.1039/c4ra16440g.

Lee, S., & Jun, B.-H. (2019). Silver nanoparticles: Synthesis and application for nanomedicine. *International Journal of Molecular Sciences, 20*(4), 865. https://doi.org/10.3390/ijms20040865.

Li, J.-X., Qin, Z.-B., Li, Y.-H., & Cui, G.-H. (2018). Sonochemical synthesis and properties of two new nanostructured silver(I) coordination polymers. *Ultrasonics Sonochemistry, 48*, 127–135. https://doi.org/10.1016/j.ultsonch.2018.05.016.

Logithkumar, R., Keshavnarayan, A., Dhivya, S., Chawla, A., Saravanan, S., & Selvamurugan, N. (2016). A review of chitosan and its derivatives in bone tissue engineering. *Carbohydrate Polymers, 151*, 172–188. https://doi.org/10.1016/j.carbpol.2016.05.049.

Machmudah, S., Sato, T., Wahyudiono, Sasaki, M., & Goto, M. (2012). Silver nanoparticles generated by pulsed laser ablation in supercritical CO_2 medium. *High Pressure Research, 32*(1), 60–66. https://doi.org/10.1080/08957959.2011.649277.

Marassi, V., Di Cristo, L., Smith, S. G. J., Ortelli, S., Blosi, M., Costa, A. L., ... Prina-Mello, A. (2018). Silver nanoparticles as a medical device in healthcare settings: A five-step approach for candidate screening of coating agents. *Royal Society Open Science, 5*(1), 171113. https://doi.org/10.1098/rsos.171113.

Masood, S., Randhawa, M. A., Butt, M. S., & Asghar, M. (2016). A potential of biopesticides to enhance the shelf life of tomatoes (Lycopersicon esculentum Mill.) in the controlled atmosphere. *Journal of Food Processing and Preservation, 40*(1), 3–13. https://doi.org/10.1111/jfpp.12550.

Michalak, M., Marek, A. A., Zawadiak, J., Kawalec, M., & Kurcok, P. (2013). Synthesis of PHB-based carrier for drug delivery systems with pH-controlled release. *European Polymer Journal, 49*(12), 4149–4156. https://doi.org/10.1016/j.eurpolymj.2013.09.021.

Moulton, M. C., Braydich-Stolle, L. K., Nadagouda, M. N., Kunzelman, S., Hussain, S. M., & Varma, R. S. (2010). Synthesis, characterization and biocompatibility of "green" synthesized silver nanoparticles using tea polyphenols. *Nanoscale, 2*(5), 763–770. https://doi.org/10.1039/c0nr00046a.

Mukherjee, P., Ahmad, A., Mandal, D., Senapati, S., Sainkar, S. R., Khan, M. I., ... Sastry, M. (2001). Fungus-mediated synthesis of silver nanoparticles and their immobilization in the mycelial matrix: A novel biological approach to nanoparticle synthesis. *Nano Letters, 1*(10), 515–519. https://doi.org/10.1021/nl0155274.

Nadagouda, M. N., Iyanna, N., Lalley, J., Han, C., Dionysiou, D. D., & Varma, R. S. (2014). Synthesis of silver and gold nanoparticles using antioxidants from blackberry, blueberry, pomegranate, and turmeric extracts. *ACS Sustainable Chemistry & Engineering, 2*(7), 1717–1723. https://doi.org/10.1021/sc500237k.

Nadagouda, M. N., Speth, T. F., & Varma, R. S. (2011). Microwave-assisted green synthesis of silver nanostructures. *Accounts of Chemical Research, 44*(7), 469–478. https://doi.org/10.1021/ar1001457.

Nadagouda, M. N., & Varma, R. S. (2008). Green synthesis of silver and palladium nanoparticles at room temperature using coffee and tea extract. *Green Chemistry, 10*(8), 859. https://doi.org/10.1039/b804703k.

Nielsen, C., Rahman, A., Rehman, A. U., Walsh, M. K., & Miller, C. D. (2017). Food waste conversion to microbial polyhydroxyalkanoates. *Microbial Biotechnology, 10*(6), 1338–1352. https://doi.org/10.1111/1751-7915.12776.

Noronha, V. T., Paula, A. J., Durán, G., Galembeck, A., Cogo-Müller, K., Franz-Montan, M., ... Durán, N. (2017). Silver nanoparticles in dentistry. *Dental Materials, 33*(10), 1110–1126. https://doi.org/10.1016/J.DENTAL.2017.07.002.

Petrangeli, M., Majone, M., Arjmand, F., Silvestri, D., Sagliaschi, M., Sucato, S., ... Pierro, L. (2016). First pilot test on the integration of GCW (Groundwater Circulation Well) with ENA (enhanced Natural Attenuation) for chlorinated solvents source remediation. *Chemical Engineering Transactions, 49*, 91–96. https://doi.org/10.3303/CET1649016.

Poirier, Y., Somerville, C., Schechtman, L. A., Satkowski, M. M., & Noda, I. (1995). Synthesis of high-molecular-weight poly([R]-(-)-3-hydroxybutyrate) in transgenic Arabidopsis thaliana plant cells. *International Journal of Biological Macromolecules, 17*(1), 7–12. https://doi.org/10.1016/0141-8130(95)93511-U.

Praveenkumar, K., Rabinal, M. K., Kalasad, M. N., Sankarappa, T., & Bedre, M. D. (2013). Chitosan capped Silver nanoparticles used as Pressure sensors. *IOSR Journal of Applied Physics, 5*(5), 43–51. https://doi.org/10.9790/4861-0554351.

Rafique, M., Sadaf, I., Rafique, M. S., & Tahir, M. B. (2017). A review on green synthesis of silver nanoparticles and their applications. *Artificial Cells, Nanomedicine, and Biotechnology, 45*(7), 1272–1291. https://doi.org/10.1080/21691401.2016.1241792.

Rai, M., Yadav, A., & Gade, A. (2009). Silver nanoparticles as a new generation of antimicrobials. *Biotechnology Advances, 27*(1), 76–83. https://doi.org/10.1016/j.biotechadv.2008.09.002.

Rannug, U. (1980). Genotoxic effects of 1,2-dibromoethane and 1,2-dichloroethane. *Mutation Research - Reviews in Genetic Toxicology, 76*(3), 269–295. https://doi.org/10.1016/0165-1110(80)90020-2.

Rashid, M. H., & Mandal, T. K. (2007). Synthesis and catalytic application of nanostructured silver dendrites. *The Journal of Physical Chemistry C, 111*(45), 16750–16760. https://doi.org/10.1021/jp074963x.

Regiel-Futyra, A., Kus-Liśkiewicz, M., Sebastian, V., Irusta, S., Arruebo, M., Kyziol, A., ... Stochel, G. (2017). Development of noncytotoxic silver-chitosan nanocomposites for efficient control of biofilm forming microbes. *RSC Advances, 7*(83), 52398–52413. https://doi.org/10.1039/c7ra08359a.

Rodriguez-Perez, S., Serrano, A., Pantión, A. A., & Alonso-Fariñas, B. (2018). Challenges of scaling-up PHA production from waste streams. A review. *Journal of Environmental Management, 205*, 215–230. https://doi.org/10.1016/j.jenvman.2017.09.083.

Rodríguez-Sánchez, L., Blanco, M. C., & Rodrı, L. (2000). Electrochemical synthesis of silver nanoparticles. *The Journal of Physical Chemistry B, 104*(41), 9683–9688. https://doi.org/10.1021/jp001761r.

Sanpui, P., Chattopadhyay, A., & Ghosh, S. S. (2011). Induction of apoptosis in cancer cells at low silver nanoparticle concentrations using chitosan nanocarrier. *ACS Applied Materials & Interfaces, 3*(2), 218–228. https://doi.org/10.1021/am100840c.

Santos, J. C. C., Moreno, P. M. D., Mansur, A. A. P., Leiro, V., Mansur, H. S., & Pêgo, A. P. (2015). Functionalized chitosan derivatives as nonviral vectors: Physicochemical properties of acylated N,N,N-trimethyl chitosan/oligonucleotide nanopolyplexes. *Soft Matter, 11*(41), 8113–8125. https://doi.org/10.1039/C5SM01403D.

Sharma, V. K., Yngard, R. A., & Lin, Y. (2009). Silver nanoparticles: Green synthesis and their antimicrobial activities. *Advances in Colloid and Interface Science, 145*(1–2), 83–96. https://doi.org/10.1016/j.cis.2008.09.002.

Silva, F., Campanari, S., Matteo, S., Valentino, F., Majone, M., & Villano, M. (2017). Impact of nitrogen feeding regulation on polyhydroxyalkanoates production by mixed microbial cultures. *New Biotechnology, 37*, 90–98. https://doi.org/10.1016/j.nbt.2016.07.013.

Silvestri, D., Wacławek, S., Ramakrishnan R, K., Venkateshaiah, A., Krawczyk, K., Padil, V. V. T., ... Černík, M. (2019). The use of a biopolymer conjugate for an eco-friendly one-pot synthesis of palladium-platinum alloys. *Polymers, 11*(12), 1948. https://doi.org/10.3390/polym11121948.

Silvestri, D., Wacławek, S., Sobel, B., Torres-Mendieta, R., Novotný, V., Nguyen, N. H. A., ... Varma, R. S. (2018). A poly(3-hydroxybutyrate)-chitosan polymer conjugate for the synthesis of safer gold nanoparticles and their applications. *Green Chemistry, 20*(21), 4975–4982. https://doi.org/10.1039/c8gc02495b.

Stephen, A. J., Rees, N. V., Mikheenko, I., & Macaskie, L. E. (2019). Platinum and palladium bio-synthesized nanoparticles as sustainable fuel cell catalysts. *Frontiers in Energy Research, 7*, 66. https://doi.org/10.3389/fenrg.2019.00066.

Stumm, W., & Morgan, J. J. (2012). *Aquatic chemistry : Chemical equilibria and rates in natural waters*. New York: Wiley.

Tang, B., Zhang, M., Hou, X., Li, J., Sun, L., & Wang, X. (2012). Coloration of cotton fibers with anisotropic silver nanoparticles. *Industrial & Engineering Chemistry Research, 51*(39), 12807–12813. https://doi.org/10.1021/ie3015704.

Tiwari, A. D., Mishra, A. K., Mishra, S. B., Arotiba, O. A., & Mamba, B. B. (2011). Green synthesis and stabilization of gold nanoparticles in chemically modified chitosan matrices. *International Journal of Biological Macromolecules, 48*(4), 682–687. https://doi.org/10.1016/J.IJBIOMAC.2011.02.008.

Tolaymat, T. M., El Badawy, A. M., Genaidy, A., Scheckel, K. G., Luxton, T. P., & Suidan, M. (2010). An evidence-based environmental perspective of manufactured silver nanoparticle in syntheses and applications: A systematic review and critical appraisal of peer-reviewed scientific papers. *The Science of the Total Environment*. https://doi.org/10.1016/j.scitotenv.2009.11.003.

Torkelson, T. R., Oyen, F., & Rowe, V. K. (1976). The toxicity of chloroform as determined by single and repeated exposure of laboratory animals. *American Industrial Hygiene Association Journal, 37*(12), 697–705. https://doi.org/10.1080/0002889768507551.

Twu, Y. K., Chen, Y. W., & Shih, C. M. (2008). Preparation of silver nanoparticles using chitosan suspensions. *Powder Technology, 185*(3), 251–257. https://doi.org/10.1016/j.powtec.2007.10.025.

Valentino, F., Morgan-Sagastume, F., Campanari, S., Villano, M., Werker, A., & Majone, M. (2017). Carbon recovery from wastewater through bioconversion into biodegradable polymers. *New Biotechnology, 37*, 9–23. https://doi.org/10.1016/j.nbt.2016.05.007.

Van Hyning, D. L., & Zukoski, C. F. (1998). Formation mechanisms and aggregation behavior of borohydride reduced silver particles. *Langmuir, 14*(24), 7034–7046. https://doi.org/10.1021/la980325h.

Virkutyte, J., & Varma, R. S. (2011). Green synthesis of metal nanoparticles: Biodegradable polymers and enzymes in stabilization and surface functionalization. *Chemical Science, 2*(5), 837–846. https://doi.org/10.1039/c0sc00338g.

Wacławek, S., Chronopoulou, L., Papini, M. P., V.T.P, V., Palocci, C., Kupčík, J., & Černík, M. (2017). Enhancement of stability and reactivity of nanosized zero-valent iron with polyhydroxybutyrate. *Desalination and Water Treatment, 69*, 302–307. https://doi.org/10.5004/dwt.2017.0704.

Wang, A., Li, J., & Zhang, T. (2018). Heterogeneous single-atom catalysis. *Nature Reviews Chemistry, 2*(6), 65–81. https://doi.org/10.1038/s41570-018-0010-1.

Wang, H., Qiao, X., Chen, J., & Ding, S. (2005). Preparation of silver nanoparticles by chemical reduction method. *Colloids and Surfaces A, Physicochemical and Engineering Aspects, 256*(2–3), 111–115. https://doi.org/10.1016/j.colsurfa.2004.12.058.

Woo, K. J., Hye, C. K., Ki, W. K., Shin, S., So, H. K., & Yong, H. P. (2008). Antibacterial activity and mechanism of action of the silver ion in Staphylococcus aureus and Escherichia coli. *Applied and Environmental Microbiology, 74*(7), 2171–2178. https://doi.org/10.1128/AEM.02001-07.

Xiong, K., Zhou, G., Zhang, H., Shen, Y., Zhang, X., Zhang, Y., ... Li, J. (2018). Bridging Mo_2 C–C and highly dispersed copper by incorporating N-functional groups to greatly enhance the catalytic activity and durability for carbon dioxide hydrogenation. *Journal of Materials Chemistry A, 6*(32), 15510–15516. https://doi.org/10.1039/C8TA04096F.

Xu, D., Hein, S., Loo, S. L., & Wang, K. (2008). The fixed-bed study of dye removal on chitosan beads at high pH. *Industrial & Engineering Chemistry Research, 47*(22), 8796–8800. https://doi.org/10.1021/ie800387z.

Zhang, J., Li, X., Sun, X., & Li, Y. (2005). Surface enhanced Raman scattering effects of silver colloids with different shapes. *The Journal of Physical Chemistry B, 109*(25), 12544–12548. https://doi.org/10.1021/jp050471d.

Zhang, W., Sun, Y., & Zhang, L. (2015). In situ synthesis of monodisperse silver nanoparticles on sulfhydryl-functionalized poly(glycidyl methacrylate) microspheres for catalytic reduction of 4-nitrophenol. *Industrial & Engineering Chemistry Research, 54*(25), 6480–6488. https://doi.org/10.1021/acs.iecr.5b01010.

Ziegler, C., Klose, M., Voitekhovich, S. V., Gaponik, N., & Eychmüller, A. (2011). Synthesis and agglomeration of silver nanoparticles stabilized with 5-R-tetrazoles. *Zeitschrift Für Physikalische Chemie, 225*(3), 363–371. https://doi.org/10.1524/zpch.2011.0049.

Modification of nZVI with a bio-conjugate containing amine and carbonyl functional groups for catalytic activation of persulfate

Abstract: Although the catalytic activation of persulfate by iron is now common in environmental sciences, there are still several obstacles, including the non–selectiveness and high cost of the production of the iron catalyst. Therefore, it is essential to develop fast and easy methods for producing an iron catalyst that exhibits high surface area properties and rapid catalytic activation of persulfate. In the present work, a chitosan–poly(3–hydroxybutyrate) conjugate (CS–PHB) was used to improve the synthesis of nanoscale zero–valent iron (nZVI). CS–PHB possesses among others two functional groups (carbonyl and amine) that are desirable for catalytic applications, including heterogeneous persulfate activation. The produced CS–PHB–nZVI particles showed an extensive surface area (113 m^2/g) and, at the same time, superior activity in heterogeneous catalysis, which was tested and compared with others persulfate activation methods (heat, Fe^{2+}, commercial nZVI). The most suitable activation conditions for complete degradation of 0.15 mM of the model pollutant (methyl orange; MO) were determined (i.e., a pH of 7, persulfate and CS–PHB–nZVI concentrations of 2 mM and 50 mg/L, respectively). The role of temperature in MO oxidation was evaluated by the Arrhenius equation, and the results showed that the estimated activation energy (E_a) was 27.1 kJ/mol. The MO degradation may be attributed to the generation of $SO_4^{\bullet-}$ in the system as a result of scavenging tests. A magnet can be used to easily separate the remaining catalyst. It is believed that due to it having several advantages over traditionally used nZVI, CS–PHB–nZVI may be successfully applied for catalytic remediation of contaminants that are reactive towards sulfate radicals.

Citation: Silvestri, D.; Wacławek, S.; Sobel, B.; Torres-Mendieta, R.; Pawlet, M.; Padil, V.V.T.; Filip, J.; Černík M. Modification of nZVI with a bio-conjugate containing amine and carbonyl functional groups for catalytic activation of persulfate. *Sep. Pur. Technol.*, **2021**, 257, 117880.
Impact Factor: **9.1** (2021), citations **14** (WOS 25.01.2023)

Separation and Purification Technology 257 (2021) 117880

Contents lists available at ScienceDirect

Separation and Purification Technology

journal homepage: www.elsevier.com/locate/seppur

Modification of nZVI with a bio-conjugate containing amine and carbonyl functional groups for catalytic activation of persulfate

Daniele Silvestri [a], Stanisław Wacławek [a,*], Bartłomiej Sobel [b], Rafael Torres–Mendieta [a], Mirosława Pawlyta [b], Vinod V.T. Padil [a], Jan Filip [c], Miroslav Černík [a]

[a] Institute for Nanomaterials, Advanced Technologies and Innovation, Technical University of Liberec, Studentská 1402/2, 461 17 Liberec 1, Czech Republic
[b] Departament of Engineering Materials and Biomaterials, Faculty of Mechanical Engineering, Silesian University of Technology, Konarskiego 18a St., 44–100 Gliwice, Poland
[c] Regional Centre of Advanced Technologies and Materials, Palacký University Olomouc, Šlechtitelů 27, 783 71 Olomouc, Czech Republic

ARTICLE INFO

Keywords:
Persulfate
nZVI
Catalytic activation
Functionalization
Remediation

ABSTRACT

Although the catalytic activation of persulfate by iron is now common in environmental sciences, there are still several obstacles, including the non-selectiveness and high cost of the production of the iron catalyst. Therefore, it is essential to develop fast and easy methods for producing an iron catalyst that exhibits high surface area properties and rapid catalytic activation of persulfate. In the present work, a chitosan-poly(3–hydroxybutyrate) conjugate (CS-PHB) was used to improve the synthesis of nanoscale zero-valent iron (nZVI). CS-PHB possesses among others two functional groups (carbonyl and amine) that are desirable for catalytic applications, including heterogeneous persulfate activation. The produced CS-PHB-nZVI particles showed an extensive surface area (113 m^2/g) and, at the same time, superior activity in heterogeneous catalysis, which was tested and compared with others persulfate activation methods (heat, Fe^{2+}, commercial nZVI). The most suitable activation conditions for complete degradation of 0.15 mM of the model pollutant (methyl orange; MO) were determined (i.e., a pH of 7, persulfate and CS-PHB-nZVI concentrations of 2 mM and 50 mg/L, respectively). The role of temperature in MO oxidation was evaluated by the Arrhenius equation, and the results showed that the estimated activation energy (E_a) was 27.1 kJ/mol. The MO degradation may be attributed to the generation of $SO_4^{\cdot-}$ in the system as a result of scavenging tests. A magnet can be used to easily separate the remaining catalyst. It is believed that due to it having several advantages over traditionally used nZVI, CS-PHB-nZVI may be successfully applied for catalytic remediation of contaminants that are reactive towards sulfate radicals.

1. Introduction

Nanoparticles of zero-valent iron (nZVI) are very widely used in environmental applications, because it is considered a rather strong reducing agent able to reduce a broad contaminants range [1], and capable of migrating from the application point towards the contamination plume. nZVI may be obtained by different methods, such as chemical reduction of Fe^{3+}, ball milling, thermal reduction of goethite or hematite precursors, electrochemical methods, and others [2]. Not only the preparation methods but also modifications are essential for nZVI properties. The most common methods for nZVI modification are emulsification [3], coating the surface [4] and the creation of bimetallic particles [5]. Due to its excellent characteristics, it can be used in both reduction and oxidation treatment. One of its most common uses is to reduce contaminants, e.g., perchloroethylene, trichloroethylene and dichloroethylene. In addition, nZVI can enhance the oxidative (catalytic) treatment by donating electrons to peroxides, e.g., for the degradation of 4-nitrophenol [6], chloramphenicol [7] and acid orange 7 [8].

The main negative issue concerning nZVI utilization in catalysis (and groundwater remediation) is particle agglomeration, which causes a reduction in the active surface area, a key parameter in the heterogeneous catalysis. Therefore, finding a way to reduce the catalyst particle size while at the same time preventing their aggregation, especially with green chemicals, is one of the leading research areas in environmental nanochemistry. Various natural chemicals have been tested for nZVI stabilization, e.g. carboxymethyl cellulose [9], gum karaya [10], chitosan [11], poly(3–hydroxybutyrate) (PHB).

Chitosan is a well-known biopolymer used in different scientific

* Corresponding author.
E-mail address: stanislaw.waclawek@tul.cz (S. Wacławek).

https://doi.org/10.1016/j.seppur.2020.117880
Received 15 July 2020; Received in revised form 23 September 2020; Accepted 9 October 2020
Available online 13 October 2020
1383-5866/© 2020 Elsevier B.V. All rights reserved.

fields and was also utilized as a coating for various catalysts [12–14].

Although PHB has shown extraordinary properties for ZVI stabilization [15,16], it has a significant drawback due to its low solubility, which forces the use of non-green solvents for the synthesis of the product [17].

A way of overcoming this obstacle is to use chitosan (CS) to form a CS-PHB conjugate [18].

Indeed, in addition to its surface reactions, nZVI may be used as a slow-releasing supply of ferrous iron for activation of hydrogen peroxide [19] or persulfate [20] to generate free radicals. In addition to commonly known advanced oxidation processes (relying on hydroxyl radical reactions [21,22]), persulfate or peroxymonosulfate have been used with success to treat different contaminants in water; however, they often requires activation to enhance its reaction rates with pollutants, which often relies on the formation of free radicals. The most common persulfate activators are heat (Eq. (1)), UV (Eq. (2)), alkaline (Eq. (3)) and in particular Fe^{2+}, which rapidity produces free radicals [23].

The reactions involved in the formation of free radicals are described in Eqs. (4), (5), and (6) (from which the reaction shown in Eq. (6) is very slow, and considered irrelevant under standard conditions).

$$S_2O_8^{2-} + \text{heat} \rightarrow 2SO_4^{\bullet-} \quad (1)$$

$$S_2O_8^{2-} + UV \rightarrow 2SO_4^{\bullet-} \quad (2)$$

$$S_2O_8^{2-} + HO_2^- \rightarrow SO_4^{\bullet-} + SO_4^{2-} + H^+ + O_2^{\bullet-} \quad (3)$$

$$Fe^0 + S_2O_8^{2-} \rightarrow Fe^{2+} + 2SO_4^{2-} \quad (4)$$

$$S_2O_8^{2-} + Fe^{2+} \rightarrow SO_4^{\bullet-} + SO_4^{2-} + Fe^{3+} \quad (5)$$

$$H_2O + SO_4^{\bullet-} \rightarrow {}^{\bullet}OH + SO_4^{2-} + H^+ \quad (6)$$

$$Fe^0 \rightarrow Fe^{2+} + 2e^- \quad (7)$$

$$Fe^{3+} + e^- \rightarrow Fe^{2+} \quad (8)$$

nZVI may not only be considered as a Fe^{2+} source (Eq. (7)) but may also regenerate ferrous ions from Fe^{3+} (Eq. (8)) by donating electrons. This, among other things, makes nZVI an interesting material for persulfate activation. Some of the already studied systems based on the persulfates/nZVI include: 4-chlorophenol degradation in an ultrasound/peroxymonosulfate/nZVI system [24], peroxymonosulfate activated by nZVI for textile wastewater decolorization [25] and persulfate activated by nZVI for brilliant blue degradation [26].

A CS-PHB conjugate has been used for the stabilization and synthesis of different metal nanoparticles [18,27,28]. The nanomaterials produced from them have shown extraordinary catalytic activity ascribable to the conjugate properties [18,27]. However, the role of a CS-PHB conjugate has not yet been studied in the activation of persulfate.

The functional groups, especially the carbonyl group and amine functional groups present on the surface of CS-PHB, may boost catalytic persulfate activation. Toshima [29] reported that the appropriate stabilization of metal nanoparticles may enhance catalytic activity and selectivity of the material. Furthermore, Mahmoud et al. [30] noticed that doping nZVI with amino groups may allow better attraction towards the species with electron deficiency. In contrast, doping materials with nitrogen functional groups may facilitate the electron transfer process [31]. On the other hand, many authors have reported possible activation of persulfates by organics and sp^2 carbons [32–34] containing the carbonyl group [35,36]. On this basis, and due to the presence of both carbonyl and amine groups, a CS-PHB conjugate was chosen as a suitable nZVI capping agent for the enhancement of persulfate activation.

In this paper, CS-PHB-nZVI nanoparticles were synthesized, characterized in various ways, such as: Brunauer–Emmett–Teller (BET), Fourier-transform infrared spectroscopy (FTIR) analysis, scanning electron microscopy [(SEM) and energy dispersive X-Ray analysis (EDX)], transmission electron microscopy [(TEM) and selected area electron diffraction (SAED)], and subsequently used for the heterogeneous activation of persulfate. According to our knowledge, this is the first work where such a modification of nZVI was performed and the created iron nanoparticles evaluated for heterogeneous activation of persulfate.

2. Materials and methods

2.1. Reagents and solutions

Chitosan (75–85% deacetylated, low molecular weight 50,000–190,000 Da) and PHB (Biomer® P209) were purchased from Biomer (Krailing, Germany). Nitric acid (65%), sodium persulfate (99%), sodium chloride (99.5%), sodium sulfate (99%) and sodium carbonate (99%) were purchased from Lach-Ner (Czech Republic). Iron (III) chloride hexahydrate (98%), sodium borohydride (98%), potassium bisulfate (99.99%), iron(II) sulfate heptahydrate (99%), methanol (99.8), *tert*-butyl alcohol (≥99.5%; TBA), humic acid sodium salt, and methyl orange were purchased from Sigma-Aldrich. Spherical and air-stable zero-valent iron nanoparticles (NANOFER STAR) were obtained from NANO IRON, s.r.o. (Czech Republic) and used as a reference material in this study. The acidity of solutions was adjusted by a stock solution of 1 M HCl or NaOH, prepared from the above-mentioned reagents. In all tests, DI (Deionized water; 18.2 MΩ·cm, ELGA, Veolia Water, Marlow, UK) was used.

2.2. Nanoparticle characterization

The morphology and composition of CS-PHB-nZVI were studied by SEM with an acceleration voltage: 0.02–30 kV (Everhardt-Thornley, ZEISS, Ultra/Plus, Germany) coupled with an energy-dispersive X-ray spectroscopy (EDX, OXFORD) for determination of the various elements in the synthesized nanoparticles.

TEM (FEI Titan 80–300 TEM/STEM, FEI) examinations were performed with a field-emission transmission electron microscope with a super twin-lens operated at 300 kV and equipped with an annular dark-field detector.

The amount of Fe^0 in the nZVI particles was determined by a nZVI tester (NANO IRON, Czech Republic) with hydrogen liberation due to the chemical reaction of Fe and $KHSO_4$ according to the reaction (Eq. (9)) [37]:

$$2KHSO_4 + Fe^0 \rightarrow FeSO_4 + K_2SO_4 + H_2 \quad (9)$$

The surface area of the samples (BET) was verified by nitrogen adsorption–desorption analysis using a Quantachrome Instruments NOVA3200 analyser and NovaWin software.

Attenuated total reflection-FTIR spectra were obtained at 700–4000 cm^{-1} (4 cm^{-1} resolution) employing a Ge ATR crystal (NICOLET IZ10, Thermo Scientific) equipped with a single reflection angle (45°) horizontal attenuated total reflection accessory.

Nanofer STAR (nZVI commercial) characterization is reported in the supplementary information (Fig. S1 and Tab. S1).

Dissolved iron concentration was checked by ICP-MS (Elan 6000, Perkin Elmer, USA).

2.3. Preparation of reagents and synthesis of CS-PHB-nZVI

Following our previous research [18], the CS-PHB conjugate was synthesized at a ratio of 4.16:1 (w chitosan: w PHB). Briefly, 5 g/L of chitosan was dissolved in acidified water (pH ~ 2.3) and stirred for five minutes. Then it was mixed with a similar volume of PHB solution (1.2 g/L), sonicated (Autotune 750 W, Bioblock Scientific; equipped with a probe and operating at a frequency of 20 kHz) for 30 min (80 °C), filtrated and dialyzed (Sigma–Aldrich, MWCO 12 kDa). Finally, the formed conjugates were freeze-dried and then stored in a refrigerator for

future use.

The CS-PHB-nZVI nanoparticles were synthesized from a ($FeCl_3$) precursor added to the CS-PHB solution at a CS-PHB to Fe^{3+} ratio (g/mol) of between 1:2.5 and 1:40. The solution was stirred in a nitrogen atmosphere for 15 min prior to continuous dropping of $NaBH_4$ to reduce Fe^{3+} to Fe^0 (zero-valent iron) (Eq. (10)):

$$2FeCl_3 + 6NaBH_4 + 18H_2O \rightarrow 2Fe^0 + 6NaCl + 6B(OH)_3 + 21H_2 \quad (10)$$

After the addition of $NaBH_4$, the reaction ran for a further 10 min. Subsequently, the CS-PHB-nZVI was washed three times in ethanol (still under a nitrogen atmosphere). After the last wash, the CS-PHB-nZVI was separated from the ethanol solution magnetically and freeze-dried for further use.

2.4. Catalytic removal of methyl orange

Methyl orange (MO) was chosen as a model contaminant as it is often reported in the literature [38–41]. An MO stock solution (0.3 mM) was prepared in a volumetric flask by dissolving MO powder in deionized water and stirring for 2 min. For the oxidation experiment, an appropriate volume of persulfate (100 mM) and CS-PHB-nZVI (1 g/L) from the stock solution was added into the reactor to obtain the desired concentrations (0.15 mM of MO, 50 mg/L of CS-PHB-nZVI, and 2 mM of persulfate). The solution was kept under vigorous stirring (200 rpm) for the whole duration of the test (30 min). For the analysis, 1 mL of the solution was taken, filtered by a syringe filter (0.22 μm), and then the samples were appropriately diluted for analysis by an ultraviolet–visible spectrophotometer (Hach Lange DR 3900) at a wavelength of 464 nm in a 1 cm cuvette. The wavelength and general procedure were adopted from Xie et al. [42]. All of the tests were performed in duplicate, and mean values and standard deviations were reported. The reaction rate was fitted by the pseudo-first-order kinetic model [43], while the degradation efficiency was calculated using the following equation (Eq. (11)).

$$\text{Conversion of the pollutant}(\%) = \frac{C_0 - C_t}{C_0} \times 100 \quad (11)$$

where C_0 and C_t are the initial MO concentration (mM) and at a specific time, respectively.

Eq. (12) was used for calculation of the reaction stoichiometric efficiency (RSE).

$$\%RSE = \frac{\Delta MO}{\Delta Persulfate} x100 \quad (12)$$

RSE is defined as the number of moles degraded of MO (ΔMO) versus the number of moles consumed of persulfate (ΔPersulfate) during the reaction.

Persulfate determination was carried out by the modified iodometric method [44,45].

The preliminary tests were performed to select the optimal CS-PHB to Fe^{3+} ratio based on the highest MO degradation efficiency (Fig. S2). From the analysis, the CS-PHB-nZVI synthesized at a ratio of 1:5 (g/mol) was found to be the most effective and was subsequently used for further tests.

To compare the catalytic activity of the prepared CS-PHB-nZVI with other activation methods (heating at 50 °C, activation by the spherical nZVI, and by ferrous iron Fe^{2+}), an MO degradation test was performed. The concentrations of catalyst and persulfate were 50 mg/L and 2 mM, respectively. They were selected as the minimum concentrations that do not cause MO adsorption/degradation under the tested conditions (Fig. S3). Typically, the nZVI amounts selected for the MO degradation were higher [43,44].

Similar experiments were carried out for various concentrations of CS-PHB-nZVI (from 6 to 50 mg/L) and persulfate (from 0.25 to 2 mM).

The effect of pH on the MO degradation was studied by changing the initial pH of the solution from 3 to 11. The pH of the solution was adjusted by adding HCl (1 M) or NaOH (1 M) drop by drop to the solution until the desired pH was obtained.

To determine the influence of other inorganic anions on persulfate activation and MO elimination, the reaction was carried out in the presence of selected anions. The chloride, sulfate and carbonate ions were added into the reactor vessel from the stock solutions (1 M) in an amount from 0.05 to 1 mL to obtain the final concentrations of 5, 10, 25, 50 and 100 mM, and were mixed for a few minutes with the MO before adding the CS-PHB-nZVI and persulfate to the reactor. All tests unless otherwise noted, were carried out at were carried out at 25 ± 1 °C.

The total iron that was dissolved from the CS-PHB-nZVI was measured by ICP-MS (Elan 6000, Perkin Elmer, USA).

The effect of the dissolved organic matter on the MO degradation was studied by adding humic acid in the concentration of 10 to 80 mg/L to the studied system. Humic acid was added into the reactor vessel from the stock solutions (100 mg/L and 320 mg/L) to obtain the final concentrations of 10, 20, 40 and 80 mg/L. Then, the MO/humic acid solutions were mixed for 10 min before the addition of the CS-PHB-nZVI and persulfate to the reactor.

To obtain more knowledge on the mechanism of the MO elimination, the reaction was run at various temperatures (laboratory, 40°, 50° and 60 °C) to reach the activation energy according to the Arrhenius equation [48].

2.5. Scavenger test

To obtain information about the radical mechanism of the reaction and to identify the primary free radical involved in the MO degradation, degradation tests were performed in excess of radical scavengers, i.e., in tert-butyl alcohol (TBA) ($^{\cdot}OH$ scavenger) and methanol ($^{\cdot}OH$ and $SO_4^{\cdot-}$ scavenger) [49]. The scavenger tests were primarily based on the evaluation of differences in the rates of the reactions between the free radical formed and the alcohols added, where sulfate and hydroxyl radicals reacted differently. While, sulfate radicals react with pollutants mainly by electron transfer reaction, hydroxyl radicals promote addition reactions [50]. MO (6.1 mM) was added to the reactor (0.25 mL) with methanol to obtain a final concentration of 0.15 mM in methanol. After filtration (0.22 μm) and appropriate dilution, the sample was analysed with an ultraviolet–visible spectrophotometer (Hach Lange DR 3900) at 464 nm. The same procedure was performed for TBA [50]. All tests unless otherwise noted, were carried out at were carried out at 25 ± 1 °C.

3. Results and discussion

3.1. CS-PHB-nZVI characterization

To confirm the surface coating of nZVI, FTIR analysis of CS-PHB-nZVI was carried out and was compared with the FTIR of the CS-PHB conjugate. The CS-PHB spectrum (Fig. 1a) showed a band at ~3330 cm^{-1}, ascribed to functional groups amide/hydroxyl, a band at ~ 2930 cm^{-1} of the symmetric or asymmetric methylene group stretching vibration, and bands at ~ 1724 and ~ 1600–1520 cm^{-1} of the ester and amino/amide groups, respectively. The CS-PHB-nZVI spectrum (Fig. 1b) showed five significant bands in the same spectral range. The first two bands may be ascribed to the asymmetric and symmetric methylene group stretching vibration (~2920 cm^{-1} and ~ 2850 cm^{-1}, respectively). A typical band appeared at ~ 1724 cm^{-1} is attributed to the stretching of the carbonyl of the ester group [51,52], while a band at ~ 1600–1530 cm^{-1} denoted the presence of amino/amide. The last identified band was ascribed to CH_2 asymmetrical deformation [51]. The presence of CH_2, the ester group and amino/amide are good indicators of the conjugate presence on the surface of the nZVI nanoparticles [18,27].

Fig. 2 shows the electron microscopy-based SEM, TEM, SAED and EDX characterization of CS-PHB-nZVI. SEM images (Fig. 2a) denoted the

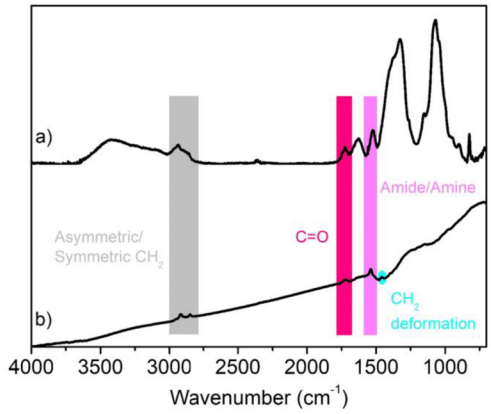

Fig. 1. FTIR spectra of (a) CS-PHB conjugate and (b) CS-PHB-nZVI.

presence of a double structure of spherical and flake shapes of the nanoparticles. The nanoparticles have a chain-like structure attributed to the magnetic effect between them. TEM images confirmed the spherical and flake shapes of the nanoparticles and indicated the presence of a coating on their surface (Fig. 2b). The coating on the surface was ascribed to the presence of CS-PHB, as suggested by the FTIR analysis. SAED confirmed the presence of polycrystalline α-Fe (space group Im-3 m, space group number 229, JCPDS 06–0696) [53] (Fig. 2c). There are no reflections from other phases, in particular from iron oxides. The results of the EDX analysis (Fig. 2d), also confirmed the presence of Fe. Light elemental analysis ($Z < 11$) by EDX must be interpreted with caution and the results obtained do not exclude the presence of oxygen. Therefore, taking into account the morphology visible on the TEM image, flake-shaped nanoparticles may be identified as amorphous iron oxide [54]. Oxygen together with carbon were found as minor elements by the EDX analysis (Fig. 2d).

The amount of Fe^0 in the prepared nZVI particles was investigated by the hydrogen liberation test (Fig. S4). There was no noteworthy difference in the Fe^0 content for nanoparticles synthesized at various ratios of CS-PCB and Fe^{3+}. The data fluctuate without a clear trend, so the mean value was ~ 65% of Fe^0, which is in the range of the commonly reported content of elemental iron in nZVI [55].

On the other hand, the surface area of the CS-PHB-ZVI determined by BET analysis was 113 m^2/g, which is significantly higher than nZVI synthesized by different approaches (Tab. S2). Such a phenomenon may be due to the formation of a polymer-nanoparticle structure, with peculiar nanoparticle shapes that are formed during the synthesis (Fig. 2a,b).

3.2. Catalytic activation of persulfate for MO elimination

To study the effect of a high surface area on the catalytic activity of CS-PHB-nZVI, persulfate activation by CS-PHB-nZVI was compared with other commonly used activation methods, i.e. heating at 50 °C, activation by the commercial nZVI [56] and ferrous iron (Fe^{2+}) all at the same concentrations [50]. Subsequently, the persulfate activity was determined for the radical decomposition of MO [57]. Under the tested conditions, CS-PHB-nZVI showed exemplary behaviour (Fig. 3). The

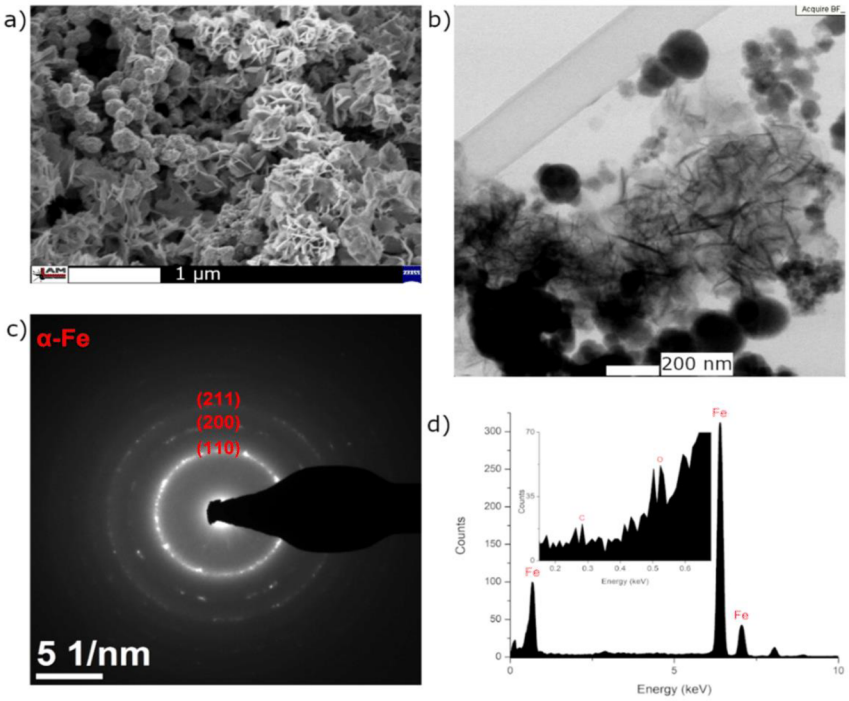

Fig. 2. (a) SEM and (b) TEM image, (c) SAED pattern and (d) EDX spectrum of CS-PHB-nZVI.

degradation of MO after 10 min was ~ 93%. The differences with the commercial iron tested were enormous. At 10 min, the recorded MO degradation was only ~ 22% and ~ 33% at 30 min. Persulfate activated by Fe^{2+} showed a much faster MO degradation at the beginning. The immediate availability of Fe^{2+} in the system, as opposed to much slower activation in the CS-PHB-nZVI/persulfate/MO system, could explain this phenomenon. This observation is in accordance with the work of Kim et al. [20], who has determined that the sulfate radical yield per mole of persulfate was more than two times higher in the persulfate/nZVI system in comparison to the persulfate/Fe^{2+} one. Persulfate activation by heating degraded the MO by a maximum of ~ 69% after 30 min.

3.3. Influence of persulfate and CS-PHB-nZVI concentrations

To understand the CS-PHB-nZVI activation process of persulfate, the influence of CS-PHB-nZVI and persulfate concentrations on MO degradation was investigated. Increasing the persulfate concentration (from 0.25 to 2 mM) caused a higher degradation efficiency (Fig. 4a), and faster MO removal (Fig. 4b). Calculated kinetic rate constants of the pseudo-first-order kinetic model plotted against the persulfate concentrations showed a linear relation (inset of Fig. 4b). Similarly, increasing the CS-PHB-nZVI concentration (from 6 to 50 mg/L) caused a higher degradation efficiency (Fig. 4c), and faster MO removal (Fig. 4d). Again, a linear relationship occurred between the kinetic rate constants and the amount of catalyst used.

To obtain information about the studied system, RSE was estimated. Under the studied condition (0.15 mM of MO, 2 mM of persulfate, 50 mg/L of CS-PHB-nZVI, pH ~ 7 and 30 min of reaction time), the calculated RSE was 23%. The obtained RSE value is in accordance with the ones reported by other research groups [58]. Amasha et al. [59] reported a maximum value of 33% for ketoprofen degradation. Conversely, Ayoub and Ghauch [60] reported a significantly smaller RSE value for sulfamethoxazole degradation. Persulfate and sulfate radicals can react not only with the target contaminant but also quenching (Eq. (13)), and other reactions may occur e.g., with the by-products formed during the oxidation [59].

$$SO_4^{\bullet-} + SO_4^{\bullet-} \rightarrow S_2O_8^{2-} \quad k = 3.1 \times 10^8\ M^{-1}\ s^{-1} \tag{13}$$

For calculating RSE, persulfate concentration was determined and shown in Figure S5. The persulfate concentration after 30 min of the reaction was ~ 60% of the starting one.

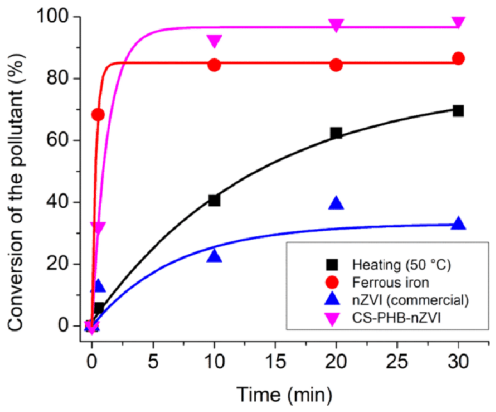

Fig. 3. Comparison of MO degradation efficiency of persulfate activated by CS-PHB-nZVI and commonly used methods (degradation time: 30 min, persulfate concentration: 2 mM, CS-PHB-nZVI concentration: 50 mg/L, MO concentration: 0.15 mM, pH ~ 7, tests were carried out at 25 ± 1 °C, deviation of duplicates less than 5%). The symbols represent experimentally determined data, whereas the solid lines show a model of the best-fit to the data ($y = y_0 + Ae^{-x/t}$).

3.4. Influence of solution pH

pH is an essential parameter in redox reactions because it determines the forms and concentrations of the redox species involved and the surface of the catalysts. For nZVI, the pH value significantly affects the reaction rates, i.e., at a low pH, the corrosion of nZVI by the available protons may occur, while at a high pH, the surface of nZVI may be passivated by OH^- species [61]. Therefore, the effect of pH on MO degradation was studied by changing the initial pH of the solution from 3 to 11. The results confirmed that the initial pH significantly influenced the MO degradation (Fig. 5). At a pH of 3 and 11, the degradation significantly decreased compared to the other pH values due to the previously mentioned rapid corrosion (and self-scavenging described below) and surface passivation, respectively. Moreover, the type of free radicals that are present in solution during the persulfate activation depends on the pH. At a low pH, the sulfate radicals from the persulfate are the predominant radical species, but their concentration is reduced due to their self-scavenging (Eq. (13)) [62].

Instead, at a pH of 10 and higher, the primary free radical species should be hydroxyl radicals [63]. Since the hydroxyl radicals are less reactive in the higher pH [63] and have a shorter lifespan than $SO_4^{\bullet-}$ [64], the dominating presence of hydroxyl radicals may decrease the overall MO degradation efficiency. Taking all of this into account, the highest value was determined for a neutral pH, when the redox activity of Fe is highest and the persulfate activation is most rapid.

3.5. Influence of anions on persulfate activation for MO elimination

To determine the influence of inorganic anions on persulfate activation and MO elimination, the reaction was carried out in the presence of different anions (chloride, carbonate and sulfate ions) in several different concentrations up to 100 mM (Fig. 6). The MO degradation efficiency significantly decreased with an increase in the concentration of anions. The results clearly showed the negative effect of other anions on the MO degradation process. The presence of ions in the reactor may create competing side reactions, namely scavenging of the $SO_4^{\bullet-}$/$^{\bullet}OH$ radicals. The influence of chlorides may be explained by the following equations (Eqs. (14) and (15)) [65,66]:

$$SO_4^{\bullet-} + Cl^- \rightleftarrows SO_4^{2-} + Cl^{\bullet} \quad k = 2.8 \times 10^8\ M^{-1}s^{-1} \tag{14}$$

$$^{\bullet}OH + Cl^- \rightleftarrows ClHO^{\bullet-} \quad k = 6 \times 10^9\ M^{-1}s^{-1} \tag{15}$$

Similarly, the carbonate ions may be have as a $SO_4^{\bullet-}$/$^{\bullet}OH$ scavenger following equation (Eqs. (16) and (17)) [66,67]:

$$SO_4^{\bullet-} + CO_3^{2-} \rightleftarrows SO_4^{2-} + CO_3^{\bullet-} \quad k = 6.1 \times 10^6\ M^{-1}\ s^{-1} \tag{16}$$

$$^{\bullet}OH + CO_3^{2-} \rightleftarrows OH^- + CO_3^{\bullet-} \quad k = 3.9 \times 10^8\ M^{-1}\ s^{-1} \tag{17}$$

These chloride and carbonate radicals often have slower reaction rates with most organic compounds [50]. Moreover, sulfate ions may destabilize the nZVI surface by corrosion, as reported by Pullin et al. [68], whereby decreasing the formation rates of the radicals. Furthermore, sulfate ions could also affect the $SO_4^{\bullet-}/SO_4^{2-}$ ORP system. Ghanbari et al. [66] reported that a high concentration of sulfate ions could harm dye removal efficiency. This conclusion was also supported in the work of Wu et al. [69], by observing the sulfate ions influence on the trichloroethene degradation.

As for the influence of the carbonate ions, they are well-known scavengers of hydroxyl (mainly) and sulfate radicals. However, as it was indicated in the work of Bennedsen et al. [70], the reactive carbonate species in a higher concentration can catalyze the propagation reactions resulting in more sulfate radicals, which could cause a slightly improved conversion of the pollutant with the increasing dose of carbonate ions.

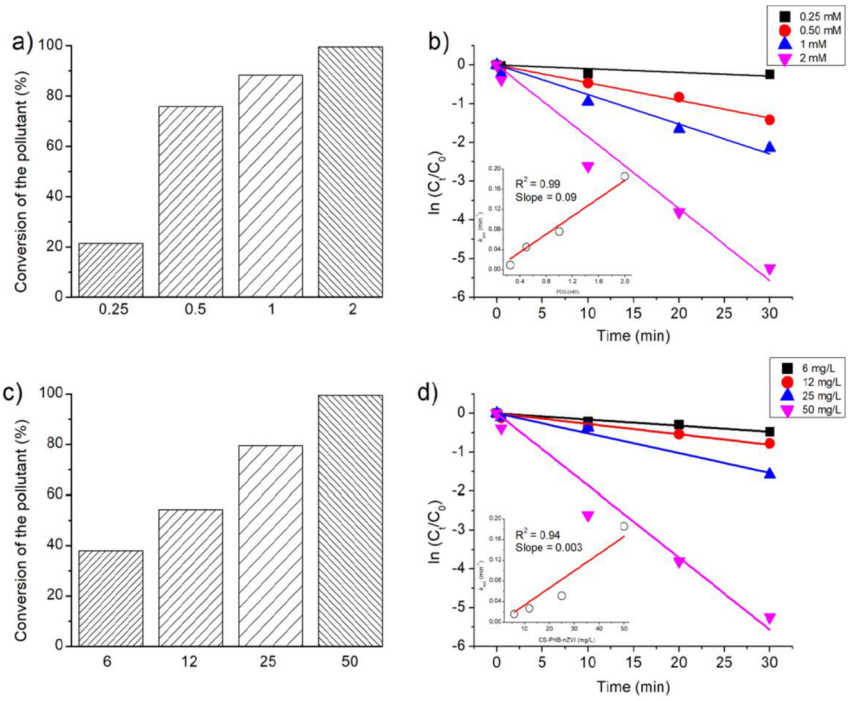

Fig. 4. Influence of persulfate and CS-PHB-nZVI concentrations on MO degradation by activated persulfate: (a) degradation efficiency for different persulfate concentration, (b) kinetics and pseudo-first-order kinetic rate constants (k_{app}), (c) degradation efficiency for different CS-PHB-nZVI concentrations, (d) kinetics and pseudo-first-order kinetic rate constants (degradation time: 30 min, persulfate concentration: 2 mM, CS-PHB-nZVI concentration: 50 mg/L, MO concentration: 0.15 mM, pH ~ 7, tests were carried out at 25 ± 1 °C, deviation of duplicates less than 5%). The symbols represent experimentally determined data, whereas the solid lines show a model of the best-fit to the data (y = a + bx).

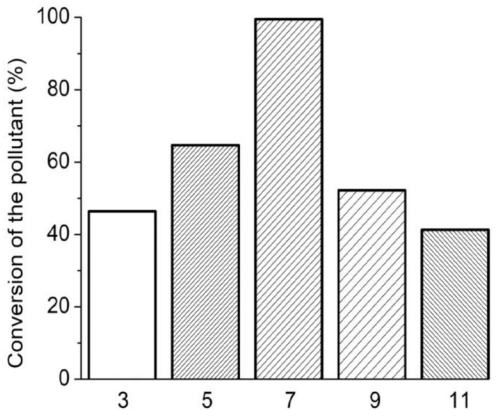

Fig. 5. Influence of pH on MO degradation by persulfate, (degradation time: 30 min, persulfate concentration: 2 mM, CS-PHB-nZVI concentration: 50 mg/L, MO concentration: 0.15 mM, tests were carried out at 25 ± 1 °C, deviation of duplicates less than 5%).

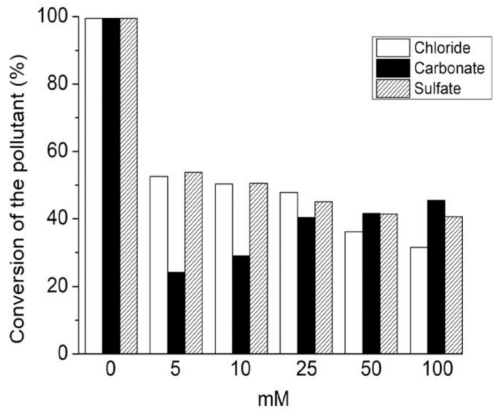

Fig. 6. Influence of chloride, carbonate and sulfate ions on the MO degradation (degradation time: 30 min, persulfate concentration: 2 mM, CS-PHB-nZVI concentration: 50 mg/L, MO concentration: 0.15 mM, tests were carried out at 25 ± 1 °C, deviation of duplicates less than 5%.). The starting pH of the reaction after adding chloride and sulfate ions was ~ 7, while the starting pH after adding carbonate ions was ~ 10 (for all the concentrations).

3.6. Influence of the dissolved organic matter

The influence of dissolved organic matter on the oxidative degradation of organic pollutants is of significant importance. In Fig. 7, the effect of humic acid on the studied system is shown. The conversion of the pollutant drops from ~ 99.4% to ~ 69%, in the presence of 80 mg/L of humic acid. All humic acid concentrations investigated in this study (10–80 mg/L) influenced the conversion of MO. Smaller conversion of the pollutant indicates the competition of humic acid with MO for the reaction with sulfate radicals. The dissolved organic matter is a known scavenger of reactive oxygen species, as reported previously by Yao et al. [71] and Ghanbari et al. [72].

Moreover, humic acid can interact with nZVI by coating its surface, as reported by Giasuddin et al. [73], which can alter nZVI's physicochemical properties [74]. The adsorption of humic acid onto the nZVI surface may harm persulfate activation and, in part, explain the reduction of the pollutant conversion. Yao et al. [71] reported a decrease of the rhodamine B removal from 100% to 48% by increasing the concentration of humic substances (fulvic acid) from 0 to 80 mg/L. In another study, Sun et al. [75] reported a substantial reduction of atrazine degradation by adding 10 mg/L of humic acid. Compared to these studies, humic substances seem to have a marginal influence on our studied system (CS-PHB-nZVI/persulfate/MO).

3.7. Calculation of activation energy

For a better comprehending of the catalytic reactions, it is essential to determine the Arrhenius activation energy, i.e., the amount of energy that the reactants have to acquire before reaching the transition state. Therefore, similar experiments were carried out at 40°, 50° and 60 °C. The pseudo-first-order kinetic model fitted the results, and the logarithm of kinetic rate constants k_{app} was plotted against 1/T (Fig. 8). The activation energy E_a, as a slope of the line, was found to be 27.1 kJ/mol. This value is in a range of values determined by other authors (Tab. S3).

3.8. Radical scavenging tests

The reaction mechanisms of persulfate decomposition presuppose the formation of two main types of radicals, hydroxyl and sulfate. To obtain the proper radical mechanism, essential free radicals can be identified by degradation tests performed in excess of different radical scavengers. Two types of scavengers were applied, namely TBA as an $^{\bullet}OH$ scavenger and methanol as both a $SO_4^{\bullet-}$ and $^{\bullet}OH$ scavenger [49]. The reaction rates of alcohols with these free radicals depend on the presence of the α-hydrogen in their molecule, because alcohols with α-hydrogen (e.g., methanol) react with both radicals (hydroxyl and sulfate radicals), while alcohols which do not possess α-hydrogen (e.g., TBA) react mainly with hydroxyl radicals (Table 1). From the changes in the reaction rates after the addition of a scavenger, it is possible to determine which radicals are significant for the reaction (Fig. 9).

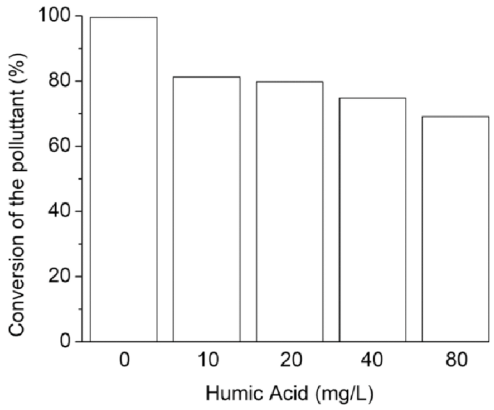

Fig. 7. Influence of humic acid on the MO degradation (degradation time: 30 min, persulfate concentration: 2 mM, CS-PHB-nZVI concentration: 50 mg/L, MO concentration: 0.15 mM, pH ~ 7, tests were carried out at 25 ± 1 °C, deviation of duplicates less than 5%).

The scavenging tests showed that after the addition of methanol, the MO concentration was almost unchanged from the initial concentration. Following the addition of TBA, the system behaved similarly to the test without the scavenger. After 10 min, the reaction stopped at ~ 76% of the MO removed. The results with TBA, which is a scavenger for hydroxyl radicals only, suggested that the $SO_4^{\bullet-}$ plays a vital role in the degradation process of MO in the nZVI/ persulfate system under the tested conditions. This is in accordance with previous studies, where the main reactive oxygen species in the systems composed by persulfate and metals in the zero oxidation state were sulfate radicals [77,78].

It should be also noted that the high TBA concentration used for carrying out these tests can influence the sulfate radical reactions with MO as well, which could explain the reaction interruption after 10 min. Similar observations had Zhu et al. [79] and Wang et al. [77] that noted a decrease of the removal efficiencies of the contaminants of concern by sulfate radicals while increasing the TBA concentration (from 50 to 300 mM [79] and from 10 to 100 mM [77]).

Because sulfate and hydroxyl radicals react in a different way, where hydroxyl radical promotes the addition reactions and sulfate radicals react mainly by electron transfer reaction [50], the mechanisms of MO removal is probably by a single electron transfer pathway.

3.9. Reusability of catalyst and iron leaching

nZVI reusability is considered an essential parameter for the evaluation of its effectiveness. Therefore, the reusability of CS-PHB-nZVI was evaluated in the MO/persulfate/CS-PHB-nZVI process. The easiness through which the CS-PHB-nZVI can be separated from the solution could be considered as an additional advantage of this catalyst (Fig. 10).

In Fig. 10a, the results obtained for MO degradation after four cycles are shown. Reusing the catalyst causes a decrease in the conversion of the pollutant in a linear way (R^2 = 0.96). The conversion of the contaminant, after the first use, was estimated to be ~ 97%. While for the second and third cycles, the conversions of the pollutant were ~ 89% and ~ 83%, respectively. At the forth reuse, the catalyst lost efficiency, and the conversion of pollutant dropped to ~ 70%. The decrease in the conversion of pollutants could be due to the passivation of the catalyst surface, which is in agreement with the work of Xie et al. [80]. They have also reported a loss of sulfamethoxazole removal up to the fourth cycle. A similar trend was observed by Khunjan and Kasikamphaiboon [81] for the decolorization of reactive black 5.

The concentration of total iron that has dissolved from the catalyst was determined as well (Fig. 10b). After 30 s of the reaction, the dissolved iron in solution equaled 6 mg/L, while, after 30 min: 14 mg/L. An increase of the catalyst dissolution after the persulfate addition can be caused by the changes in the pH and ORP values in the system. The dissolution of the iron in the persulfate/nZVI system is in agreement with Du et al. [82]. However, it should be noted that our stabilization resulted in reduced iron leaching after 30 min of the reaction (28% in comparison to ~ 40% that was reported by Du et al. [82]).

For further assessment of the CS-PHB-nZVI passivation mechanism, it was analyzed by FTIR after the reaction (Fig. S6). The nanoparticles spectrum shows broadband ascribed to O-H vibration (~3250 cm^{-1}). The new bands at ~ 1110–1000 cm^{-1} could be attributed to the sulfate ions presence [83]. Going to the lower wavenumbers, the newly formed bands could be due to the presence of iron oxides in larger concentration in the CS-PHB-nZVI catalyst after reuse. In general, the spectrum has

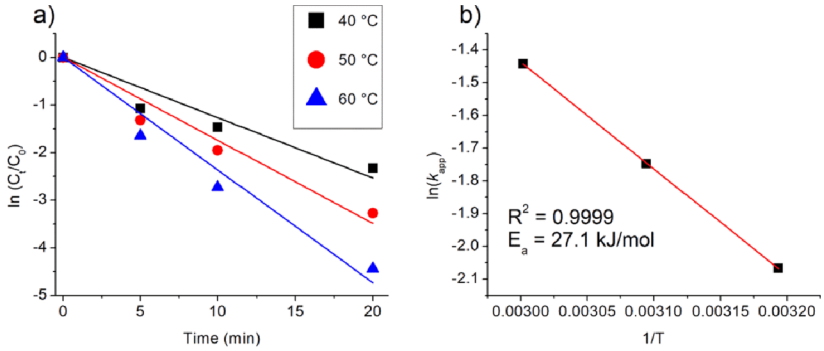

Fig. 8. (a) Influence of the temperature (40°, 50° and 60 °C) on MO degradation kinetics, (b) activation energy E_a estimated by the Arrhenius equation (reaction time: 30 min, persulfate concentration: 2 mM, CS-PHB-nZVI concentration: 50 mg/L, MO concentration: 0.15 mM, pH ~ 7, deviation of duplicates less than 5%.). The symbols represent experimentally determined data, whereas the solid lines show a model of the best-fit to the data (y = a + bx).

Table 1
Rate constants (2nd order) of methanol and TBA with hydroxyl and sulfate radicals [76].

Radical scavengers	$SO_4^{\bullet-}$	$^{\bullet}OH$
Methanol	3.2×10^9 M^{-1} s^{-1}	9.7×10^9 M^{-1} s^{-1}
TBA	$(4.0–9.1) \times 10^5$ M^{-1} s^{-1}	$(3.8–7.6) \times 10^8$ M^{-1} s^{-1}

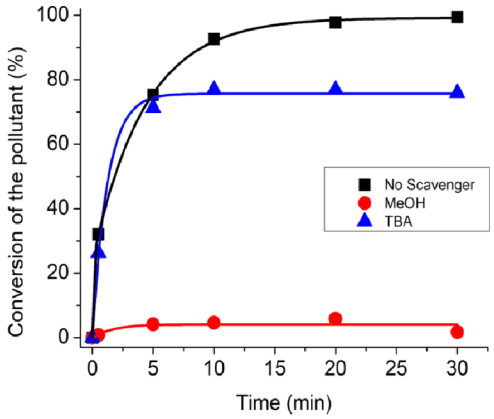

Fig. 9. Radical scavenging tests of MO elimination. No scavenger (degradation: 99.5%), in methanol (MeOH) (degradation: ~2%) and TBA (degradation: ~76%), (degradation time: 30 min, persulfate concentration: 2 mM, CS-PHB-nZVI concentration: 50 mg/L, MO concentration: 0.15 mM, pH ~ 7, tests were carried out at 25 ± 1 °C, deviation of duplicates less than 5%, detailed experimental conditions are reported in Table S4). The symbols represent experimentally determined data, whereas the solid lines show a model of the best-fit to the data ($y = y_0 + Ae^{-x/t}$).

changed after the use of the catalyst. It should be noted that the presence of sulfate ions and the oxidized Fe could cause the reduced oxidation efficiency of MO.

The results of this work were compared with other catalytic processes used for the degradation of MO (Tab. S5). Our activation method exhibits fast reaction kinetics, which may probably be attributed to the larger surface area of CS-PHB-nZVI and the functional groups presented on the nanoparticle surface. The functional groups identified by FTIR analysis have been reported to be able to enhance the catalytic/adsorption properties of nZVI and other materials [30,32,84,85]. The synergic effect of carbonyl and amine groups may further boost the persulfate activation.

4. Conclusions

This research investigated the effectiveness of nZVI coated by a bio-conjugate CS-PHB for the heterogeneous activation of persulfate. CS-PHB-nZVI was synthesized by the chemical reduction of Fe^{3+} in the presence of CS-PHB at a ratio of 1:5 (g CS-PHB: mol Fe^{3+}). The nanomaterial synthesized by the current methodology exhibits a large surface area of 113 m^2/g, which is one of the highest that could be found in the literature and leads to unusual catalytic activity. The CS-PHB-nZVI was tested as a persulfate activator for the degradation of methyl orange. The analysis showed that the CS-PHB-nZVI exhibits a better performance than the other catalysts tested.

The different activation mechanism may be attributed to the synergic effect of the carbonyl and amine groups present on the surface of the nZVI, as confirmed by FTIR. The large surface area of CS-PHB-nZVI may also play an essential role in the activation of persulfate. The best conditions for MO removal were determined to be 2 mM of persulfate and 50 mg/L of nZVI, at a pH of ~ 7. The addition of anions (chlorides, carbonates and sulfates) dramatically decreased the reactivity of persulfate for MO degradation. The activation energy for the MO degradation was found to be 27.1 kJ/mol, which is, on average, lower than the activation energies of other persulfate -nZVI systems reported in the literature.

The performed scavenging test suggested that $SO_4^{\bullet-}$ is involved as the leading free radical species in the reaction, playing an essential role in the MO degradation, which is in agreement with the literature data for the systems composed of persulfate and metals in the zero-oxidation state. It is believed that such a modification of nanoparticles may be implemented with success for other catalytic reactions.

CRediT authorship contribution statement

Daniele Silvestri: Validation, Formal analysis, Investigation, Writing - original draft, Visualization. **Stanisław Wacławek:** Conceptualization, Writing - original draft, Supervision, Project administration, Funding acquisition. **Bartłomiej Sobel:** Writing - review & editing, Methodology. **Rafael Torres–Mendieta:** Methodology. **Mirosława Pawlyta:** Writing - review & editing, Methodology. **Vinod V.T. Padil:** Methodology. **Jan Filip:** Writing - review & editing, Methodology.

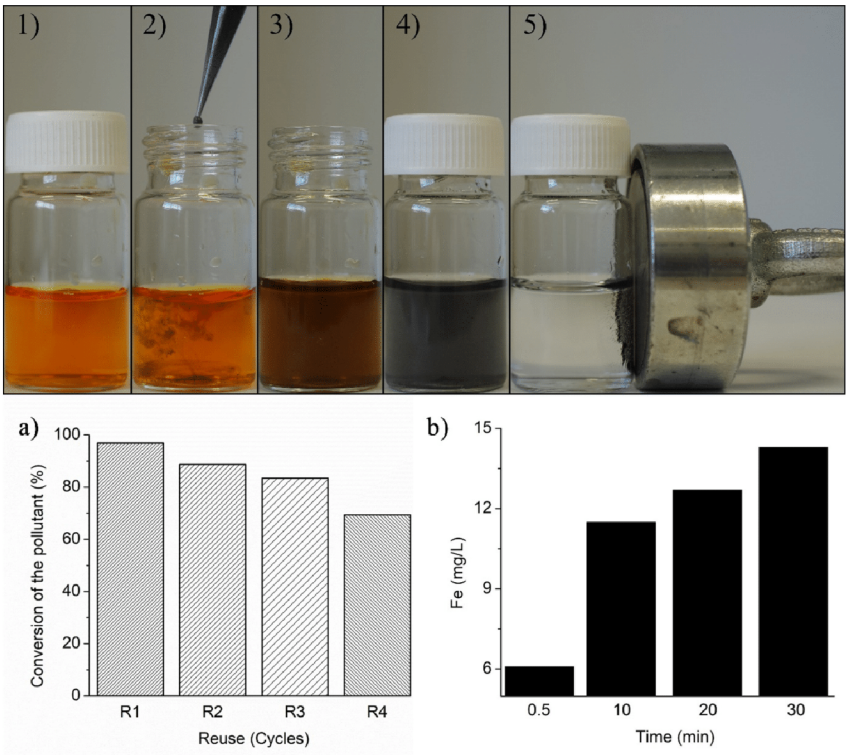

Fig. 10. Process of MO degradation (persulfate activated by CS-PHB-nZVI) and separation of nanoparticles from the reaction solution by a magnet. (1) MO/persulfate solution; (2) addition of CS-PHB-nZVI, (3) solution after 5 s of the reaction (4)) solution after 30 min of the reaction (5)) separation of CS-PHB-nZVI by a magnet; (a) reusability of CS-PHB-nZVI (reaction time: 15 min); (b) concentration of the total iron dissolved from the catalyst during the reaction (persulfate concentration: 2 mM, CS-PHB-nZVI concentration: 50 mg/L, MO concentration: 0.15 mM, pH ~ 7, tests were carried out at 25 ± 1 °C, deviation of duplicates less than 5%).

Miroslav Černík: Conceptualization, Writing - review & editing, Supervision, Funding acquisition.

Declaration of Competing Interest

The authors declare that they have no conflict of interest.

Acknowledgments

This work was partly supported by the Student Grant Scheme at the Technical University of Liberec through project number SGS-2020-3055. The authors would also like to acknowledge help of the Ministry of Education, Youth and Sports in the Czech Republic under the Research Infrastructures NanoEnviCz (Project No. LM2015073) and "Inter Excellence – Action programme" within the framework of project "Exploring the role of ferrates and modified nano zero-valent iron in the activation process of persulfates" (reg. nr: LTAUSA18078). This work was also supported by the Ministry of Education, Youth and Sports of the Czech Republic and the European Union - European Structural and Investment Funds in the frames of Operational Programme Research, Development and Education - project Hybrid Materials for Hierarchical Structures (HyHi, Reg. no. CZ.02.1.01/0.0/0.0/16_019/0000843). Stanisław Wacławek also gratefully thanks for the support provided by Grant Agency of the Czech Republic (GA ČR) GJ20-17028Y Nano Zero-Valent Iron and Cyclodextrins – Their Synergistic Action for Water Purification. This project was supported by the Operational Programme Research, Development and Education - European Regional Development Fund, project No. CZ.02.1.01/0.0/0.0/16_019/0000754 of the Ministry of Education, Youth and Sports of the Czech Republic.

Appendix A. Supplementary material

Supplementary data to this article can be found online at https://doi.org/10.1016/j.seppur.2020.117880.

References

[1] C.M. Dominguez, J. Parchão, S. Rodriguez, D. Lorenzo, A. Romero, A. Santos, Kinetics of Lindane Dechlorination by Zerovalent Iron Microparticles: Effect of Different Salts and Stability Study, Ind. Eng. Chem. Res. 55 (2016) 12776–12785, https://doi.org/10.1021/acs.iecr.6b03434.
[2] F. Fu, D.D. Dionysiou, H. Liu, The use of zero-valent iron for groundwater remediation and wastewater treatment: A review, J. Hazard. Mater. 267 (2014) 194–205, https://doi.org/10.1016/j.jhazmat.2013.12.062.
[3] N.D. Berge, C.A. Ramsburg, Oil-in-Water Emulsions for Encapsulated Delivery of Reactive Iron Particles, Environ. Sci. Technol. 43 (2009) 5060–5066, https://doi.org/10.1021/es900358p.
[4] F. He, D. Zhao, Preparation and characterization of a new class of starch-stabilized bimetallic nanoparticles for degradation of chlorinated hydrocarbons in water, Environ. Sci. Technol. 39 (2005) 3314–3320, https://doi.org/10.1021/es048743y.
[5] T. Wang, J. Su, X. Jin, Z. Chen, M. Megharaj, R. Naidu, Functional clay supported bimetallic nZVI/Pd nanoparticles used for removal of methyl orange from aqueous solution, J. Hazard. Mater. 262 (2013) 819–825, https://doi.org/10.1016/J.JHAZMAT.2013.09.028.

[6] Z. He, S. Mahmud, Y. Yang, L. Zhu, Y. Zhao, Q. Zeng, Z. Xiong, S. Zhao, Polyvinylidene fluoride membrane functionalized with zero valent iron for highly efficient degradation of organic contaminants, Sep. Purif. Technol. 250 (2020), 117266, https://doi.org/10.1016/j.seppur.2020.117266.

[7] T. Zhang, Y. Yang, J. Gao, X. Li, H. Yu, N. Wang, P. Du, R. Yu, H. Li, X. Fan, Z. Zhou, Synergistic degradation of chloramphenicol by ultrasound-enhanced nanoscale zero-valent iron/persulfate treatment, Sep. Purif. Technol. 240 (2020), 116575, https://doi.org/10.1016/j.seppur.2020.116575.

[8] X. Fu, J. Zhang, H. Zhao, S. Zhang, T. Nie, Y. Zhang, J. Lu, Enhanced peroxymonosulfate activation by coupling zeolite-supported nano-zero-valent iron with weak magnetic field, Sep. Purif. Technol. 230 (2020), 115886, https://doi.org/10.1016/j.seppur.2019.115886.

[9] Y.-F. Yang, P.-J. Chen, V.H.-C. Liao, Nanoscale zerovalent iron (nZVI) at environmentally relevant concentrations induced multigenerational reproductive toxicity in *Caenorhabditis elegans*, Chemosphere 150 (2016) 615–623, https://doi.org/10.1016/j.chemosphere.2016.01.068.

[10] V.T. Padil Vinod, S. Wacławek, C. Senan, J. Kupčík, K. Pešková, M. Černík, H. M. Somashekarappa, Gum karaya (*Sterculia urens*) stabilized zero-valent iron nanoparticles: characterization and applications for the removal of chromium and volatile organic pollutants from water, RSC Adv. 7 (2017) 13997–14009, https://doi.org/10.1039/C7RA00464H.

[11] M. Ahmadi, M. Foladivanda, N. Jaafarzadeh, Z. Ramezani, B. Ramavandi, S. Jorfi, B. Kakavandi, Synthesis of chitosan zero-valent iron nanoparticles-supported for cadmium removal: Characterization, optimization and modeling approach, J. Water Supply Res. Technol. - Aqua. 66 (2017) 116–130, https://doi.org/10.2166/aqua.2017.027.

[12] R.B.N. Baig, R.S. Varma, Copper on chitosan: a recyclable heterogeneous catalyst for azide–alkyne cycloaddition reactions in water, Green Chem. 15 (2013) 1839, https://doi.org/10.1039/c3gc40401c.

[13] R.B.N. Baig, M.N. Nadagouda, R.S. Varma, Ruthenium on chitosan: A recyclable heterogeneous catalyst for aqueous hydration of nitriles to amides, Green Chem. 16 (2014) 2122–2127, https://doi.org/10.1039/c3gc42004c.

[14] N. Motahharifar, M. Nasrollahzadeh, A. Taheri-Kafrani, R.S. Varma, M. Shokouhimehr, Magnetic chitosan-copper nanocomposite: A plant assembled catalyst for the synthesis of amino- and N-sulfonyl tetrazoles in eco-friendly media, Carbohydr. Polym. 232 (2020), 115819, https://doi.org/10.1016/j.carbpol.2019.115819.

[15] L. Chronopoulou, C. Palocci, F. Valentino, I. Pettiti, S. Wacławek, M. Černík, Petrangeli Papini, Stabilization of Iron (Micro)Particles with Polyhydroxybutyrate for In Situ Remediation Applications, Appl. Sci. 6 (2016) 417, https://doi.org/10.3390/app6120417.

[16] S. Wacławek, L. Chronopoulou, M. Petrangeli Papini, V.T.P. Vinod, C. Palocci, J. Kupčík, M. Černík, Enhancement of stability and reactivity of nanosized zero-valent iron with polyhydroxybutyrate, Desalin, Water Treat. 69 (2017) 302–307, https://doi.org/10.5004/dwt.2017.0704.

[17] R.R.N. Reusch, The role of short-chain conjugated poly-(R)-3-hydroxybutyrate (cPHB) in protein folding, Int. J. Mol. Sci. 14 (2013) 10727–10748, https://doi.org/10.3390/ijms140610727.

[18] D. Silvestri, S. Wacławek, B. Sobel, R. Torres-Mendieta, V. Novotný, N.H. A. Nguyen, A. Ševců, V.V.T. Padil, J. Müllerová, M. Stuchlík, M.P. Papini, M. Černík, R.S. Varma, A poly(3-hydroxybutyrate)-chitosan polymer conjugate for the synthesis of safer gold nanoparticles and their applications, Green Chem. 20 (2018) 4975–4982, https://doi.org/10.1039/c8gc02495b.

[19] S. Zha, Y. Cheng, Y. Gao, Z. Chen, M. Megharaj, R. Naidu, Nanoscale zero-valent iron as a catalyst for heterogeneous Fenton oxidation of amoxicillin, Chem. Eng. J. 255 (2014) 141–148, https://doi.org/10.1016/J.CEJ.2014.06.057.

[20] C. Kim, J.-Y. Ahn, T.Y. Kim, W.S. Shin, I. Hwang, Activation of Persulfate by Nanosized Zero-Valent Iron (NZVI): Mechanisms and Transformation Products of NZVI, Environ. Sci. Technol. 52 (2018) 3625–3633, https://doi.org/10.1021/acs.est.7b05847.

[21] A. Fernandes, M. Gagol, P. Makoś, J.A. Khan, G. Boczkaj, Integrated photocatalytic advanced oxidation system (TiO_2/UV/O_3/H_2O_2) for degradation of volatile organic compounds, Sep. Purif. Technol. 224 (2019) 1–14, https://doi.org/10.1016/j.seppur.2019.05.012.

[22] G. Boczkaj, A. Fernandes, Wastewater treatment by means of advanced oxidation processes at basic pH conditions: A review, Chem. Eng. J. 320 (2017) 608–633, https://doi.org/10.1016/j.cej.2017.03.084.

[23] B.D. Yirsaw, M. Megharaj, Z. Chen, R. Naidu, Environmental application and ecological significance of nano-zero valent iron, J. Environ. Sci. 44 (2016) 88–98, https://doi.org/10.1016/J.JES.2015.07.016.

[24] G. Barzegar, S. Jorfi, V. Zarezade, M. Khatebasreh, F. Mehdipour, F. Ghanbari, 4-Chlorophenol degradation using ultrasound/peroxymonosulfate/nanoscale zero valent iron: Reusability, identification of degradation intermediates and potential application for real wastewater, Chemosphere 201 (2018) 370–379, https://doi.org/10.1016/j.chemosphere.2018.02.143.

[25] F. Ghanbari, M. Moradi, M. Manshouri, Textile wastewater decolorization by zero valent iron activated peroxymonosulfate: Compared with zero valent copper, J. Environ. Chem. Eng. 2 (2014) 1846–1851, https://doi.org/10.1016/j.jece.2014.08.003.

[26] M. Yousefi, F. Ghanbari, M.A. Zazouli, S. Madihi-Bidgoli, Brilliant Blue FCF degradation by persulfate/zero valent iron: the effects of influencing parameters and anions, 70 (2017) 364-371. doi:10.5004/dwt.2017.20478.

[27] D. Silvestri, S. Wacławek, A. Venkateshaiah, K. Krawczyk, B. Sobel, V.V.T. Padil, M. Černík, R.S. Varma, Synthesis of Ag nanoparticles by a chitosan-poly(3-hydroxybutyrate) polymer conjugate and their superb catalytic activity, Carbohydr. Polym. 232 (2020), 115806, https://doi.org/10.1016/j.carbpol.2019.115806.

[28] D. Silvestri, S. Wacławek, R.K. Ramakrishnan, A. Venkateshaiah, K. Krawczyk, V.V. T. Padil, B. Sobel, M. Černík, The use of a biopolymer conjugate for an eco-friendly one-pot synthesis of palladium-platinum alloys, Polymers 11 (2019) 1948, https://doi.org/10.3390/polym11121948.

[29] N. Toshima, Metal Nanoparticles Used as Catalysts, in: Dekker Encycl. Nanosci. Nanotechnology, Second Ed. - Six Vol., Marcel Dekker, New York, NY, USA 2004: p. 1869. https://doi.org/10.1201/9781439834398.ch125.

[30] M.E. Mahmoud, E.A. Saad, M.A. Soliman, M.S. Abdelwahab, Synthesis and surface protection of nano zerovalent iron (NZVI) with 3-aminopropyltrimethoxysilane for water remediation of cobalt and zinc and their radioactive isotopes, RSC Adv. 6 (2016) 66242–66251, https://doi.org/10.1039/c6ra11049e.

[31] K. Scott, E.H. Yu, Microbial Electrochemical and Fuel Cells: Fundamentals and Applications, Woodhead, Illinois, USA, 2015, pp 126.

[32] X. Duan, H. Sun, J. Kang, Y. Wang, S. Indrawirawan, S. Wang, Insights into heterogeneous catalysis of persulfate activation on dimensional-structured nanocarbons, ACS Catal. 5 (2015) 4629–4636, https://doi.org/10.1021/acscatal.5b00774.

[33] W. Ren, G. Nie, P. Zhou, H. Zhang, X. Duan, S. Wang, The Intrinsic Nature of Persulfate Activation and N-Doping in Carbocatalysis, Environ. Sci. Technol. 54 (2020) 6438–6447, https://doi.org/10.1021/acs.est.0c01161.

[34] W. Ren, L. Xiong, G. Nie, H. Zhang, X. Duan, S. Wang, Insights into the Electron-Transfer Regime of Peroxydisulfate Activation on Carbon Nanotubes: The Role of Oxygen Functional Groups, Environ. Sci. Technol. 54 (2020) 1267–1275, https://doi.org/10.1021/acs.est.9b06208.

[35] A.M. Ocampo, Persulfate Activation by Organic Compounds, Washington State University, Department of Civil and Environmental Engineering, 2009.

[36] S. Selvarani, B. Medona, M.S. Ramachandran, Studies on the ketone-catalyzed decomposition of caroate in aqueous alkaline medium, Int. J. Chem. Kinet. 37 (2005) 483–488, https://doi.org/10.1002/kin.20093.

[37] J. Filip, J. Soukupova, J. Kaslík, J. Slunsky, R. Zboril, Nanoscale Zerovalent Iron Particles for Groundwater and Soil Treatment: Monitoring and Control of their Solid- State Synthesis, Stability, and Activity, in: Iron Nanomater. Water Soil Treat., Jenny Stanford Publishing, 2018: pp. 119–147. doi:10.1201/b22501-6.

[38] Y. Yang, H. Zhang, S. Lee, D. Kim, W. Hwang, Z.L. Wang, Hybrid Energy Cell for Degradation of Methyl Orange by Self-Powered Electrocatalytic Oxidation, Nano Lett. 13 (2013) 803–808, https://doi.org/10.1021/nl3046188.

[39] Q. Liu, Q. Liu, Z. Wu, Y. Wu, T. Gao, J. Yao, Efficient Removal of Methyl Orange and Alizarin Red S from pH-Unregulated Aqueous Solution by the Catechol-Amine Resin Composite Using Hydrocellulose as Precursor, ACS Sustain. Chem. Eng. 5 (2017) 1871–1880, https://doi.org/10.1021/acssuschemeng.6b02593.

[40] Y. Shi, J. Zhu, G. Yuan, G. Liu, Q. Wang, W. Sun, B. Zhao, L. Wang, H. Zhang, Activation of persulfate by EDTA-2K-derived nitrogen-doped porous carbons for organic contaminant removal: Radical and non-radical pathways, Chem. Eng. J. 386 (2020), 124009, https://doi.org/10.1016/j.cej.2019.124009.

[41] N. Guettaï, H. Ait Amar, Photocatalytic oxidation of methyl orange in presence of titanium dioxide in aqueous suspension. Part I: Parametric study, Desalination 185 (2005) 427–437, https://doi.org/10.1016/j.desal.2005.04.048.

[42] S. Xie, P. Huang, J.J. Kruzic, X. Zeng, H. Qian, A highly efficient degradation mechanism of methyl orange using Fe-based metallic glass powders, Sci. Rep. 6 (2016) 21947, https://doi.org/10.1038/srep21947.

[43] W. Stumm, J.J. Morgan, Aquatic chemistry: Chemical Equilibria and Rates in Natural Waters, Wiley, Hoboken, New Jersey, USA, 2012.

[44] C. Liang, C.F. Huang, N. Mohanty, R.M. Kurakalva, A rapid spectrophotometric determination of persulfate anion in ISCO, Chemosphere 73 (2008) 1540–1543, https://doi.org/10.1016/j.chemosphere.2008.08.043.

[45] S. Wacławek, K. Grübel, M. Černík, Simple spectrophotometric determination of monopersulfate, Spectrochim. Acta - Part A Mol Biomol. Spectrosc. 149 (2015) 928–933, https://doi.org/10.1016/j.saa.2015.05.029.

[48] S.A. Ashter, Mechanics of Materials, in: Thermoforming of Single and Multilayer Laminates, Elsevier, Amsterdam, Netherlands, 2014, pp. 123–145, https://doi.org/10.1016/B978-1-4557-3172-5.00006-2.

[49] Y. Feng, P.H. Lee, D. Wu, K. Shih, Surface-bound sulfate radical-dominated degradation of 1,4-dioxane by alumina-supported palladium (Pd/Al_2O_3) catalyzed peroxymonosulfate, Water Res. 120 (2017) 12–21, https://doi.org/10.1016/j.watres.2017.04.070.

[50] S. Wacławek, H.V. Lutze, K. Grübel, V.V.T. Padil, M. Černík, D.D. Dionysiou, Chemistry of persulfates in water and wastewater treatment: A review, Chem. Eng. J. 330 (2017) 44–62, https://doi.org/10.1016/j.cej.2017.07.132.

[51] B. Alkotaini, S. Abdellaoui, K. Hasan, M. Grattieri, T. Quah, R. Cai, M. Yuan, S. D. Minteer, Sustainable Bioelectrosynthesis of the Bioplastic Polyhydroxybutyrate: Overcoming Substrate Requirement for NADH Regeneration, ACS Sustain. Chem. Eng. 6 (2018) 4909–4915, https://doi.org/10.1021/acssuschemeng.7b04392.

[52] Y.S. Mostafa, S.A. Alrumman, K.A. Otaif, S.A. Alamri, M.S. Mostafa, T. Sahlabji, Production and Characterization of Bioplastic by Polyhydroxybutyrate Accumulating Erythrobacter aquimaris Isolated from Mangrove Rhizosphere, Molecules 25 (2020) 179, https://doi.org/10.3390/molecules25010179.

[53] J Wyckoff, R.W.G. Cubic Closest Packed, Structure. In Crystal Structures, 2nd ed.; Interscience Publishers, New York, NY, USA, 1963; pp. 7–83.

[54] J. Filip, F. Karlický, Z. Marušák, P. Lazar, M. Černík, M. Otyepka, R. Zbořil, Anaerobic reaction of nanoscale zerovalent iron with water: Mechanism and kinetics, J. Phys. Chem. C. 118 (2014) 13817–13825, https://doi.org/10.1021/jp501846f.

[55] T. Tosco, M. Petrangeli Papini, C. Cruz Viggi, R. Sethi, Nanoscale zerovalent iron particles for groundwater remediation: a review, J. Clean. Prod. 77 (2014) 10–21, https://doi.org/10.1016/J.JCLEPRO.2013.12.026.
[56] S. Wacławek, J. Nosek, L. Cádrová, V. Antoš, M. Černík, Use of Various Zero Valent Irons for Degradation of Chlorinated Ethenes and Ethanes, Ecol. Chem. Eng. S. 22 (2016) 577–587, https://doi.org/10.1515/eces-2015-0034.
[57] L. Gomathi Devi, S. Girish Kumar, K. Mohan Reddy, C. Munikrishnappa, Photo degradation of Methyl Orange an azo dye by Advanced Fenton Process using zero valent metallic iron: Influence of various reaction parameters and its degradation mechanism, J. Hazard. Mater. 164 (2009) 459–467, https://doi.org/10.1016/J.JHAZMAT.2008.08.017.
[58] A. Ghauch, A. Baalbaki, M. Amasha, R. El Asmar, O. Tantawi, Contribution of persulfate in UV-254nm activated systems for complete degradation of chloramphenicol antibiotic in water, Chem. Eng. J. 317 (2017) 1012–1025, https://doi.org/10.1016/j.cej.2017.02.133.
[59] M. Amasha, A. Baalbaki, A. Ghauch, A comparative study of the common persulfate activation techniques for the complete degradation of an NSAID: The case of ketoprofen, Chem. Eng. J. 350 (2018) 395–410, https://doi.org/10.1016/j.cej.2018.05.118.
[60] G. Ayoub, A. Ghauch, Assessment of bimetallic and trimetallic iron-based systems for persulfate activation: Application to sulfamethoxazole degradation, Chem. Eng. J. 256 (2014) 280–292, https://doi.org/10.1016/j.cej.2014.07.002.
[61] H. Song, E.R. Carraway, Reduction of chlorinated ethanes by nanosized zero-valent iron: Kinetics, pathways, and effects of reaction conditions, Environ. Sci. Technol. 39 (2005) 6237–6245, https://doi.org/10.1021/es048262e.
[62] I. Hussain, Y. Zhang, S. Huang, Degradation of aniline with zero-valent iron as an activator of persulfate in aqueous solution, RSC Adv. 4 (2014) 3502–3511, https://doi.org/10.1039/C3RA43364A.
[63] H. Li, J. Guo, L. Yang, Y. Lan, Degradation of methyl orange by sodium persulfate activated with zero-valent zinc, Sep. Purif. Technol. 132 (2014) 168–173, https://doi.org/10.1016/j.seppur.2014.05.015.
[64] M. Brienza, I.A. Katsoyiannis, Sulfate radical technologies as tertiary treatment for the removal of emerging contaminants from wastewater, Sustain. 9 (2017) 1604, https://doi.org/10.3390/su9091604.
[65] R.E. Huie, C.L. Clifton, P. Neta, Electron transfer reaction rates and equilibria of the carbonate and sulfate radical anions, Int. J. Radiat. Appl. Instrumentation. Part C Radiat. Phys. Chem. 38 (1991) 477–481, https://doi.org/10.1016/1359-0197(91)90065-A.
[66] F. Ghanbari, M. Riahi, B. Kakavandi, X. Hong, K.Y.A. Lin, Intensified peroxydisulfate/microparticles-zero valent iron process through aeration for degradation of organic pollutants: Kinetic studies, mechanism and effect of anions, J. Water Process Eng. 36 (2020), 101321, https://doi.org/10.1016/j.jwpe.2020.101321.
[67] Z. Zuo, Z. Cai, Y. Katsumura, N. Chitose, Y. Muroya, Reinvestigation of the acid–base equilibrium of the (bi)carbonate radical and pH dependence of its reactivity with inorganic reactants, Radiat. Phys. Chem. 55 (1999) 15–23, https://doi.org/10.1016/S0969-806X(98)00308-9.
[68] H. Pullin, R.A. Crane, D.J. Morgan, T.B. Scott, The effect of common groundwater anions on the aqueous corrosion of zero-valent iron nanoparticles and associated removal of aqueous copper and zinc, J. Environ. Chem. Eng. 5 (2017) 1166–1173, https://doi.org/10.1016/j.jece.2017.01.038.
[69] X. Wu, X. Gu, S. Lu, Z. Qiu, Q. Sui, X. Zang, Z. Miao, M. Xu, Strong enhancement of trichloroethylene degradation in ferrous ion activated persulfate system by promoting ferric and ferrous ion cycles with hydroxylamine, Sep. Purif. Technol. 147 (2015) 186–193, https://doi.org/10.1016/j.seppur.2015.04.031.
[70] L.R. Bennedsen, J. Muff, E.G. Søgaard, Influence of chloride and carbonates on the reactivity of activated persulfate, Chemosphere 86 (2012) 1092–1097, https://doi.org/10.1016/j.chemosphere.2011.12.011.
[71] Y. Yao, Y. Cai, G. Wu, F. Wei, X. Li, H. Chen, S. Wang, Sulfate radicals induced from peroxymonosulfate by cobalt manganese oxides ($Co_xMn_{3-x}O_4$) for Fenton-Like reaction in water, J. Hazard. Mater. 296 (2015) 128–137, https://doi.org/10.1016/j.jhazmat.2015.04.014.
[72] F. Ghanbari, M. Ahmadi, F. Gohari, Heterogeneous activation of peroxymonosulfate via nanocomposite CeO_2-Fe_3O_4 for organic pollutants removal: The effect of UV and US irradiation and application for real wastewater, Sep. Purif. Technol. 228 (2019), https://doi.org/10.1016/j.seppur.2019.115732.
[73] A.B.M. Giasuddin, S.R. Kanel, H. Choi, Adsorption of humic acid onto nanoscale zerovalent iron and its effect on arsenic removal, Environ. Sci. Technol. 41 (2007) 2022–2027, https://doi.org/10.1021/es0616534.
[74] H.H. Dong, I.M.C. Lo, Influence of humic acid on the colloidal stability of surface-modified nano zero-valent iron, Water Res. 47 (2013) 419–427, https://doi.org/10.1016/j.watres.2012.10.013.
[75] X. Sun, H. Liu, Y. Zhang, Y. Zhao, X. Quan, Effects of Cu(II) and humic acid on atrazine photodegradation, J. Environ. Sci. 23 (2011) 773–777, https://doi.org/10.1016/S1001-0742(10)60476-7.
[76] B.-T. Zhang, Y. Zhang, Y. Teng, M. Fan, Sulfate Radical and Its Application in Decontamination Technologies, Crit. Rev. Environ. Sci. Technol. 45 (2014) 1756–1800, https://doi.org/10.1080/10643389.2014.970681.
[77] Z. Wang, W. Qiu, S. Pang, Y. Gao, Y. Zhou, Y. Cao, J. Jiang, Relative contribution of ferryl ion species (Fe(IV)) and sulfate radical formed in nanoscale zero valent iron activated peroxydisulfate and peroxymonosulfate processes, Water Res. 172 (2020), 115504, https://doi.org/10.1016/j.watres.2020.115504.
[78] T. Zhang, Y. Yang, X. Li, H. Yu, N. Wang, H. Li, P. Du, Y. Jiang, X. Fan, Z. Zhou, Degradation of sulfamethazine by persulfate activated with nanosized zero-valent copper in combination with ultrasonic irradiation, Sep. Purif. Technol. 239 (2020), 116537, https://doi.org/10.1016/j.seppur.2020.116537.
[79] C. Zhu, G. Fang, D.D. Dionysiou, C. Liu, J. Gao, W. Qin, D. Zhou, Efficient transformation of DDTs with Persulfate Activation by Zero-valent Iron Nanoparticles: A Mechanistic Study, J. Hazard. Mater. 316 (2016) 232–241, https://doi.org/10.1016/j.jhazmat.2016.05.040.
[80] Y. Xie, X. Wang, W. Tong, W. Hu, P. Li, L. Dai, Y. Wang, Y. Zhang, Fe_xP/biochar composites induced oxygen-driven Fenton-like reaction for sulfamethoxazole removal: Performance and reaction mechanism, Chem. Eng. J. 396 (2020), 125321, https://doi.org/10.1016/j.cej.2020.125321.
[81] U. Khunjan, P. Kasikamphaiboon, Green Synthesis of Kaolin-Supported Nanoscale Zero-Valent Iron Using *Ruellia tuberosa* Leaf Extract for Effective Decolorization of Azo Dye Reactive Black 5, Arab. J. Sci. Eng. (2020) 1–12, https://doi.org/10.1007/s13369-020-04831-w.
[82] J. Du, Y. Wang, T. Faheem, H. Xu, J. Zheng, Bao, Synergistic degradation of PNP via coupling H_2O_2 with persulfate catalyzed by nano zero valent iron, RSC Adv. 9 (2019) 20323–20331, https://doi.org/10.1039/c9ra02901j.
[83] H. Dong, F. Zhao, Q. He, Y. Xie, Y. Zeng, L. Zhang, L. Tang, G. Zeng, Physicochemical transformation of carboxymethyl cellulose-coated zero-valent iron nanoparticles (nZVI) in simulated groundwater under anaerobic conditions, Sep. Purif. Technol. 175 (2017) 376–383, https://doi.org/10.1016/j.seppur.2016.11.053.
[84] Z. Guan, Y. Shu, Y. Ma, J. Wan, Factors affecting the physicochemical properties of the modified core/shell NH_2-SiO_2@NZVI nanoparticles, Colloids Surf. A Physicochem. Eng. Asp. 482 (2015) 18–26, https://doi.org/10.1016/j.colsurfa.2015.03.057.
[85] H. Yao, Q. Ding, H. Zhou, Z. Zhao, G. Liu, G. Wang, An adsorption-reduction synergistic effect of mesoporous Fe/SiO_2-NH_2 hollow spheres for the removal of Cr (VI) ions, RSC Adv. 6 (2016) 27039–27046, https://doi.org/10.1039/c6ra03172b.

CONCLUSIONS

My work demonstrated the feasibility of conjugating chitosan and PHB in a greener procedure under certain conditions. Cs–PHB conjugate was characterised by several techniques. In addition, Cs–PHB was employed for the greener synthesis of several nanostructures. Furthermore, the synthesis conditions were studied by investigating the influence of parameters, such as the concentrations of Cs–PHB and metal salt precursors, as well as temperature. From this investigation, results emerged that Pd/Pt nanoparticles can change shape under certain conditions by varying the synthesis procedure. Data on degradation kinetics using TMNPs reveal that the nanoparticles coated by Cs–PHB exhibit extraordinary behaviour through 4–NP hydrogenation. Parameters such as pseudo–first order kinetics, activity parameter and specific surface area were used to describe the catalytic performance of nano–catalysts. Furthermore, Cs–PHB–nZVI, due to the large surface area recorded by Brunauer–Emmett–Teller theory, was used as a persulfate activator for the degradation of a model pollutant with extraordinary results. As a long-term impact, it is belived that the Cs–PHB polymer conjugate can find application in other fields such as greener food packaging.

Attachments

Articles

- Kudlek, E.; Silvestri, D.; Wacławek, S.; Padil, V.V.T.; Stuchlík, M.; Voleský, L.; Kejzlar, P.; ČERNíK, M. TiO_2 immobilised on biopolymer nanofibers for the removal of bisphenol A and diclofenac from water. *Ecol. Chem. Eng. S* **2017**, *24*, 417–429, doi:10.1515/eces-2017-0028.
- Silvestri, D.; Wacławek, S.; Sobel, B.; Torres-Mendieta, R.; Novotný, V.; Nguyen, N.H.A.; Ševců, A.; Padil, V.V.T.; Müllerová, J.; Stuchlík, M.; et al. A poly(3-hydroxybutyrate)-chitosan polymer conjugate for the synthesis of safer gold nanoparticles and their applications. *Green Chem.* **2018**, *20*, 4975–4982, doi:10.1039/c8gc02495b
- Silvestri, D.; Chłąd, Z.; Wacławek, S.; Adach, K.; Fijałkowski, M.; Padil, V.T.V.; Černík, M. A comparative study of gold nanoparticles synthesized with a "green" approach. In Proceedings of the NANOCON 2017 - Conference Proceedings, 9th International Conference on Nanomaterials - Research and Application; **2018**; 416-421
- Silvestri, D.; Wacławek, S.; Gončuková, Z.; Padil, V.V.T.; Grübel, K.; Černík, M. A new method for assessment of the sludge disintegration degree with the use of differential centrifugal sedimentation. *Env. Tech.* **2018**, *40*, 3086-3093, doi:10.1080/09593330.2018.1477839
- Wacławek, S.; Grübel, K.; Silvestri, D.; Padil, V.V.T.; Ząbkowska-Wacławek, M.; Černík, M. Disintegration of wastewater activated sludge (WAS) for improved biogas production: a mini review. *Energies* **2019**, *12*, 21, https://doi.org/10.3390/en12010021.
- Krawczyk, K.; Wacławek, S.; Silvestri, D.; Torres-Mendieta, R.; Padil, V.V.T.; Řezanka, M.; Černík, M. Synergistic effect of nano zero-valent iron and cyclodextrins: a nano-structure for water purification. In Proceedings of the NANOCON 2019 Conference Proeedings; **2019**, 279–286 https://doi.org/10.37904/nanocon.2019.8575
- Silvestri, D.; Mikšíček, J.; Wacławek, S.; Torres-Mendieta, R.; Padil, V.V.T.; Černík, M. Production of electrospun nanofibers based on graphene oxide/gum Arabic. *Int. J. Biol. Macromol.* **2019**, *124*, 396–402, doi:10.1016/j.ijbiomac.2018.11.243
- Wacławek, S.; Silvestri, D.; Hrabák, P.; Padil, V.V.T.; Torres-Mendieta, R.; Wacławek, M.; Černík, M.; Dionysiou, D.D. Chemical oxidation and reduction of hexachlorocyclohexanes: A review. *Wat. Res.* **2019**; *162*, 302–319, https://doi.org/10.1016/j.watres.2019.06.072

- Venkateshaiah, A.; Silvestri, D.; Ramakrishnan, R.K.; Wacławek, S.; Padil, V.V.T.; Černík, M.; Varma, R.S. Gum kondagogu/reduced graphene oxide framed platinum nanoparticles and their catalytic role. *Molecules* **2019**, *24*, 3643, doi:10.3390/molecules24203643
- Silvestri, D.; Wacławek, S.; Ramakrishnan, R.K.; Venkateshaiah, A.; Krawczyk, K.; Padil, V.V.T.; Sobel, B.; Černík, M. The use of a biopolymer conjugate for an eco-friendly one-pot synthesis of palladium-platinum alloys. *Polymers* **2019**, *11*, 1948, doi:10.3390/polym11121948
- Silvestri, D.; Wacławek, S.; Venkateshaiah, A.; Krawczyk, K.; Sobel, B.; Padil, V.V.T.; Černík, M.; Varma, R.S. Synthesis of Ag nanoparticles by a chitosan-poly(3-hydroxybutyrate) polymer conjugate and their superb catalytic activity. *Carbohydr. Polym.* **2020**, *232*, doi:10.1016/j.carbpol.2019.115806
- Krawczyk, K.; Wacławek, S.; Kudlek, E.; Silvestri, D.; Kukulski, T.; Grübel, K.; Padil, V.V.T.; Černík, M. Uv-catalyzed persulfate oxidation of an anthraquinone based dye. *Catalysts* **2020**, *10*, 456, doi:10.3390/catal10040456.
- Kukulski, T.; Wacławek, S.; Silvestri, D.; Krawczyk, K.; Padil, V.V.T.; Fryczkowski, R.; Janicki, J.; Černík, M. A polymeric composite material (RGO/PANI) for acid blue 129 adsorption. *Polymers* **2020**, *12*, 1051, doi:10.3390/polym12051051.
- Silvestri, D.; Krawczyk, K.; Pawlyta, M.; Krzywiecki, M.; Padil, V.V.T.; Torres-Mendieta, R.; Ghanbari, F.; Dinc, O.; Černík, M.; Dionysiou, D.D.; et al. Influence of catalyst zeta potential on the activation of persulfate. *Chem. Commun.* **2021**, *57*, 7814–7817, doi:10.1039/d1cc01946e
- Silvestri, D.; Wacławek, S.; Sobel, B.; Torres–Mendieta, R.; Pawlyta, M.; Padil, V.V.T.; Filip, J.; Černík, M. Modification of nZVI with a bio-conjugate containing amine and carbonyl functional groups for catalytic activation of persulfate. *Sep. Purif. Technol.* **2021**, *257*, 117880, doi:10.1016/j.seppur.2020.117880
- Krawczyk, K.; Wacławek, S.; Silvestri, D.; Padil, V.V.T.; Řezanka, M.; Černík, M.; Jaroniec, M. Surface modification of zero-valent iron nanoparticles with β-cyclodextrin for 4-nitrophenol conversion. *J. Colloid Interface Sci.* **2020**, *586*, 655–662, doi:10.1016/j.jcis.2020.10.135

- Wacławek, S.; Silvestri, D.; Padil, V.V.T.; Černík, M.; Dionysiou, D.D. Selective spectrophotometric determination of peroxydisulfate based on a by-product formation. *Sensors Actuators B Chem.* **2021**, *344*, 130214, doi:10.1016/j.snb.2021.130214
- Ettel, D.; Havelka, O.; Isik, S.; Silvestri, D.; Wacławek, S.; Urbánek, M.; Padil, V.V.T.; Černík, M.; Yalcinkaya, F.; Torres-Mendieta, R. Laser-synthesized Ag/TiO nanoparticles to integrate catalytic pollutant degradation and antifouling enhancement in nanofibrous membranes for oil–water separation. *Appl. Surf. Sci.* **2021**, *564*, 150471, doi:10.1016/j.apsusc.2021.150471
- Venkateshaiah, A.; Silvestri, D.; Wacławek, S.; Ramakrishnan, R.K.; Krawczyk, K.; Saravanan, P.; Pawlyta, M.; Padil, V.V.T.; Černík, M.; Dionysiou, D.D. A comparative study of the degradation efficiency of chlorinated organic compounds by bimetallic zero-valent iron nanoparticles. *Environ. Sci. Water Res. Technol.* **2022**, *8,* 162-172 doi:10.1039/d1ew00791b
- Kończak, B.; Gzyl, G.; Wacławek, S.; Łabaj, P.; Silvestri, D.; Hrabák, P.; Černík, M. Application of zero-valent iron/peat permeable reactive barrier for in-situ remediation of lindane and chlorobenzenes. *Des. Water Treat.* **2022**, *252*, 287-299 doi:10.5004/dwt.2022.28264
- Krawczyk, K.; Silvestri, D.; Nguyen, N.H.A.; Ševců, A.; Łukowiec, D.; Padil, V.V.T.; Řezanka, M.; Černík, M.; Dionysiou, D.D.; Wacławek, S. Enhanced degradation of sulfamethoxazole by a modified nano zero-valent iron with a β-cyclodextrin polymer: Mechanism and toxicity evaluation. *Sci. Total Environ.* **2022**, *817*, 152888, doi:10.1016/j.scitotenv.2021.152888
- Socha, B.; Silvestri, D.; Grübel, K.; Padil, V.V.T.; Dudziak, M.; Ghanbari, F.; Černík, M.; Wacławek, S. Activation of peroxydisulfate by bimetallic nano zero-valent iron for waste-activated sludge disintegration. *Catalysts* **2022**, *12*, 590, doi:10.3390/catal12060590
- Ramakrishnan, R.K.; Silvestri, D.; Sumitha, N.S.; Nguyen, N.H.A.; Havlíček, K.; Łukowiec, D.; Wacławek, S.; Černík, M.; Tiwari, D.; Padil, V.V.T.; et al. Gum Hydrocolloids Reinforced Silver Nanoparticle Sponge for Catalytic Degradation of Water Pollutants. *Polymers* **2022**, *14*, 3120, doi:10.3390/polym14153120/s1
- Wacławek, S.; Krawczyk, K.; Silvestri, D.; Padil, V.V.T.; Řezanka, M.; Černík, M.; Jaroniec, M. Cyclodextrin-based strategies for removal of persistent organic pollutants. *Adv. Colloid Interface Sci.* **2022**, *310*, 102807, doi:10.1016/J.CIS.2022.102807

- Świsłowski, P.; Nowak, A.;Wacławek S.; Silvestri D.; Rajfur, M. Bioaccumulation of trace elements from aqueous solutions by selected terrestrial moss species. *Biol.* **2022**, 11, 1692, doi:10.3390/biology11121692.

Patent

- WACLAWEK, S., SILVESTRI, D. a ČERNÍK, M. *Způsob stanovení přítomnosti a koncentrace persíranu(ů) ve vodě, zejména v podzemní vodě, ve které je navíc obsažené alespoň jedno jiné oxidační činidlo* [patent] Udělen 20220223 pod číslem 309167.

Cover page

- Polymers, Volume 11, Issue 12 (December 2019)

REFERENCES

[1] R. Langer, D.A. Tirrell, Designing materials for biology and medicine, Nat. 2004 4286982. 428 (2004) 487–492. https://doi.org/10.1038/nature02388.

[2] W.J. Ong, L.L. Tan, Y.H. Ng, S.T. Yong, S.P. Chai, Graphitic Carbon Nitride (g-C_3N_4)-Based photocatalysts for artificial photosynthesis and environmental remediation: are we a step closer to achieving sustainability?, Chem. Rev. 116 (2016) 7159–7329. https://doi.org/10.1021/acs.chemrev.6b00075.

[3] B. Thomas, M.C. Raj, B.K. Athira, H.M. Rubiyah, J. Joy, A. Moores, G.L. Drisko, C. Sanchez, Nanocellulose, a versatile green platform: from biosources to materials and their applications, Chem. Rev. 118 (2018) 11575–11625. https://doi.org/10.1021/acs.chemrev.7b00627.

[4] M.P. Lutolf, J.A. Hubbell, Synthetic biomaterials as instructive extracellular microenvironments for morphogenesis in tissue engineering, Nat. Biotechnol. 23 (2005) 47–55. https://doi.org/10.1038/nbt1055.

[5] K. Rezwan, Q.Z. Chen, J.J. Blaker, A.R. Boccaccini, Biodegradable and bioactive porous polymer/inorganic composite scaffolds for bone

tissue engineering, Biomaterials. 27 (2006) 3413–3431. https://doi.org/10.1016/j.biomaterials.2006.01.039.

[6] A. Venkateshaiah, K. Havlíček, R.L. Timmins, M. Röhrl, S. Wacławek, N.H.A. Nguyen, M. Černík, V.V.T. Padil, S. Agarwal, Alkenyl succinic anhydride modified tree-gum kondagogu: A bio-based material with potential for food packaging, Carbohydr. Polym. 266 (2021) 118126. https://doi.org/10.1016/j.carbpol.2021.118126.

[7] A. George, M.R. Sanjay, R. Srisuk, J. Parameswaranpillai, S. Siengchin, A comprehensive review on chemical properties and applications of biopolymers and their composites, Int. J. Biol. Macromol. 154 (2020) 329–338. https://doi.org/10.1016/j.ijbiomac.2020.03.120.

[8] R. Yang, H. Li, M. Huang, H. Yang, A. Li, A review on chitosan-based flocculants and their applications in water treatment, Water Res. 95 (2016) 59–89. https://doi.org/10.1016/j.watres.2016.02.068.

[9] S. (Gabriel) Kou, L. Peters, M. Mucalo, Chitosan: A review of molecular structure, bioactivities and interactions with the human body and micro-organisms, Carbohydr. Polym. 282 (2022) 119132. https://doi.org/10.1016/j.carbpol.2022.119132.

[10] G.Q. Chen, Q. Wu, The application of polyhydroxyalkanoates as

tissue engineering materials, Biomaterials. 26 (2005) 6565–6578. https://doi.org/10.1016/j.biomaterials.2005.04.036.

[11] A.A. Amadu, S. Qiu, S. Ge, G.N.D. Addico, G.K. Ameka, Z. Yu, W. Xia, A.W. Abbew, D. Shao, P. Champagne, S. Wang, A review of biopolymer (Poly-β-hydroxybutyrate) synthesis in microbes cultivated on wastewater, Sci. Total Environ. 756 (2021) 143729. https://doi.org/10.1016/j.scitotenv.2020.143729.

[12] F. Hempel, A.S. Bozarth, N. Lindenkamp, A. Klingl, S. Zauner, U. Linne, A. Steinbüchel, U.G. Maier, Microalgae as bioreactors for bioplastic production, Microb. Cell Fact. 10 (2011) 1–6. https://doi.org/10.1186/1475-2859-10-81.

[13] P.G. Jamkhande, N.W. Ghule, A.H. Bamer, M.G. Kalaskar, Metal nanoparticles synthesis: An overview on methods of preparation, advantages and disadvantages, and applications, J. Drug Deliv. Sci. Technol. 53 (2019) 101174. https://doi.org/10.1016/j.jddst.2019.101174.

[14] A. Venkateshaiah, D. Silvestri, S. Wacławek, R.K. Ramakrishnan, K. Krawczyk, P. Saravanan, M. Pawlyta, V.V.T. Padil, M. Černík, D.D. Dionysiou, A comparative study of the degradation efficiency of chlorinated organic compounds by bimetallic zero-valent iron nanoparticles, Environ. Sci. Water Res. Technol. (2022).

https://doi.org/10.1039/d1ew00791b.

[15] P. Endla, V. Radhika, Fabrication and evaluation of gold nanoparticles by ball milling, Hall-Williamson and x-ray diffraction method, Mater. Today Proc. 47 (2021) 4993–4995. https://doi.org/10.1016/j.matpr.2021.04.451.

[16] F. Mafuné, J.Y. Kohno, Y. Takeda, T. Kondow, H. Sawabe, Formation of gold nanoparticles by laser ablation in aqueous solution of surfactant, J. Phys. Chem. B. 105 (2001) 5114–5120. https://doi.org/10.1021/JP0037091.

[17] F. Mafuné, J.Y. Kohno, Y. Takeda, T. Kondow, Formation of stable platinum nanoparticles by laser ablation in water, J. Phys. Chem. B. 107 (2003) 4218–4223. https://doi.org/10.1021/JP021580K.

[18] P.A. Pandey, G.R. Bell, J.P. Rourke, A.M. Sanchez, M.D. Elkin, B.J. Hickey, N.R. Wilson, P.A. Pandey, G.R. Bell, A.M. Sanchez, N.R. Wilson, J.P. Rourke, M.D. Elkin, B.J. Hickey, Physical vapor deposition of metal nanoparticles on chemically modified graphene: observations on metal–graphene interactions, Small 7 (2011) 3202–3210. https://doi.org/10.1002/smll.201101430.

[19] C.B.D. Marien, C. Marchal, A. Koch, D. Robert, P. Drogui, Sol-gel synthesis of TiO_2 nanoparticles: effect of Pluronic P123 on particle's

morphology and photocatalytic degradation of paraquat, Environ. Sci. Pollut. Res. 24 (2017) 12582–12588. https://doi.org/10.1007/s11356-016-7681-2.

[20] E. Petala, K. Dimos, A. Douvalis, T. Bakas, J. Tucek, R. Zbořil, M.A. Karakassides, Nanoscale zero-valent iron supported on mesoporous silica: characterization and reactivity for Cr(VI) removal from aqueous solution, J. Hazard. Mater. 261 (2013) 295–306. https://doi.org/10.1016/j.jhazmat.2013.07.046.

[21] B. Bari, J. Lee, T. Jang, P. Won, S.H. Ko, K. Alamgir, M. Arshad, L.J. Guo, Simple hydrothermal synthesis of very-long and thin silver nanowires and their application in high quality transparent electrodes, J. Mater. Chem. A. 4 (2016) 11365–11371. https://doi.org/10.1039/c6ta03308c.

[22] J. Choi, S. Park, Z. Stojanović, H.S. Han, J. Lee, H.K. Seok, D. Uskoković, K.H. Lee, Facile solvothermal preparation of monodisperse gold nanoparticles and their engineered assembly of ferritin-gold nanoclusters, Langmuir. 29 (2013) 15698–15703. https://doi.org/10.1021/la403888f.

[23] S. Kango, S. Kalia, A. Celli, J. Njuguna, Y. Habibi, R. Kumar, Surface modification of inorganic nanoparticles for development of organic–inorganic nanocomposites—A review, Prog. Polym. Sci. 38

(2013) 1232–1261.
https://doi.org/10.1016/j.progpolymsci.2013.02.003.

[24] A.R. Studart, E. Amstad, L.J. Gauckler, Colloidal stabilization of nanoparticles in concentrated suspensions, Langmuir. 23 (2007) 1081–1090. https://doi.org/10.1021/la062042s.

[25] Y. Wang, Y. Han, X. Tan, Y. Dai, F. Xia, X. Zhang, Cyclodextrin capped gold nanoparticles (AuNP@CDs): from synthesis to applications, J. Mater. Chem. B. 9 (2021) 2584–2593.
https://doi.org/10.1039/d0tb02857f.

[26] L.A. Frank, G.R. Onzi, A.S. Morawski, A.R. Pohlmann, S.S. Guterres, R. V. Contri, Chitosan as a coating material for nanoparticles intended for biomedical applications, React. Funct. Polym. 147 (2020) 104459.
https://doi.org/10.1016/j.reactfunctpolym.2019.104459.

[27] H. Tian, Y. Liang, D. Yang, Y. Sun, Characteristics of PVP–stabilised NZVI and application to dechlorination of soil–sorbed TCE with ionic surfactant, Chemosphere 239 (2020) 124807.
https://doi.org/10.1016/j.chemosphere.2019.124807.

[28] M.E. Mahmoud, E.A. Saad, M.A. Soliman, M.S. Abdelwahab, Synthesis and surface protection of nano zerovalent iron (NZVI)

with 3-aminopropyltrimethoxysilane for water remediation of cobalt and zinc and their radioactive isotopes, RSC Adv. 6 (2016) 66242–66251. https://doi.org/10.1039/c6ra11049e.

[29] X. Duan, H. Sun, J. Kang, Y. Wang, S. Indrawirawan, S. Wang, Insights into heterogeneous catalysis of persulfate activation on dimensional-structured nanocarbons, ACS Catal. 5 (2015) 4629–4636. https://doi.org/10.1021/acscatal.5b00774.

[30] W. Ren, G. Nie, P. Zhou, H. Zhang, X. Duan, S. Wang, The Intrinsic nature of persulfate activation and N-doping in carbocatalysis, Environ. Sci. Technol. 54 (2020) 6438–6447. https://doi.org/10.1021/acs.est.0c01161.

[31] W. Ren, L. Xiong, G. Nie, H. Zhang, X. Duan, S. Wang, Insights into the electron-transfer regime of peroxydisulfate activation on carbon nanotubes: the role of oxygen functional groups, Environ. Sci. Technol. 54 (2020) 1267–1275. https://doi.org/10.1021/acs.est.9b06208.

[32] D. Silvestri, K. Krawczyk, M. Pawlyta, M. Krzywiecki, V.V.T. Padil, R. Torres-Mendieta, F. Ghanbari, O. Dinc, M. Černík, D.D. Dionysiou, S. Wacławek, Influence of catalyst zeta potential on the activation of persulfate, Chem. Commun. 57 (2021) 7814–7817. https://doi.org/10.1039/d1cc01946e.

[33] M. Stefaniuk, P. Oleszczuk, Y.S. Ok, Review on nano zerovalent iron (nZVI): From synthesis to environmental applications, Chem. Eng. J. 287 (2016) 618–632. https://doi.org/10.1016/j.cej.2015.11.046.

[34] T.A. Salem, N.A. Fetian, N.I. Elsheery, Nanotechnology for polluted soil remediation, Nanotechnol. Agric. Adv. Sustain. Agric. (2019) 285–305. doi: 10.1007/978-981-32-9370-0_15.

[35] S.I. Siddiqui, S.A. Chaudhry, Iron oxide and its modified forms as an adsorbent for arsenic removal: A comprehensive recent advancement, Process Saf. Environ. Prot. 111 (2017) 592–626. https://doi.org/10.1016/j.psep.2017.08.009.

[36] Y.S. Seo, E.Y. Ahn, J. Park, T.Y. Kim, J.E. Hong, K. Kim, Y. Park, Y. Park, Catalytic reduction of 4-nitrophenol with gold nanoparticles synthesized by caffeic acid, Nanoscale Res. Lett. 12 (2017) 1–11. https://doi.org/10.1186/s11671-016-1776-z.

[37] Y. Li, L. Pan, Y. Zhu, Y. Yu, D. Wang, G. Yang, X. Yuan, X. Liu, H. Li, J. Zhang, How does zero valent iron activating peroxydisulfate improve the dewatering of anaerobically digested sludge?, Water Res. 163 (2019) 114912. https://doi.org/10.1016/j.watres.2019.114912.

[38] G. Yu, X. Wang, J. Liu, P. Jiang, S. You, N. Ding, Q. Guo, F. Lin,

Applications of nanomaterials for heavy metal removal from water and soil: a review, Sustain. 13 (2021) 713. https://doi.org/10.3390/su13020713.

[39] A. Gangula, R. Podila, R. M, L. Karanam, C. Janardhana, A.M. Rao, Catalytic reduction of 4-nitrophenol using biogenic gold and silver nanoparticles derived from *Breynia rhamnoides*, Langmuir. 27 (2011) 15268–15274. https://doi.org/10.1021/la2034559.

[40] X. Li, Y. Zhao, B. Xi, X. Meng, B. Gong, R. Li, X. Peng, H. Liu, Decolorization of methyl orange by a new clay-supported nanoscale zero-valent iron: synergetic effect, efficiency optimization and mechanism, J. Environ. Sci. 52 (2017) 8–17. https://doi.org/10.1016/j.jes.2016.03.022.

[41] J. Li, X. Sun, S. Subhan, W. Gong, W. Li, W. Sun, Y. Zhang, M. Lu, H. Ji, Z. Zhao, Z. Zhao, Construction of novel Cu-based bimetal polycrystal@carbon catalyst prepared from bimetal HKUST-1 type MOFs (MOF-199s) for ultrafast reduction of 4-nitrophenol via interfacial synergistic catalysis, Chem. Eng. J. 446 (2022) 137314. https://doi.org/10.1016/j.cej.2022.137314.

[42] L. Cai, L. Zhang, X. Xu, One-step synthesis of ultra-small silver nanoparticles-loaded triple-helix β-glucan nanocomposite for highly catalytic hydrogenation of 4-nitrophenol and dyes, Chem. Eng. J.

442 (2022) 136114. https://doi.org/10.1016/j.cej.2022.136114.

[43] X. Sun, D. Xu, P. Dai, X. Liu, F. Tan, Q. Guo, Efficient degradation of methyl orange in water via both radical and non-radical pathways using Fe-Co bimetal-doped MCM-41 as peroxymonosulfate activator, Chem. Eng. J. 402 (2020) 125881. https://doi.org/10.1016/j.cej.2020.125881.

[44] D. Robati, B. Mirza, M. Rajabi, O. Moradi, I. Tyagi, S. Agarwal, V.K. Gupta, Removal of hazardous dyes-BR 12 and methyl orange using graphene oxide as an adsorbent from aqueous phase, Chem. Eng. J. 284 (2016) 687–697. https://doi.org/10.1016/j.cej.2015.08.131.

[45] E.B. Mano, Natural Polymer Characterization, Macromol. Symp. 258 (2007) 1–4. https://doi.org/10.1002/masy.200751201.

[46] R.N. Tharanathan, F.S. Kittur, Chitin — the undisputed biomolecule of great potential, Crit. Rev. Food Sci. Nutr. 43 (2003) 61–87. https://doi.org/10.1080/10408690390826455.

[47] B. H., Sur la nature des champibnons, Ann Chi. 79 (1881) 265–304.

[48] N.K. Mathur, C.K. Narang, Chitin and chitosan, versatile polysaccharides from marine animals, J. Chem. Educ. 67 (1990) 938–942. https://doi.org/10.1021/ed067p938.

[49] M.M. Abo Elsoud, E.M. El Kady, Current trends in fungal

biosynthesis of chitin and chitosan, Bull. Natl. Res. Cent. 2019 431. 43 (2019) 1–12. https://doi.org/10.1186/s42269-019-0105-y.

[50] M. Seenuvasan, G. Sarojini, M. Dineshkumar, Recovery of chitosan from natural biotic waste, Curr. Dev. Biotechnol. Bioeng. Resour. Recover. from Wastes. (2020) 115–133. https://doi.org/10.1016/b978-0-444-64321-6.00006-9.

[51] A. Usman, S. Khalid, A. Usman, Z. Hussain, Y. Wang, Algal polysaccharides, novel application, and outlook, Algae Based Polym. Blends, Compos. Chem. Biotechnol. Mater. Sci. (2017) 115–153. https://doi.org/10.1016/b978-0-12-812360-7.00005-7.

[52] I. Younes, M. Rinaudo, Chitin and chitosan preparation from marine sources. structure, properties and applications, Mar. Drugs. 13 (2015) 1133–1174. https://doi.org/10.3390/md13031133.

[53] M.K. Jang, B.G. Kong, Y. Il Jeong, C.H. Lee, J.W. Nah, Physicochemical characterization of α-chitin, β-chitin, and γ-chitin separated from natural resources, J. Polym. Sci. Part A Polym. Chem. 42 (2004) 3423–3432. https://doi.org/10.1002/pola.20176.

[54] K. Kurita, K. Tomita, S. Ishii, S. -I Nishimura, K. Shimoda, β-chitin as a convenient starting material for acetolysis for efficient preparation of N-acetylchitooligosaccharides, J. Polym. Sci. Part A Polym. Chem.

31 (1993) 2393–2395.
https://doi.org/10.1002/pola.1993.080310923.

[55] H. El Knidri, R. Belaabed, A. Addaou, A. Laajeb, A. Lahsini, Extraction, chemical modification and characterization of chitin and chitosan, Int. J. Biol. Macromol. 120 (2018) 1181–1189. https://doi.org/10.1016/j.ijbiomac.2018.08.139.

[56] M. Nasrollahzadeh, M. Sajjadi, S. Iravani, R.S. Varma, Starch, cellulose, pectin, gum, alginate, chitin and chitosan derived (nano)materials for sustainable water treatment: A review, Carbohydr. Polym. 251 (2021) 116986. https://doi.org/10.1016/j.carbpol.2020.116986.

[57] M.N.V. Ravi Kumar, A review of chitin and chitosan applications, React. Funct. Polym. 46 (2000) 1–27. https://doi.org/10.1016/s1381-5148(00)00038-9.

[58] S. Kou, L.M. Peters, M.R. Mucalo, Chitosan: A review of sources and preparation methods, Int. J. Biol. Macromol. 169 (2021) 85–94. https://doi.org/10.1016/j.ijbiomac.2020.12.005.

[59] P.R. Sivashankari, M. Prabaharan, Deacetylation modification techniques of chitin and chitosan, Chitosan Based Biomater. 1 (2017) 117–133. https://doi.org/10.1016/b978-0-08-100230-

8.00005-4.

[60] F.A. Vicente, M. Huš, B. Likozar, U. Novak, Chitin deacetylation using deep eutectic solvents: *Ab Initio*-supported process optimization, ACS Sustain. Chem. Eng. 9 (2021) 3874–3886. https://doi.org/10.1021/acssuschemeng.0c08976.

[61] M.B. Kaczmarek, K. Struszczyk-Swita, X. Li, M. Szczęsna-Antczak, M. Daroch, Enzymatic modifications of chitin, chitosan, and chitooligosaccharides, Front. Bioeng. Biotechnol. 27 (2019) 243. https://doi.org/10.3389/fbioe.2019.00243.

[62] T.S. Tan, H.Y. Chin, M.L. Tsai, C.L. Liu, Structural alterations, pore generation, and deacetylation of α- and β-chitin submitted to steam explosion, Carbohydr. Polym. 122 (2015) 321–328. https://doi.org/10.1016/j.carbpol.2015.01.016.

[63] R.N. Wijesena, N. Tissera, Y.Y. Kannangara, Y. Lin, G.A.J. Amaratunga, K.M.N. De Silva, A method for top down preparation of chitosan nanoparticles and nanofibers, Carbohydr. Polym. 117 (2015) 731–738. https://doi.org/10.1016/j.carbpol.2014.10.055.

[64] R. Czechowska-Biskup, D. Jarosińska, B. Rokita, P. Ulański, J.M. Rosiak, Determination of degree of deacetylation of chitosan - comparision of methods, Prog. Chem. Appl. Chitin Its Deriv. 17

(2012) 5–20.

[65] R.A.A. Muzzarelli, R. Rocchetti, Determination of the degree of acetylation of chitosans by first derivative ultraviolet spectrophotometry, Carbohydr. Polym. 5 (1985) 461–472. https://doi.org/10.1016/0144-8617(85)90005-0.

[66] J. Jennings, J. Bumgardner, Chitosan Based Biomaterials Volume 1 - 1st Edition (2017),

[67] D. Tahtat, C. Uzun, M. Mahlous, O. Güven, Beneficial effect of gamma irradiation on the N-deacetylation of chitin to form chitosan, Nucl. Instruments Methods Phys. Res. Sect. B Beam Interact. with Mater. Atoms. 265 (2007) 425–428. https://doi.org/10.1016/j.nimb.2007.09.016.

[68] A. Baxter, M. Dillon, K.D. Anthony Taylor, G.A.F. Roberts, Improved method for i.r. determination of the degree of N-acetylation of chitosan, Int. J. Biol. Macromol. 14 (1992) 166–169. https://doi.org/10.1016/s0141-8130(05)80007-8.

[69] Y. Zhang, X. Zhang, R. Ding, J. Zhang, J. Liu, Determination of the degree of deacetylation of chitosan by potentiometric titration preceded by enzymatic pretreatment, Carbohydr. Polym. 83 (2011) 813–817. https://doi.org/10.1016/j.carbpol.2010.08.058.

[70] A. Pelletier, I. Lemire, J. Sygusch, E. Chornet, R.P. Overend, Chitin/chitosan transformation by thermo-mechano-chemical treatment including characterization by enzymatic depolymerization, Biotechnol. Bioeng. 36 (1990) 310–315. https://doi.org/10.1002/bit.260360313.

[71] A. Zając, J. Hanuza, M. Wandas, L. Dymińska, Determination of N-acetylation degree in chitosan using Raman spectroscopy, Spectrochim. Acta Part A Mol. Biomol. Spectrosc. 134 (2015) 114–120. https://doi.org/10.1016/j.saa.2014.06.071.

[72] A. Pavinatto, F.J. Pavinatto, J.A. d. M. Delezuk, T.M. Nobre, A.L. Souza, S.P. Campana-Filho, O.N. Oliveira, Low molecular-weight chitosans are stronger biomembrane model perturbants, Colloids Surfaces B Biointerfaces. 104 (2013) 48–53. https://doi.org/10.1016/j.colsurfb.2012.11.047.

[73] Y. Atay, Antibacterial Activity of Chitosan-Based Systems. Functional Chitosan. Springer, Singapore (2019). doi: 10.1007/978-981-15-0263-7_15.

[74] X. Liu, L. Song, L. Li, S. Li, K. Yao, Antibacterial effects of chitosan and its water-soluble derivatives on E. coli, plasmids DNA, and mRNA, J. Appl. Polym. Sci. 103 (2007) 3521–3528. https://doi.org/10.1002/app.25421.

[75] K. Divya, S. Vijayan, T.K. George, M.S. Jisha, Antimicrobial properties of chitosan nanoparticles: Mode of action and factors affecting activity, Fibers Polym. 2017 182. 18 (2017) 221–230. https://doi.org/10.1007/s12221-017-6690-1.

[76] F. Ding, H. Deng, Y. Du, X. Shi, Q. Wang, Emerging chitin and chitosan nanofibrous materials for biomedical applications, Nanoscale. 6 (2014) 9477–9493. https://doi.org/10.1039/c4nr02814g.

[77] K. Kurita, Chemistry and application of chitin and chitosan, Polym. Degrad. Stab. 59 (1998) 117–120. https://doi.org/10.1016/s0141-3910(97)00160-2.

[78] M. Kong, X.G. Chen, K. Xing, H.J. Park, Antimicrobial properties of chitosan and mode of action: A state of the art review, Int. J. Food Microbiol. 144 (2010) 51–63. https://doi.org/10.1016/j.ijfoodmicro.2010.09.012.

[79] M. Kong, X.G. Chen, Y.P. Xue, C.S. Liu, L.J. Yu, Q.X. Ji, D.S. Cha, H.J. Park, Preparation and antibacterial activity of chitosan microshperes in a solid dispersing system, Front. Mater. Sci. China 2008 22. 2 (2008) 214–220. https://doi.org/10.1007/s11706-008-0036-2.

[80] T. Takahashi, M. Imai, I. Suzuki, J. Sawai, Growth inhibitory effect on bacteria of chitosan membranes regulated with deacetylation degree, Biochem. Eng. J. 40 (2008) 485–491. https://doi.org/10.1016/j.bej.2008.02.009.

[81] T.C. Yang, C.C. Chou, C.F. Li, Antibacterial activity of N-alkylated disaccharide chitosan derivatives, Int. J. Food Microbiol. 97 (2005) 237–245. https://doi.org/10.1016/s0168-1605(03)00083-7.

[82] V.E. Tikhonov, E.A. Stepnova, V.G. Babak, I.A. Yamskov, J. Palma-Guerrero, H.B. Jansson, L. V. Lopez-Llorca, J. Salinas, D. V. Gerasimenko, I.D. Avdienko, V.P. Varlamov, Bactericidal and antifungal activities of a low molecular weight chitosan and its N-/2(3)-(dodec-2-enyl)succinoyl/-derivatives, Carbohydr. Polym. 64 (2006) 66–72. https://doi.org/10.1016/j.carbpol.2005.10.021.

[83] S. Tokura, K. Ueno, S. Miyazaki, N. Nishi, Molecular weight dependent antimicrobial activity by chitosan, New Macromol. Archit. Funct. (1996) 199–207. https://doi.org/10.1007/978-3-642-80289-8_21.

[84] M.S.S. Benhabiles, R. Salah, H. Lounici, N. Drouiche, M.F.A. Goosen, N. Mameri, Antibacterial activity of chitin, chitosan and its oligomers prepared from shrimp shell waste, Food Hydrocoll. 29 (2012) 48–56. https://doi.org/10.1016/j.foodhyd.2012.02.013.

[85] S.H. Lim, S.M. Hudson, Synthesis and antimicrobial activity of a water-soluble chitosan derivative with a fiber-reactive group, Carbohydr. Res. 339 (2004) 313–319. https://doi.org/10.1016/j.carres.2003.10.024.

[86] D.H. Young, H. Köhle, H. Kauss, Effect of chitosan on membrane permeability of suspension-cultured glycine max and *Phaseolus vulgaris* cells, Plant Physiol. 70 (1982) 1449–1454. https://doi.org/10.1104/PP.70.5.1449.

[87] D. Zhao, S. Yu, B. Sun, S. Gao, S. Guo, K. Zhao, Biomedical applications of chitosan and its derivative nanoparticles, Polymers. 10 (2018). https://doi.org/10.3390/polym10040462.

[88] N. Morin-Crini, E. Lichtfouse, G. Torri, G. Crini, Applications of chitosan in food, pharmaceuticals, medicine, cosmetics, agriculture, textiles, pulp and paper, biotechnology, and environmental chemistry, Environ. Chem. Lett. 17 (2019) 1667–1692. https://doi.org/10.1007/s10311-019-00904-x.

[89] M.N.V. Ravi Kumar, A review of chitin and chitosan applications, React. Funct. Polym. 46 (2000) 1–27. https://doi.org/10.1016/S1381-5148(00)00038-9.

[90] H. Huang, X. Yang, Synthesis of chitosan-stabilized gold

nanoparticles in the absence/presence of tripolyphosphate, Biomacromolecules. 5 (2004) 2340–2346. https://doi.org/10.1021/bm0497116.

[91] M. Bin Ahmad, J.J. Lim, K. Shameli, N.A. Ibrahim, M.Y. Tay, Synthesis of silver nanoparticles in chitosan, gelatin and chitosan/gelatin bionanocomposites by a chemical reducing agent and their characterization, Molecules 16 (2011) 7237. https://doi.org/10.3390/molecules16097237.

[92] Y. Duan, R. Duan, R. Liu, M. Guan, W. Chen, J. Ma, M. Chen, B. Du, Q. Zhang, Chitosan-stabilized self-assembled fluorescent gold nanoclusters for cell imaging and biodistribution in vivo, ACS Biomater. Sci. Eng. 4 (2018) 1055–1063. https://doi.org/10.1021/acsbiomaterials.7b00975.

[93] F. Tao, Y. Cheng, X. Shi, H. Zheng, Y. Du, W. Xiang, H. Deng, Applications of chitin and chitosan nanofibers in bone regenerative engineering, Carbohydr. Polym. 230 (2020) 115658. https://doi.org/10.1016/j.carbpol.2019.115658.

[94] P. Feng, Y. Luo, C. Ke, H. Qiu, W. Wang, Y. Zhu, R. Hou, L. Xu, S. Wu, Chitosan-based functional materials for skin wound repair: mechanisms and applications, Front. Bioeng. Biotechnol. 18 (2021) 111. https://doi.org/10.3389/fbioe.2021.650598.

[95] R. Priyadarshi, J.W. Rhim, Chitosan-based biodegradable functional films for food packaging applications, Innov. Food Sci. Emerg. Technol. 62 (2020) 102346. https://doi.org/10.1016/j.ifset.2020.102346.

[96] E. Guzmán, F. Ortega, R.G. Rubio, Chitosan: A promising multifunctional cosmetic ingredient for skin and hair care, Cosmet. 9 (2022) 99. https://doi.org/10.3390/cosmetics9050099.

[97] Y. Qin, P. Li, Antimicrobial chitosan conjugates: current synthetic strategies and potential applications, Int. J. Mol. Sci. 21 (2020) 499. https://doi.org/10.3390/ijms21020499.

[98] K. Esumi, N. Takei, T. Yoshimura, Antioxidant-potentiality of gold–chitosan nanocomposites, Colloids Surfaces B Biointerfaces. 32 (2003) 117–123. https://doi.org/10.1016/s0927-7765(03)00151-6.

[99] H. Huang, Q. Yuan, X. Yang, Morphology study of gold–chitosan nanocomposites, J. Colloid Interface Sci. 282 (2005) 26–31. https://doi.org/10.1016/j.jcis.2004.08.063.

[100] J. Esther, V. Sridevi, Synthesis and characterization of chitosan-stabilized gold nanoparticles through a facile and green approach, Gold Bull. 50 (2017) 1–5. https://doi.org/10.1007/s13404-016-0189-1.

[101] L. Sun, J. Li, J. Cai, L. Zhong, G. Ren, Q. Ma, One pot synthesis of gold nanoparticles using chitosan with varying degree of deacetylation and molecular weight, Carbohydr. Polym. 178 (2017) 105–114. https://doi.org/10.1016/j.carbpol.2017.09.032.

[102] Y.C. Chang, D.H. Chen, Catalytic reduction of 4-nitrophenol by magnetically recoverable Au nanocatalyst, J. Hazard. Mater. 165 (2009) 664–669. https://doi.org/10.1016/j.jhazmat.2008.10.034.

[103] X.F. Zhang, Z.G. Liu, W. Shen, S. Gurunathan, Silver Nanoparticles: Synthesis, Characterization, Properties, Applications, and Therapeutic Approaches, Int. J. Mol. Sci. 17 (2016) 1534. https://doi.org/10.3390/ijms17091534.

[104] Y.K. Twu, Y.W. Chen, C.M. Shih, Preparation of silver nanoparticles using chitosan suspensions, Powder Technol. 185 (2008) 251–257. https://doi.org/10.1016/j.powtec.2007.10.025.

[105] R. Kalaivani, M. Maruthupandy, T. Muneeswaran, A. Hameedha Beevi, M. Anand, C.M. Ramakritinan, A.K. Kumaraguru, Synthesis of chitosan mediated silver nanoparticles (Ag NPs) for potential antimicrobial applications, Front. Lab. Med. 2 (2018) 30–35. https://doi.org/10.1016/j.flm.2018.04.002.

[106] D. Wei, Y. Ye, X. Jia, C. Yuan, W. Qian, Chitosan as an active support

for assembly of metal nanoparticles and application of the resultant bioconjugates in catalysis, Carbohydr. Res. 345 (2010) 74–81. https://doi.org/10.1016/j.carres.2009.10.008.

[107] K. Praveenkumar, M.K. Rabinal, M.N. Kalasad, T. Sankarappa, M.D. Bedre, Chitosan capped Silver nanoparticles used as Pressure sensors, IOSR J. Appl. Phys. 5 (2013) 43–51. https://doi.org/10.9790/4861-0554351.

[108] V.V.T. Padil, S. Wacławek, M. Černík, Green synthesis: nanoparticles and nanofibres based on tree gums for environmental applications, Ecol. Chem. Eng. S. 23 (2016) 533–557. https://doi.org/10.1515/eces-2016-0038.

[109] H.-H. Deng, X.-L. Lin, Y.-H. Liu, K.-L. Li, Q.-Q. Zhuang, H.-P. Peng, A.-L. Liu, X.-H. Xia, W. Chen, Chitosan-stabilized platinum nanoparticles as effective oxidase mimics for colorimetric detection of acid phosphatase, Nanoscale 9 (2017) 10292–10300. https://doi.org/10.1039/c7nr03399k.

[110] J. Liu, W. Bai, J. Zhang, J. Zheng, Novel synthesis of chitosan protected platinum nanoparticles based on gas–liquid interfacial reactions and their application for electrochemical sensing of hydrogen peroxide, Anal. Methods. 8 (2016) 7903–7909. https://doi.org/10.1039/c6ay02376b.

[111] T.K.L. Nguyen, N.D. Nguyen, V.P. Dang, D.T. Phan, T.H. Tran, Q.H. Nguyen, H.D. Mai, Synthesis of platinum nanoparticles by gamma Co-60 ray irradiation method using chitosan as stabilizer, Adv. Mater. Sci. Eng. 2019 (2019) 9624374 . https://doi.org/10.1155/2019/9624374.

[112] X. Chen, X.-J. Xu, X.-C. Zheng, X.-X. Guan, P. Liu, Chitosan supported palladium nanoparticles: The novel catalysts for hydrogen generation from hydrolysis of ammonia borane, Mater. Res. Bull. 103 (2018) 89–95. https://doi.org/10.1016/j.materresbull.2018.03.013.

[113] D. Gao, Q. Zhang, Z. Liu, F. Zhang, F. Gou, G. Xing, S. Zhou, L. Shao, J. Li, Y. Du, C. Qi, Stabilization of palladium nanoparticles inside chitosan derived N-doped carbon nanofibers for Heck reaction, J. Appl. Polym. Sci. 139 (2022) 51742. https://doi.org/10.1002/app.51742.

[114] L.O. Ferreira, A.C.C. Lemos, F.G.E. Nogueira, I.R. Guimaraes, M.C. Guerreiro, M.V.J. Rocha, R.M.L. Savedra, P. Hammer, A.D.B. Brito, E.F.F. Da Cunha, J.P. Silva, T.C. Ramalho, Degradation of organic compounds in a fenton system based on chitosan/Fe^0/Fe_2O_3 composites: A theoretical and experimental study, J. Iran. Chem. Soc. 13 (2016) 377–386. https://doi.org/10.1007/s13738-015-0746-

1.

[115] A.A. Caetano, P.M.B. Chagas, S.S. Vieira, T.F. Moratta, J.C.S. Terra, J.D. Ardisson, I.D.R. Guimarães, Nanostructured iron oxides stabilized by chitosan: using copper to enhance degradation by a combined mechanism, Catal. Sci. Technol. 10 (2020) 5013–5026. https://doi.org/10.1039/d0cy00473a.

[116] A. Maleki, N. Ghamari, M. Kamalzare, Chitosan-supported Fe_3O_4 nanoparticles: a magnetically recyclable heterogeneous nanocatalyst for the syntheses of multifunctional benzimidazoles and benzodiazepines, RSC Adv. 4 (2014) 9416–9423. https://doi.org/10.1039/c3ra47366j.

[117] M. Raji, S.A. Mirbagheri, F. Ye, J. Dutta, Nano zero-valent iron on activated carbon cloth support as Fenton-like catalyst for efficient color and COD removal from melanoidin wastewater, Chemosphere 263 (2021) 127945. https://doi.org/10.1016/j.chemosphere.2020.127945.

[118] Q. Hu, Y. Luo, Polyphenol-chitosan conjugates: Synthesis, characterization, and applications, Carbohydr. Polym. 151 (2016) 624–639. https://doi.org/10.1016/j.carbpol.2016.05.109.

[119] Y. Luo, Q. Wang, Recent development of chitosan-based

polyelectrolyte complexes with natural polysaccharides for drug delivery, Int. J. Biol. Macromol. 64 (2014) 353–367. https://doi.org/10.1016/j.ijbiomac.2013.12.017.

[120] M. Prabaharan, Review Paper: Chitosan Derivatives as Promising Materials for Controlled Drug Delivery. 23 (2008) 5–36. https://doi.org/10.1177/0885328208091562.

[121] Z. Shariatinia, Carboxymethyl chitosan: Properties and biomedical applications, Int. J. Biol. Macromol. 120 (2018) 1406–1419. https://doi.org/10.1016/j.ijbiomac.2018.09.131.

[122] J. Ge, P. Yue, J. Chi, J. Liang, X. Gao, Formation and stability of anthocyanins-loaded nanocomplexes prepared with chitosan hydrochloride and carboxymethyl chitosan, Food Hydrocoll. 74 (2018) 23–31. https://doi.org/10.1016/j.foodhyd.2017.07.029.

[123] V.M. Ramos, M.S. Rodríguez, E. Agulló, N.M. Rodríguez, A. Heras, Chitosan with phosphonic and carboxylic group: New multidentate ligands, Int. J. Pol. Mat. Pol. Biomat. 51 (2010) 711–720. https://doi.org/10.1080/714975833.

[124] C. Federer, M. Kurpiers, A. Bernkop-Schnürch, Thiolated chitosans: a multi-talented class of polymers for various applications, Biomacromolecules 22 (2021) 24–56.

https://doi.org/10.1021/acs.biomac.0c00663.

[125] A. Anitha, N. Deepa, K.P. Chennazhi, S. V. Nair, H. Tamura, R. Jayakumar, Development of mucoadhesive thiolated chitosan nanoparticles for biomedical applications, Carbohydr. Polym. 83 (2011) 66–73. https://doi.org/10.1016/j.carbpol.2010.07.028.

[126] A.O. Aytekin, S. Morimura, K. Kida, Synthesis of chitosan–caffeic acid derivatives and evaluation of their antioxidant activities, J. Biosci. Bioeng. 111 (2011) 212–216. https://doi.org/10.1016/j.jbiosc.2010.09.018.

[127] K. Crouvisier-Urion, P.R. Bodart, P. Winckler, J. Raya, R.D. Gougeon, P. Cayot, S. Domenek, F. Debeaufort, T. Karbowiak, Biobased composite films from chitosan and lignin: antioxidant activity related to structure and moisture, ACS Sustain. Chem. Eng. 4 (2016) 6371–6381. https://doi.org/10.1021/acssuschemeng.6b00956.

[128] E. Rosova, N. Smirnova, E. Dresvyanina, V. Smirnova, E. Vlasova, E. Ivan'kova, M. Sokolova, T. Maslennikova, K. Malafeev, K. Kolbe, M. Kanerva, V. Yudin, Biocomposite Materials Based on Chitosan and Lignin: Preparation and Characterization, Cosmet. 8 (2021) 24. https://doi.org/10.3390/cosmetics8010024.

[129] F.L. Mi, Synthesis and characterization of a novel chitosan−gelatin

bioconjugate with fluorescence emission, Biomacromolecules 6 (2005) 975–987. https://doi.org/10.1021/bm049335p.

[130] G. Cirillo, M. Curcio, U.G. Spizzirri, O. Vittorio, E. Valli, A. Farfalla, A. Leggio, F.P. Nicoletta, F. Iemma, Chitosan–quercetin bioconjugate as multi-functional component of antioxidants and dual-responsive hydrogel networks, Macromol. Mater. Eng. 304 (2019) 1800728. https://doi.org/10.1002/mame.201800728.

[131] H.S. Mansur, A.A.P. Mansur, E. Curti, M. V. De Almeida, Bioconjugation of quantum-dots with chitosan and N,N,N-trimethyl chitosan, Carbohydr. Polym. 90 (2012) 189–196. https://doi.org/10.1016/j.carbpol.2012.05.022.

[132] M. Yalpani, R.H. Marchessault, F.G. Morin, C.J. Monasteries, Syntheses of Poly(3-hydroxyalkanoate) (PHA) conjugates: PHA-carbohydrate and PHA-synthetic polymer conjugates, Macromolecules 24 (1991) 6046–6049. https://doi.org/10.1021/ma00022a024.

[133] E. Korkakaki, M.C.M. van Loosdrecht, R. Kleerebezem, Survival of the fastest: Selective removal of the side population for enhanced PHA production in a mixed substrate enrichment, Bioresour. Technol. 216 (2016) 1022–1029. https://doi.org/10.1016/j.biortech.2016.05.125.

[134] J. Rajesh Banu, G. Ginni, S. Kavitha, R. Yukesh Kannah, V. Kumar, S. Adish Kumar, M. Gunasekaran, V.K. Tyagi, G. Kumar, Polyhydroxyalkanoates synthesis using acidogenic fermentative effluents, Int. J. Biol. Macromol. 193 (2021) 2079–2092. https://doi.org/10.1016/j.ijbiomac.2021.11.040.

[135] T.M.M.M. Amaro, D. Rosa, G. Comi, L. Iacumin, Prospects for the use of whey for polyhydroxyalkanoate (PHA) production, Front. Microbiol. 10 (2019) 992. https://doi.org/10.3389/fmicb.2019.00992.

[136] A. Anjum, M. Zuber, K.M. Zia, A. Noreen, M.N. Anjum, S. Tabasum, Microbial production of polyhydroxyalkanoates (PHAs) and its copolymers: A review of recent advancements, Int. J. Biol. Macromol. 89 (2016) 161–174. https://doi.org/10.1016/j.ijbiomac.2016.04.069.

[137] M.G.E. Albuquerque, V. Martino, E. Pollet, L. Avérous, M.A.M. Reis, Mixed culture polyhydroxyalkanoate (PHA) production from volatile fatty acid (VFA)-rich streams: Effect of substrate composition and feeding regime on PHA productivity, composition and properties, J. Biotechnol. 151 (2011) 66–76. https://doi.org/10.1016/j.jbiotec.2010.10.070.

[138] C. Kourmentza, J. Plácido, N. Venetsaneas, A. Burniol-Figols, C.

Varrone, H.N. Gavala, M.A.M. Reis, Recent Advances and challenges towards sustainable polyhydroxyalkanoate (PHA) production, Bioeng. 4 (2017) 55. https://doi.org/10.3390/bioengineering4020055.

[139] Z. Li, X.J. Loh, Water soluble polyhydroxyalkanoates: future materials for therapeutic applications, Chem. Soc. Rev. 44 (2015) 2865–2879. https://doi.org/10.1039/c5cs00089k.

[140] T.S.M. Amelia, S. Govindasamy, A.M. Tamothran, S. Vigneswari, K. Bhubalan, Applications of PHA in agriculture, Biotechnol. Appl. Polyhydroxyalkanoates. (2019) 347–361. https://doi.org/10.1007/978-981-13-3759-8_13.

[141] S. Dhania, M. Bernela, R. Rani, M. Parsad, S. Grewal, S. Kumari, R. Thakur, Scaffolds the backbone of tissue engineering: Advancements in use of polyhydroxyalkanoates (PHA), Int. J. Biol. Macromol. 208 (2022) 243–259. https://doi.org/10.1016/j.ijbiomac.2022.03.030.

[142] S.Y. Lee, J. Il Choi, H.H. Wong, Recent advances in polyhydroxyalkanoate production by bacterial fermentation: mini-review, Int. J. Biol. Macromol. 25 (1999) 31–36. https://doi.org/10.1016/s0141-8130(99)00012-4.

[143] Y. Zheng, J.C. Chen, Y.M. Ma, G.Q. Chen, Engineering biosynthesis of polyhydroxyalkanoates (PHA) for diversity and cost reduction, Metab. Eng. 58 (2020) 82–93. https://doi.org/10.1016/j.ymben.2019.07.004.

[144] P. Chakraborty, W. Gibbons, K. Muthukumarappan, Conversion of volatile fatty acids into polyhydroxyalkanoate by Ralstonia eutropha, J. Appl. Microbiol. 106 (2009) 1996–2005. https://doi.org/10.1111/j.1365-2672.2009.04158.x.

[145] F.C. de Paula, S. Kakazu, C.B.C. de Paula, J.G.C. Gomez, J. Contiero, Polyhydroxyalkanoate production from crude glycerol by newly isolated Pandoraea sp., J. King Saud Univ. - Sci. 29 (2017) 166–173. https://doi.org/10.1016/j.jksus.2016.07.002.

[146] P.M. Halami, Production of polyhydroxyalkanoate from starch by the native isolate Bacillus cereus CFR06, World J. Microbiol. Biotechnol. 24 (2008) 805–812. https://doi.org/10.1007/s11274-007-9543-z.

[147] L.R. Castilho, D.A. Mitchell, D.M.G. Freire, Production of polyhydroxyalkanoates (PHAs) from waste materials and by-products by submerged and solid-state fermentation, Bioresour. Technol. 100 (2009) 5996–6009. https://doi.org/10.1016/j.biortech.2009.03.088.

[148] H. Al Battashi, S. Al-Kindi, V.K. Gupta, N. Sivakumar, Polyhydroxyalkanoate (PHA) production using volatile fatty acids derived from the anaerobic digestion of waste paper, J. Polym. Environ. 29 (2021) 250–259. https://doi.org/10.1007/s10924-020-01870-0.

[149] I.S. Al Rowaihi, B. Kick, S.W. Grötzinger, C. Burger, R. Karan, D. Weuster-Botz, J. Eppinger, S.T. Arold, A two-stage biological gas to liquid transfer process to convert carbon dioxide into bioplastic, Bioresour. Technol. Reports. 1 (2018) 61–68. https://doi.org/10.1016/j.biteb.2018.02.007.

[150] K. Sudesh, H. Abe, Y. Doi, Synthesis, structure and properties of polyhydroxyalkanoates: biological polyesters, Prog. Polym. Sci. 25 (2000) 1503–1555. https://doi.org/10.1016/s0079-6700(00)00035-6.

[151] L. M., Produits de Deshydration et de Polymerisation de L'acide β=Oxybutyrique, Bull. Soc. Chim. Biol. 8 (1926) 770–782.

[152] S. Khanna, A.K. Srivastava, Statistical media optimization studies for growth and PHB production by Ralstonia eutropha, Process Biochem. 40 (2005) 2173–2182. https://doi.org/10.1016/j.procbio.2004.08.011.

[153] P. Anbukarasu, D. Sauvageau, A. Elias, Tuning the properties of polyhydroxybutyrate films using acetic acid via solvent casting, Sci. Rep. 5 (2015). https://doi.org/10.1038/srep17884.

[154] B. McAdam, M. Brennan Fournet, P. McDonald, M. Mojicevic, Production of polyhydroxybutyrate (PHB) and factors impacting its chemical and mechanical characteristics, Polymers 12 (2020) 2908. https://doi.org/10.3390/polym12122908.

[155] S.L. Riedel, S. Jahns, S. Koenig, M.C.E. Bock, C.J. Brigham, J. Bader, U. Stahl, Polyhydroxyalkanoates production with *Ralstonia eutropha* from low quality waste animal fats, J. Biotechnol. 214 (2015) 119–127. https://doi.org/10.1016/j.jbiotec.2015.09.002.

[156] A.M. Díez-Pascual, A.L. Díez-Vicente, Poly(3-hydroxybutyrate)/ZnO bionanocomposites with improved mechanical, barrier and antibacterial properties, Int. J. Mol. Sci. 15 (2014) 10950. https://doi.org/10.3390/ijms150610950.

[157] A. Jayakumar, K. Prabhu, L. Shah, P. Radha, Biologically and environmentally benign approach for PHB-silver nanocomposite synthesis and its characterization, Polym. Test. 81 (2020) 106197. https://doi.org/10.1016/j.polymertesting.2019.106197.

[158] J.L. Castro-Mayorga, F. Freitas, M.A.M. Reis, M.A. Prieto, J.M.

Lagaron, Biosynthesis of silver nanoparticles and polyhydroxybutyrate nanocomposites of interest in antimicrobial applications, Int. J. Biol. Macromol. 108 (2018) 426–435. https://doi.org/10.1016/j.ijbiomac.2017.12.007.

[159] S. Yalcin, R. Khodadust, G. Unsoy, I.C. Garip, Z.D. Mumcuoglu, U. Gunduz, Synthesis and characterization of polyhydroxybutyrate coated magnetic nanoparticles: toxicity analyses on different cell lines, Synt. Reac. Inorg. Metal-Org. Nano-Metal Chem.45 (2015) 700–708. https://doi.org/10.1080/15533174.2013.831448.

[160] Y.S. Mostafa, S.A. Alrumman, S.A. Alamri, K.A. Otaif, M.S. Mostafa, A.M. Alfaify, Bioplastic (poly-3-hydroxybutyrate) production by the marine bacterium *Pseudodonghicola xiamenensis* through date syrup valorization and structural assessment of the biopolymer, Sci. Reports 10 (2020) 8815. https://doi.org/10.1038/s41598-020-65858-5.

[161] M. Degli Esposti, F. Chiellini, F. Bondioli, D. Morselli, P. Fabbri, Highly porous PHB-based bioactive scaffolds for bone tissue engineering by in situ synthesis of hydroxyapatite, Mater. Sci. Eng. C. 100 (2019) 286–296. https://doi.org/10.1016/j.msec.2019.03.014.

[162] D.Z. Bucci, L.B.B. Tavares, I. Sell, PHB packaging for the storage of

food products, Polym. Test. 24 (2005) 564–571. https://doi.org/10.1016/j.polymertesting.2005.02.008.

[163] M.M.E. Costa, E.C.M. Cabral-Albuquerque, T.L.M. Alves, J.C. Pinto, R.L. Fialho, Use of polyhydroxybutyrate and ethyl cellulose for coating of urea granules, J. Agric. Food Chem. 61 (2013) 9984–9991. https://doi.org/10.1021/jf401185y.

[164] S. Wacławek, L. Chronopoulou, M. Petrangeli Papini, V.V.T. Padil, C. Palocci, J. Kupčík, M. Černík, Enhancement of stability and reactivity of nanosized zero-valent iron with polyhydroxybutyrate, Desalin. Water Treat. 69 (2017). https://doi.org/10.5004/dwt.2017.0704.

[165] P.D. Sruthi, C.S. Sahithya, C. Justin, C. SaiPriya, K.S. Bhavya, P. Senthilkumar, A. V. Samrot, Utilization of chemically synthesized super paramagnetic iron oxide nanoparticles in drug delivery, imaging and heavy metal removal, J. Clust. Sci. 30 (2019) 11–24. https://doi.org/10.1007/s10876-018-1454-7.

[166] D. D'Amico, L.A. Fasce, C.E. Hoppe, M. Arturo López-Quintela, V.P. Cyras, Superparamagnetic nanocomposites obtained by dispersion of ultrafine magnetic iron oxide nanoparticles in poly(3-hydroxybutyrate), Eur. Polym. J. 55 (2014) 160–169. https://doi.org/10.1016/j.eurpolymj.2014.03.033.

[167] R. Yadav, K. Balasubramanian, X. Wang, Encapsulation of gold nanoparticles with PHB based on coffee ring effect, RSC Adv. 5 (2015) 18501–18505. https://doi.org/10.1039/c4ra15269g.

[168] S. Riaz, Z.A. Raza, M.I. Majeed, T. Jan, Synthesis of zinc sulfide nanoparticles and their incorporation into poly(hydroxybutyrate) matrix in the formation of a novel nanocomposite, Mater. Res. Express. 5 (2018) 055027. https://doi.org/10.1088/2053-1591/aac1f9.

[169] A.M. Díez-Pascual, Poly(3-hydroxybutyrate-co-3-hydroxyhexanoate) with zinc oxide nanoparticles for food packaging, J. Food Process Eng. 45 (2022) e13814. https://doi.org/10.1111/jfpe.13814.

[170] L. Dan, M.A. Pope, A.L. Elias, Solution-processed conductive biocomposites based on polyhydroxybutyrate and reduced graphene oxide, J. Phys. Chem. C. 122 (2018) 17490–17500. https://doi.org/10.1021/acs.jpcc.8b02515.

[171] V. Sridhar, I. Lee, H.H. Chun, H. Park, Graphene reinforced biodegradable poly(3-hydroxybutyrate-co-4-hydroxybutyrate) nano-composites, Express Polym. Lett. 7 (2013) 320–328. https://doi.org/10.3144/expresspolymlett.2013.29.

[172] J.A. Damasco, S.Y. Huang, J.V.D. Perez, J.A.T. Manongdo, K.A. Dixon, M.L. Williams, M.C. Jacobsen, R. Barbosa, G.M. Canlas, G. Chintalapani, A.D. Melancon, R.R. Layman, N.W. Fowlkes, E.M. Whitley, M.P. Melancon, Bismuth nanoparticle and polyhydroxybutyrate coatings enhance the radiopacity of absorbable inferior vena cava filters for fluoroscopy-guided placement and longitudinal computed tomography monitoring in pigs, ACS Biomater. Sci. Eng. 8 (2022) 1676–1685. https://doi.org/10.1021/acsbiomaterials.1c01449.

[173] A.R. Kolahchi, M. Kontopoulou, Chain extended poly(3-hydroxybutyrate) with improved rheological properties and thermal stability, through reactive modification in the melt state, Polym. Degrad. Stab. 121 (2015) 222–229. https://doi.org/10.1016/j.polymdegradstab.2015.09.008.

[174] H. Arslan, B. Hazer, S.C. Yoon, Grafting of poly(3-hydroxyalkanoate) and linoleic acid onto chitosan, J. Appl. Polym. Sci. 103 (2007) 81–89. https://doi.org/10.1002/app.24276.

[175] B. Hazer, A. Steinbüchel, Increased diversification of polyhydroxyalkanoates by modification reactions for industrial and medical applications, Appl. Microbiol. Biotechnol. 74 (2007) 1–12. doi:10.1007/s00253-006-0732-8.

[176] D. Briassoulis, P. Tserotas, I.G. Athanasoulia, Alternative optimization routes for improving the performance of poly(3-hydroxybutyrate) (PHB) based plastics, J. Clean. Prod. 318 (2021) 128555. https://doi.org/10.1016/j.jclepro.2021.128555.

[177] W. Cao, A. Wang, D. Jing, Y. Gong, N. Zhao, X. Zhang, Novel biodegradable films and scaffolds of chitosan blended with poly(3-hydroxybutyrate), J. Biomater. Sci. Polym. Ed. 16 (2005) 1379–1394. https://doi.org/10.1163/156856205774472308.

[178] I. Lugoloobi, X. Li, Y. Zhang, Z. Mao, B. Wang, X. Sui, X. Feng, Fabrication of lignin/poly(3-hydroxybutyrate) nanocomposites with enhanced properties via a Pickering emulsion approach, Int. J. Biol. Macromol. 165 (2020) 3078–3087. https://doi.org/10.1016/j.ijbiomac.2020.10.156.

[179] J.C.C. Yeo, X.Y. Ong, J.J. Koh, J. Kong, X. Zhang, W. Thitsartarn, Z. Li, C. He, Dual-phase poly(lactic acid)/poly(hydroxybutyrate)-rubber copolymer as high-performance shape memory materials, ACS Appl. Polym. Mater. 3 (2021) 389–399. https://doi.org/10.1021/acsapm.0c01158.

[180] M.L. Tebaldi, A.L.C. Maia, F. Poletto, F.V. de Andrade, D.C.F. Soares, Poly(-3-hydroxybutyrate-co-3-hydroxyvalerate) (PHBV): Current advances in synthesis methodologies, antitumor applications and

biocompatibility, J. Drug Deliv. Sci. Technol. 51 (2019) 115–126. https://doi.org/10.1016/j.jddst.2019.02.007.

[181] A. Balakrishna Pillai, A. Jaya Kumar, H. Kumarapillai, Biosynthesis of poly(3-hydroxybutyrate-co-3-hydroxyvalerate) (PHBV) in *Bacillus aryabhattai* and cytotoxicity evaluation of PHBV/poly(ethylene glycol) blends, 3 Biotech 10 (2020) 32. https://doi.org/10.1007/s13205-019-2017-9.

[182] A.L. Rivera-Briso, Á. Serrano-Aroca, Poly(3-Hydroxybutyrate-co-3-Hydroxyvalerate): enhancement strategies for advanced applications, Polymers 10 (2018). https://doi.org/10.3390/polym10070732.

[183] S.A. Varghese, H. Pulikkalparambil, S.M. Rangappa, S. Siengchin, J. Parameswaranpillai, Novel biodegradable polymer films based on poly(3-hydroxybutyrate-co-3-hydroxyvalerate) and *Ceiba pentandra* natural fibers for packaging applications, Food Packag. Shelf Life 25 (2020) 100538. https://doi.org/10.1016/j.fpsl.2020.100538.

[184] L. Xia, Y. Li, Z. Zhou, Y. Dai, H. Liu, H. Liu, Icariin delivery porous PHBV scaffolds for promoting osteoblast expansion in vitro, Mater. Sci. Eng. C. 33 (2013) 3545–3552. https://doi.org/10.1016/j.msec.2013.04.050.

[185] K.W. Meereboer, K.W. Meereboer, A.K. Pal, M. Misra, M. Misra, A.K. Mohanty, A.K. Mohanty, Sustainable PHBV/cellulose acetate blends: effect of a chain extender and a plasticizer, ACS Omega 5 (2020) 14221–14231. https://doi.org/10.1021/acsomega.9b03369.

[186] M.M. Quispe, O. V. Lopez, D.A. Boina, J.F. Stumbé, M.A. Villar, Glycerol-based additives of poly(3-hydroxybutyrate) films, Polym. Test. 93 (2021) 107005. https://doi.org/10.1016/j.polymertesting.2020.107005.

[187] H.K. Lee, J. Ismail, H.W. Kammer, M.A. Bakar, Melt reaction in blends of poly(3-hydroxybutyrate) (PHB) and epoxidized natural rubber (ENR-50), J. Appl. Polym. Sci. 95 (2005) 113–129. https://doi.org/10.1002/app.20808.

[188] T. Ikejima, K. Yagi, Y. Inoue, Thermal properties and crystallization behavior of poly(3-hydroxybutyric acid) in blends with chitin and chitosan, Macromol. Chem. Phys. 200 (1999) 413–421. https://doi.org/10.1002/(sici)1521-3935(19990201)200:2<413::aid-macp413>3.0.co;2-q.

[189] P. Mousavioun, W.O.S. Doherty, G. George, Thermal stability and miscibility of poly(hydroxybutyrate) and soda lignin blends, Ind. Crops Prod. 32 (2010) 656–661. https://doi.org/10.1016/j.indcrop.2010.08.001.

[190] S. Godbole, S. Gote, M. Latkar, T. Chakrabarti, Preparation and characterization of biodegradable poly-3-hydroxybutyrate–starch blend films, Bioresour. Technol. 86 (2003) 33–37. https://doi.org/10.1016/s0960-8524(02)00110-4.

[191] M. Zhang, N.L. Thomas, Blending polylactic acid with polyhydroxybutyrate: The effect on thermal, mechanical, and biodegradation properties, Adv. Polym. Technol. 30 (2011) 67–79. https://doi.org/10.1002/adv.20235.

[192] M.P. Arrieta, M. Perdiguero, S. Fiori, J.M. Kenny, L. Peponi, Biodegradable electrospun PLA-PHB fibers plasticized with oligomeric lactic acid, Polym. Degrad. Stab. 179 (2020) 109226. https://doi.org/10.1016/j.polymdegradstab.2020.109226.

[193] D.M. Panaitescu, C.A. Nicolae, A.R. Gabor, R. Trusca, Thermal and mechanical properties of poly(3-hydroxybutyrate) reinforced with cellulose fibers from wood waste, Ind. Crops Prod. 145 (2020) 112071. https://doi.org/10.1016/j.indcrop.2019.112071.

[194] J. Li, Y. Wang, Z. Wang, J. Wang, D. Wu, Surface chain engineering of chitin nanocrystals towards tailoring the nucleating capacities for poly(β-hydroxybutyrate), Int. J. Biol. Macromol. 166 (2021) 967–976. https://doi.org/10.1016/j.ijbiomac.2020.10.253.

[195] E.I. Ochoa-Segundo, M. González-Torres, A. Cabrera-Wrooman, R. Sánchez-Sánchez, B.M. Huerta-Martínez, Y. Melgarejo-Ramírez, G. Leyva-Gómez, E.M. Rivera-Muñoz, H. Cortés, C. Velasquillo, S. Vargas-Muñoz, R. Rodríguez-Talavera, Gamma radiation-induced grafting of n-hydroxyethyl acrylamide onto poly(3-hydroxybutyrate): A companion study on its polyurethane scaffolds meant for potential skin tissue engineering applications, Mater. Sci. Eng. C. 116 (2020) 111176. https://doi.org/10.1016/j.msec.2020.111176.

[196] E. V. Torres-Tello, J.R. Robledo-Ortíz, Y. González-García, A.A. Pérez-Fonseca, C.F. Jasso-Gastinel, E. Mendizábal, Effect of agave fiber content in the thermal and mechanical properties of green composites based on polyhydroxybutyrate or poly(hydroxybutyrate-co-hydroxyvalerate), Ind. Crops Prod. 99 (2017) 117–125. https://doi.org/10.1016/j.indcrop.2017.01.035.

[197] B. Gomez-Ruiz, P. Ribao, N. Diban, M.J. Rivero, I. Ortiz, A. Urtiaga, Photocatalytic degradation and mineralization of perfluorooctanoic acid (PFOA) using a composite TiO_2–rGO catalyst, J. Hazard. Mater. 344 (2018) 950–957. https://doi.org/10.1016/j.jhazmat.2017.11.048.

[198] A. Modak, P. Bhanja, S. Dutta, B. Chowdhury, A. Bhaumik, Catalytic

reduction of CO_2 into fuels and fine chemicals, Green Chem. 22 (2020) 4002–4033. https://doi.org/10.1039/d0gc01092h.

[199] X. Zou, Y. Zhang, Noble metal-free hydrogen evolution catalysts for water splitting, Chem. Soc. Rev. 44 (2015) 5148–5180. https://doi.org/10.1039/c4cs00448e.

[200] S. Wacławek, V.V.T. Padil, M. Černík, Major Advances and Challenges in Heterogeneous Catalysis for Environmental Applications: A Review, Ecol. Chem. Eng. S 25 (2018) 9–34. https://doi.org/10.1515/eces-2018-0001.

[201] J. Wang, L. Yu, L. Hu, G. Chen, H. Xin, X. Feng, Ambient ammonia synthesis via palladium-catalyzed electrohydrogenation of dinitrogen at low overpotential, Nat. Commun. 2018 91. 9 (2018) 1–7. https://doi.org/10.1038/s41467-018-04213-9.

[202] Y. Zhang, Q. Jiang, S. Jiang, H. Li, R. Zhang, J. Qu, S. Zhang, W. Han, One-step synthesis of biochar supported nZVI composites for highly efficient activating persulfate to oxidatively degrade atrazine, Chem. Eng. J. 420 (2021) 129868. https://doi.org/10.1016/j.cej.2021.129868.

[203] C. Kästner, A.F. Thünemann, Catalytic Reduction of 4-Nitrophenol Using Silver Nanoparticles with Adjustable Activity, Langmuir 32

(2016) 7383–7391. https://doi.org/10.1021/acs.langmuir.6b01477.

[204] S. Pandey, S.B. Mishra, Catalytic reduction of p-nitrophenol by using platinum nanoparticles stabilised by guar gum, Carbohydr. Polym. 113 (2014) 525–531. https://doi.org/10.1016/j.carbpol.2014.07.047.

[205] Y. Yu, E. Jung, H.J. Kim, A. Cho, J. Kim, T. Yu, J. Lee, Protein particles decorated with Pd nanoparticles for the catalytic reduction of p-nitrophenol to p-aminophenol, ACS Appl. Nano Mater. 3 (2020) 10487–10496. https://doi.org/10.1021/acsanm.0c02406.

[206] P. Zhao, X. Feng, D. Huang, G. Yang, D. Astruc, Basic concepts and recent advances in nitrophenol reduction by gold- and other transition metal nanoparticles, Coor. Chem.Rev. 287 (2015) 114-136. https://doi.org/10.1016/j.ccr.2015.01.002.

[207] E. Seo, J. Kim, Y. Hong, Y.S. Kim, D. Lee, B.S. Kim, Double hydrophilic block copolymer templated au nanoparticles with enhanced catalytic activity toward nitroarene reduction, J. Phys. Chem. C 117 (2013) 11686–11693. https://doi.org/10.1021/jp4027139.

[208] I. V. Asharani, D. Thirumalai, Synthesis of Dendrimer-Encapsulated Silver Nanoparticles and Its Catalytic Activity on the Reduction of 4-Nitrophenol, J. Chinese Chem. Soc. 59 (2012) 1455–1460.

https://doi.org/10.1002/jccs.201100734.

[209] Q. Zhu, W. Zhang, J. Cai, J. Li, L. Zhong, S. Pu, A. Li, Morphology-controlled synthesis of gold nanoparticles with chitosan for catalytic reduction of nitrophenol, Colloids Surfaces A Physicochem. Eng. Asp. 640 (2022) 128471. https://doi.org/10.1016/j.colsurfa.2022.128471.

[210] Y.G. Kang, H. Yoon, W. Lee, E. ju Kim, Y.S. Chang, Comparative study of peroxide oxidants activated by nZVI: Removal of 1,4-Dioxane and arsenic(III) in contaminated waters, Chem. Eng. J. 334 (2018) 2511–2519. https://doi.org/10.1016/j.cej.2017.11.076.

[211] N. Toshima, Metal Nanoparticles Used as Catalysts, in: Dekker Encycl. Nanosci. Nanotechnology, Second Ed. - Six Vol. Set, New York, (2004) 1869.

[212] A. Romero García, Ł. Klapiszewski, Y. Zhuikova, V. Zhuikov, V. Varlamov, Biocomposite materials based on poly(3-hydroxybutyrate) and chitosan: A Review, Polym. 14 (2022) 5549. https://doi.org/10.3390/polym14245549.

[213] F. Neese, The ORCA program system, Wiley Interdiscip. Rev. Comput. Mol. Sci. 2 (2012) 73–78. https://doi.org/10.1002/wcms.81.

[214] T. Lu, F. Chen, Multiwfn: A multifunctional wavefunction analyzer, J. Comput. Chem. 33 (2012) 580–592. https://doi.org/10.1002/jcc.22885.

[215] M.D. Hanwell, D.E. Curtis, D.C. Lonie, T. Vandermeerschd, E. Zurek, G.R. Hutchison, Avogadro: An advanced semantic chemical editor, visualization, and analysis platform, J. Cheminform. 4 (2012) 17. https://doi.org/10.1186/1758-2946-4-17